NASA Contractor Report 3926

General Design Method for Three-Dimensional, Potential Flow Fields

II—Computer Program DIN3D1 for Simple, Unbranched Ducts

John D. Stanitz

NASA

NASA Contractor Report 3926

General Design Method for Three-Dimensional, Potential Flow Fields

II—Computer Program DIN3D1 for Simple, Unbranched Ducts

John D. Stanitz, *Consulting Engineer*
University Heights, Ohio

NASA

National Aeronautics
and Space Administration

Scientific and Technical
Information Branch

1985

CONTENTS

SUMMARY

The general design method for three-dimensional, potential, incompressible or subsonic-compressible flow developed in part I of this report is applied to the design of simple, unbranched ducts. A computer program, DIN3D1, is developed and five numerical examples are presented: a nozzle, two elbows, an S-duct, and the preliminary design of a side inlet for turbomachines. The two major inputs to the program are the upstream boundary shape and the lateral velocity distribution on the duct wall. As a result of these inputs, boundary conditions are overprescribed and the problem is ill posed. However, it appears that there are degrees of "compatibility" between these two major inputs and that, for reasonably compatible inputs, satisfactory solutions can be obtained. By not prescribing the shape of the upstream boundary, the problem presumably becomes well posed, but it is not clear how to formulate a practical design method under this circumstance. Nor does it appear desirable, because the designer usually needs to retain control over the upstream (or downstream) boundary shape.

The problem is further complicated by the fact that, unlike the two-dimensional case, and irrespective of the upstream boundary shape, some prescribed lateral velocity distributions do not have proper solutions.

1.0 INTRODUCTION

In part I of this report (ref. 1), a general design method is developed for three-dimensional, potential, incompressible or subsonic-compressible flow fields with arbitrary, prescribed velocity distributions as a function of arc length along streamlines on the boundary of the field. For (the present) part II of this report, a computer program, DIN3D1, has been developed for the design of simple, unbranched ducts with uniform velocities at the upstream and downstream boundaries and with arbitrary, prescribed velocity distributions along streamlines on the lateral boundaries.

The design of flow fields with satisfactory velocities along the boundary is important for the following reasons:

(1) Boundary-layer separation losses can be avoided by prescribing velocity distributions in the direction of flow, along the surfaces of the boundary, that do not decrease too rapidly.

(2) Shock losses in compressible flow and cavitation in incompressible flow can be avoided by prescribing velocities that do not exceed certain maximum values dictated by these phenomena.

(3) For compressible flow in ducts, the desired flow rate can be assured by prescribing velocities that do not result in premature choked flow.

However, the first objective of fluid dynamic design is to determine the shape of the flow-field boundary for which losses are minimum. For both incompressible and shock-free compressible flow, the fluid losses originate at the material surfaces along the flow-field boundary, and the magnitude of these losses depends on the velocity distribution along these surfaces. The characteristics of a desirable velocity distribution are relatively well known from boundary-layer theory.

The main program, DIN3D1, together with 21 major subroutines is described herein. The program input and output are also described and several numerical examples are presented.

2.0 SYMBOLS

All quantities are nondimensional; velocity is expressed as a ratio of the upstream velocity; linear quantities, expressed in any consistent unit for input, are made dimensionless in the program by dividing by the square root of the upstream boundary area; names for variables and parameters used in the computer program are not listed.

A	local continuity parameter, eq. (3.3.2)
a	distance between adjacent nodal points of finite-difference star, figs. in section 3.2
B	local continuity parameter, eq. (3.3.3)
$C_C, C_0,$ $C_1, ..., C_6$	coefficients in governing finite-difference eqs. (3.3.4) and (3.3.5)
$C_1^*, C_2^*,$ C_3^*, C_4^*	coefficients given by eqs. (3.4.3) to (3.4.5)
$\bar{e}$	unit vector
$\bar{e}_1$	unit vector in direction of q along streamlines, which are intersections of ψ and η stream surfaces, fig. in section 3.1
$\bar{e}_2$	unit vector tangent to intersection of η stream surface and φ potential surface, fig. in section 3.1
$\bar{e}_3$	unit vector tangent to intersection of ψ stream surface and φ potential surface, fig. in section 3.1
I, J, K	indices in φ, ψ, and η directions, respectively
$\bar{i}, \bar{j}, \bar{k}$	unit vectors in x, y, and z directions, respectively, fig. in section 3.1
JX, KX	indices for location of primary streamline, fig. in section 3.5
k	adjustment factors for constraints, eqs. (4.2.2) and (4.2.9)
m	path length in direction of $\bar{e}_3$ along intersection of ψ stream surface and φ potential surface, fig. in section 3.1

2

n	path length in direction of $\bar{e}_2$ along intersection of η stream surface and φ potential surface, fig. in section 3.1
p_U	path length along perimeter of upstream boundary, fig. in section 3.5
Q	ln q
q	velocity, expressed as ratio of upstream velocity
$\bar{q}$	velocity vector, $\bar{e}_1 q$, fig. in section 3.1
$\mathscr{R}$	residual error, eq. (3.3.4)
r	radius from axis of duct turn, fig. in appendix A
s	path length along streamline in direction of $\bar{e}_1$, fig. in section 3.1
x,y,z	Cartesian coordinates in physical space
α,β,γ	angles of direction cosines in x,y,z space, fig. in section 3.1
Δ	finite increment
Θ	angle with which ψ and η stream surfaces intersect on potential surface, fig. in section 3.1; any angle
ρ	local static density of fluid as ratio of upstream static density
φ	velocity potential, eq. (3.0.1)
φ,ψ,η	curvilinear coordinates in physical x,y,z space, or orthogonal coordinates of transformed φ,ψ,η space
(·)	dot-product operator of two vectors

Subscripts:

amp	amplitude
D	downstream boundary
max	maximum
min	minimum
o	outer radius
P	principal streamline, IP on first fig. in section 7.1
U	upstream boundary
0,1,...,6	grid points in finite-difference star, figs. in section 3.2
1,2,3	variables or components of variables associated with directions of $\bar{e}_1$, $\bar{e}_2$, and $\bar{e}_3$, respectively

3.0 GOVERNING DIFFERENTIAL EQUATION AND CONSTRUCTION OF FLOW FIELD

A major difficulty faced by all classical design methods is that they are boundary-value problems in which the velocity is specified along physical boundaries, the shapes of which are not known until the problem is solved. In this report, the difficulty was avoided by solving the problem in transformed φ,ψ,η space, where φ and ψ are the velocity potential and a stream function, respectively, and η is a second stream function associated with continuity in three-dimensional flow. The velocity distribution can then be expressed as a function of φ along the boundary streamlines (lines of constant ψ and η) from the relation

$$\varphi = \int q(s)\ ds + const \tag{3.0.1}$$

where $q(s)$ is the prescribed velocity as a function of arc length s along the boundary streamline in physical x,y,z space.

3.1 Physical x,y,z space. - The flow field at a point in physical x,y,z space has two stream surfaces of constant ψ and η, respectively, that intersect the potential surface at $90°$ and intersect one another at an angle Θ measured on the potential surface (ref. 1). The directions of these three intersections are given by the unit vectors $\bar{e}_1$, $\bar{e}_2$, and $\bar{e}_3$, each defined by its direction cosines $\cos \alpha$, $\cos \beta$, and $\cos \gamma$. Differential lengths along the intersections are given by ds, dm, and dn, as shown in the following figure.

4
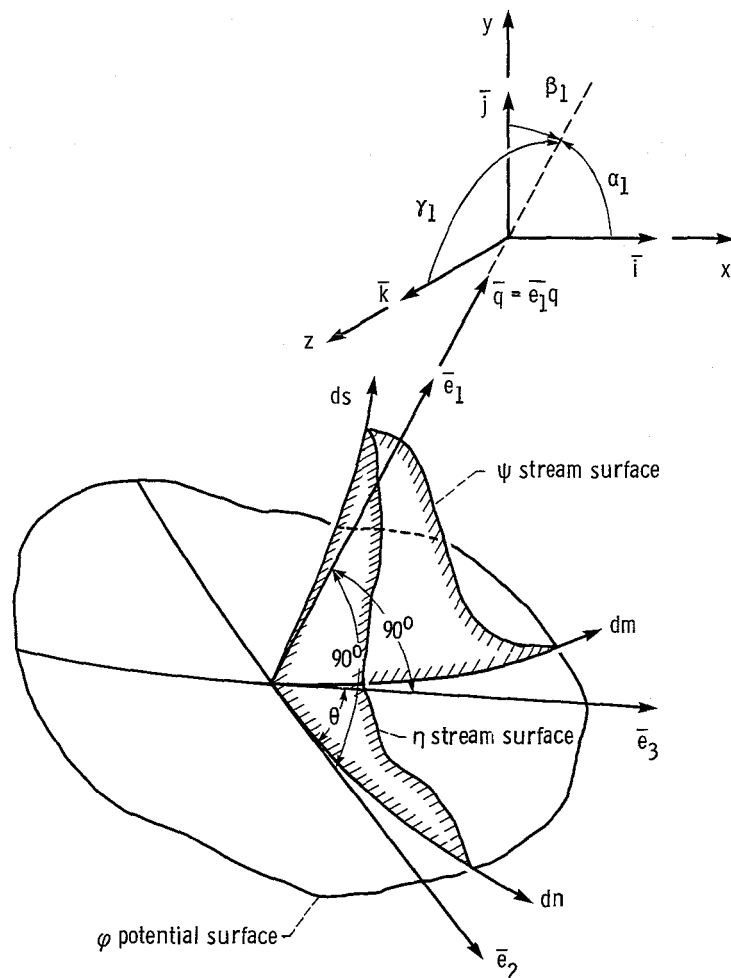
The velocity vector $\bar{q}$ ($\bar{e}_1 q$) is tangent to the intersection of the ψ and η stream surfaces so that $\bar{q}$ is normal to the potential surface φ and ψ and η are constant along the streamline.

3.2 Transformed φ, ψ, η space. - For a duct, the flow field in transformed φ, ψ, η space becomes a cylinder with a cross section
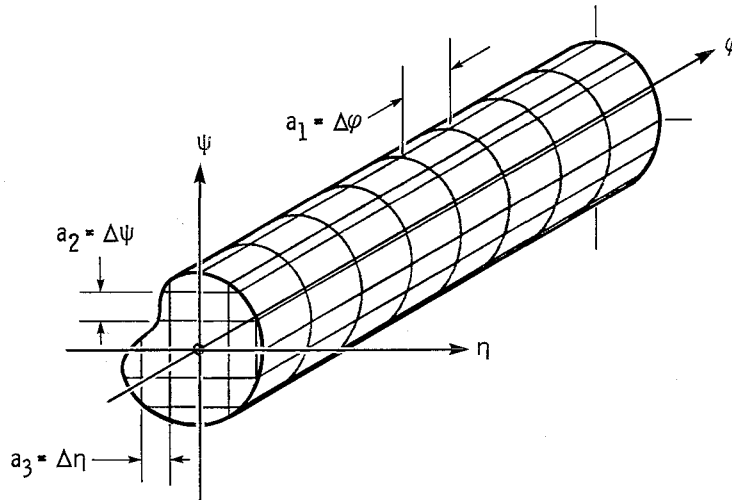
the same shape as the upstream boundary configuration in x, y, z space, provided that the stream surfaces ψ and η at the upstream boundary are defined by lines of constant y and z, respectively (ref. 1). Lines of constant ψ and η (paired values) on the lateral boundary are streamlines, and the velocity vector $\bar{q}$ is everywhere parallel to the φ axis. The rectangular grid resulting from the intersections of surfaces of constant φ, ψ, and η, for various specified values of grid spacing a_1, a_2, and a_3, respectively, is used to solve the governing differential equation by finite-difference methods. (The procedure is outlined in ref. 1.) Thus, for every internal grid point (numbered 0) in the flow field, at which points the finite-difference form of the governing equation must be satisfied, a finite-difference star is formed with six adjacent grid points numbered 1 to 6 and spaced $a_1, \ldots, a_6$ distance away.

3.3 Governing differential equation.
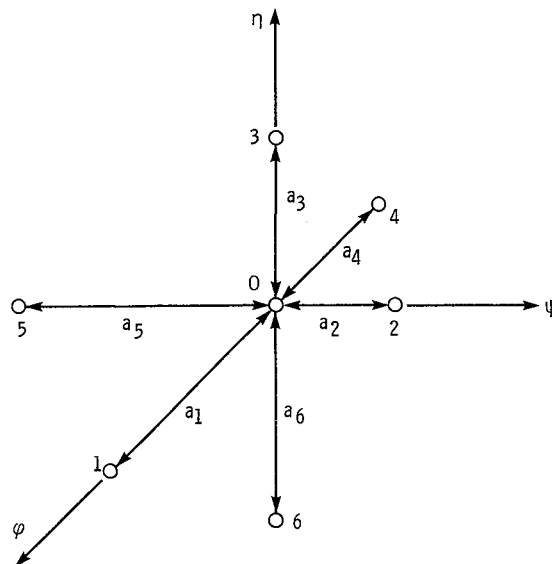
3.3 Governing differential equation. - From page 28 of part I, the governing, second-order, partial-differential equation for the distribution of $\ln q$ in transformed φ, ψ, η space is

$$\frac{\partial^2 \ln q}{\partial \varphi^2} + \frac{\partial^2 \ln \rho}{\partial \varphi^2} + \frac{\partial^2 \ln \sin \Theta}{\partial \varphi^2} - \frac{K_\eta}{q^2} - \frac{K_\psi}{q^2}$$

$$+ B^2 \left(\frac{\partial \ln B}{\partial \psi} \frac{\partial \ln q}{\partial \psi} + \frac{\partial^2 \ln q}{\partial \psi^2} \right) - \frac{\partial \ln B}{\partial \varphi} \left(\frac{\partial \ln q}{\partial \varphi} + \frac{\partial \ln B}{\partial \varphi} \right)$$

$$+ A^2 \left(\frac{\partial \ln A}{\partial \eta} \frac{\partial \ln q}{\partial \eta} + \frac{\partial^2 \ln q}{\partial \eta^2} \right) - \frac{\partial \ln A}{\partial \varphi} \left(\frac{\partial \ln q}{\partial \varphi} + \frac{\partial \ln A}{\partial \varphi} \right) = 0 \qquad (3.3.1)$$

where q is the local velocity expressed as a ratio of the upstream velocity ($q = 1.0$ at the upstream boundary), ρ is the density expressed as a ratio of the upstream static density ($\rho = 1.0$ at the upstream boundary), Θ is the distortion angle, which is the angle of intersection between the ψ and η stream surfaces, as shown by the figure in section 3.1 (at the upstream boundary where the specified grid is rectangular, Θ equals $90°$, i.e., there is no "distortion"), K_ψ and K_η are the total curvatures in x,y,z space of the ψ and η stream surfaces (K_ψ and K_η equal 0 at the upstream boundary), and A and B are the "continuity" parameters defined by (ref. 1)

$$A = \rho \frac{dn}{d\psi} \sin \Theta \qquad (3.3.2)$$

$$B = \rho \frac{dm}{d\eta} \sin \Theta \qquad (3.3.3)$$

(A and B equal 1.0 at the upstream boundary, because there $d\psi = dn$ and $d\eta = dm$.)

In finite-difference form, equation (3.3.1) becomes (ref. 1)

$$C_C + C_1 Q_1 + C_2 Q_2 + C_3 Q_3 + C_4 Q_4 + C_5 Q_5 + C_6 Q_6 - C_0 Q_0 = \mathscr{R} \qquad (3.3.4)$$

where

$$C_C = \frac{\partial^2 \ln \rho}{\partial \varphi^2} + \frac{\partial^2 \ln \sin \Theta}{\partial \varphi^2} - \left(\frac{\partial \ln B}{\partial \varphi}\right)^2 - \left(\frac{\partial \ln A}{\partial \varphi}\right)^2 - \frac{K_\eta + K_\psi}{\exp(2Q_0)}$$

$$C_1 = \frac{a_4}{a_1(a_1 + a_4)} \left(\frac{2}{a_4} - \frac{\partial \ln B}{\partial \varphi} - \frac{\partial \ln A}{\partial \varphi}\right)$$

$$C_2 = \frac{a_5 B^2}{a_2(a_2 + a_5)} \left(\frac{2}{a_5} + \frac{\partial \ln B}{\partial \psi}\right)$$

$$C_3 = \frac{a_6 A^2}{a_3(a_3 + a_6)} \left(\frac{2}{a_6} + \frac{\partial \ln A}{\partial \eta}\right)$$

$$C_4 = \frac{a_1}{a_4(a_1 + a_4)} \left(\frac{2}{a_1} + \frac{\partial \ln B}{\partial \varphi} + \frac{\partial \ln A}{\partial \varphi}\right)$$

$$C_5 = \frac{a_2 B^2}{a_5(a_2 + a_5)} \left(\frac{2}{a_2} - \frac{\partial \ln B}{\partial \psi}\right)$$

$$C_6 = \frac{a_3 A^2}{a_6(a_3 + a_6)} \left(\frac{2}{a_3} - \frac{\partial \ln A}{\partial \eta}\right)$$

$$C_0 = \frac{2}{a_1 a_4} + B^2 \left(\frac{\partial \ln B}{\partial \psi} \frac{a_5 - a_2}{a_2 a_5} + \frac{2}{a_2 a_5}\right) + A^2 \left(\frac{\partial \ln A}{\partial \eta} \frac{a_6 - a_3}{a_3 a_6} + \frac{2}{a_3 a_6}\right)$$
$$- \left(\frac{\partial \ln B}{\partial \varphi} + \frac{\partial \ln A}{\partial \varphi}\right) \left(\frac{a_4 - a_1}{a_1 a_4}\right)$$

(3.3.5)

where Q is $\ln q$, the numerical subscripts refer to the six adjacent grid points in the finite-difference star shown in the second figure of section 3.2, and the residual error $\mathscr{R}$ equals 0 when the governing equation (3.3.1) is satisfied locally. With the coefficients C_C, C_1,...,C_6, C_0 at each internal grid point held constant, equation (3.3.4) is solved globally by changing the values of Q_0 according to standard relaxation procedures. These procedures involve repeated passes (IT counter) through the entire flow field, starting at the upstream boundary, until the maximum value of $\mathscr{R}$ in the entire field is less than the input value of EPSR. This set of calculations, involving fixed values of the coefficients, constitutes one major iteration (ITER counter). The coefficients are then recomputed from the new values of Q_0, and the procedure is repeated until the solution is complete.

3.4 Direction cosines. - With the velocity gradients known from the solution of the governing equation (3.3.1), the nine direction cosines associated with the three unit vectors $\bar{e}_1$, $\bar{e}_2$, and $\bar{e}_3$ (fig. in section 3.1) are obtained from their gradients in the φ direction starting from the upstream boundary. (The boundary is assumed to lie on a y,z plane so that $\cos \alpha_1$, $\cos \beta_2$, and $\cos \gamma_3$ are 1.0 and the other six direction cosines are zero.) For example, the gradients of the direction cosines of the unit vector $\bar{e}_1$, which is in the direction of the velocity vector $\bar{q}$, are obtained (ref. 1) from the components of the irrotationality equation normal to the ψ and η surfaces and from the direction-cosine law

$$\cos^2 \alpha + \cos^2 \beta + \cos^2 \gamma = 1 \qquad (3.4.1)$$

Thus,

$$\frac{\partial \cos \alpha_1}{\partial \varphi} = \frac{\begin{vmatrix} 0 & \cos \beta_1 & \cos \gamma_1 \\ C_1^* & \cos \beta_2 & \cos \gamma_2 \\ C_2^* & \cos \beta_3 & \cos \gamma_3 \end{vmatrix}}{D_1}$$

$$\frac{\partial \cos \beta_1}{\partial \varphi} = \frac{\begin{vmatrix} \cos \alpha_1 & 0 & \cos \gamma_1 \\ \cos \alpha_2 & C_1^* & \cos \gamma_2 \\ \cos \alpha_3 & C_2^* & \cos \gamma_3 \end{vmatrix}}{D_1}$$

$$\frac{\partial \cos \gamma_1}{\partial \varphi} = \frac{\begin{vmatrix} \cos \alpha_1 & \cos \beta_1 & 0 \\ \cos \alpha_2 & \cos \beta_2 & C_1^* \\ \cos \alpha_3 & \cos \beta_3 & C_2^* \end{vmatrix}}{D_1}$$

$$\left.\rule{0pt}{60pt}\right\} \quad (3.4.2)$$

where

$$D_1 = \begin{vmatrix} \cos \alpha_1 & \cos \beta_1 & \cos \gamma_1 \\ \cos \alpha_2 & \cos \beta_2 & \cos \gamma_2 \\ \cos \alpha_3 & \cos \beta_3 & \cos \gamma_3 \end{vmatrix}$$

and

$$C_1^* = B \frac{\partial \ln q}{\partial \psi}$$

$$\text{(3.4.3)}$$

$$C_2^* = A \frac{\partial \ln q}{\partial \eta}$$

$$\text{(3.4.4)}$$

Equations for the gradients of the direction cosines of $\bar{e}_2$ and $\bar{e}_3$ in the φ direction are obtained in part I of this report (ref. 1) in a similar manner. In (the present) part II, however, the expressions for C_3^* and C_4^* (eqs. (22f) and (23f) in part I) have been reformulated, by making use of the continuity equations (16c) and (16d) in reference 1, to give

and

$$C_3^* = \frac{1}{2}\left[\frac{\partial \cos \Theta}{\partial \varphi} - \cos \Theta \left(\frac{\partial \ln A}{\partial \varphi} - \frac{\partial \ln B}{\partial \varphi}\right)\right]$$

$$C_4^* = \frac{1}{2}\left[\frac{\partial \cos \Theta}{\partial \varphi} + \cos \Theta \left(\frac{\partial \ln A}{\partial \varphi} - \frac{\partial \ln B}{\partial \varphi}\right)\right]$$

$$\text{(3.4.5)}$$

Finally, again by making use of the continuity and irrotationality equations in part I, equations can be developed (section 5.2) for the gradients of the direction cosines of the unit vector $\bar{e}_1$ in the ψ and η directions on potential surfaces. These gradients are used in subroutine ANGL (section 5.5).

3.5 Construction of flow field in x,y,z space. - With the velocity distribution known from the solution of equation (3.3.1) in φ,ψ,η space, and with the distribution of the direction cosines likewise known from section 3.4, the shape of the flow field in x,y,z space can be constructed. The boundary of this flow field constitutes the design of the duct.

The construction starts in x,y,z space with the arbitrarily specified shape of the upstream boundary on the y_U, z_U plane at $x_U = 0$, where, for nondimensional variables (as defined in ref. 1), ψ and η equal y_U and z_U, respectively, because the grid is rectangular (but not necessarily square).
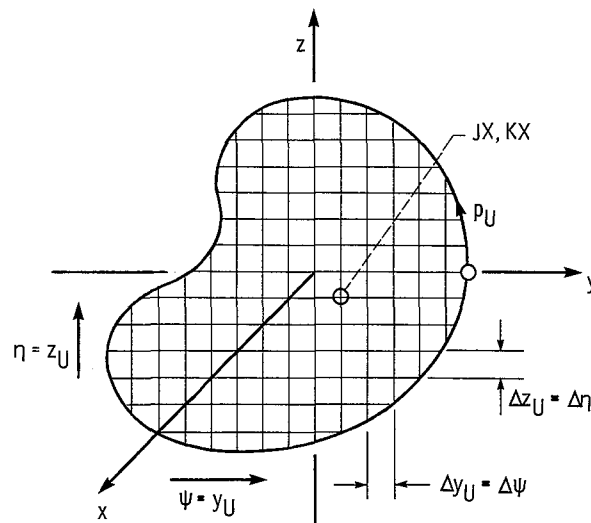
From each intersection of the grid lines in the figure, a streamline (with constant paired values of ψ and η) extends to the downstream boundary. The x,y,z coordinates of the streamline at each successive potential surface (constant φ) are obtained by integrating the following equations (eqs. (26a), (26b), and (26c), ref. 1):

$$x = x_U + \int_0^\varphi \frac{\cos \alpha_1}{q} \, d\varphi \qquad (3.5.1)$$

$$y = y_U + \int_0^\varphi \left(\frac{\cos \beta_1}{q} \right) d\varphi \qquad (3.5.2)$$

and

$$z = z_U + \int_0^\varphi \left(\frac{\cos \gamma_1}{q} \right) d\varphi \qquad (3.5.3)$$

3.6 Alternative construction of flow field in x,y,z space. - An alternative method for constructing the flow field is to select one streamline (designated by the indices JX and KX as shown on the figure in section 3.5), obtained from equations (3.5.1) to (3.5.3), and to use this primary streamline as a backbone from which to obtain the x,y,z coordinates of every grid point on each successive potential surface by integrating the following equations (ref. 1) in the ψ direction on a potential surface,

$$x = x_x + \int_{\psi_x}^\psi \left(\frac{\cos \alpha_2}{qB} \right) d\psi \qquad (3.6.1)$$

$$y = y_x + \int_{\psi_x}^\psi \left(\frac{\cos \beta_2}{qB} \right) d\psi \qquad (3.6.2)$$

and

$$z = z_x + \int_{\psi_x}^\psi \left(\frac{\cos \gamma_2}{qB} \right) d\psi \qquad (3.6.3)$$

and in the η direction on a potential surface,

$$x = x_x + \int_{\eta_x}^\eta \left(\frac{\cos \alpha_3}{qA} \right) d\eta \qquad (3.6.4)$$

$$y = y_x + \int_{\eta_x}^\eta \left(\frac{\cos \beta_3}{qA} \right) d\eta \qquad (3.6.5)$$

11

and

$$z = z_x + \int_{\eta_x}^{\eta} \left(\frac{\cos \gamma_3}{qA} \right) d\eta \qquad (3.6.6)$$

The continuity parameters A and B in equations (3.6.1) to (3.6.6) are computed by the program from equations (3.3.2) and (3.3.3), respectively, by using values of Δn and Δm from the previous iteration.

The location JX, KX of the <u>primary streamline</u> is arbitrary. However, results should be best for locations near the center of gravity of the upstream boundary and should be biased somewhat toward the boundary streamlines with the highest prescribed velocities if the duct bends. For solutions with planar symmetry, the computer program DIN3D1 requires that JX, KX be on the plane of symmetry.

In the program, both methods (sections 3.5 and 3.6) are used to find the x, y, z coordinates. This is further discussed in section 4.7, where the input coefficient CAVP is introduced to allow a weighted average of the two methods. The first method (section 3.5) is used in subroutine VARI (section 5.2), where CAVP also is used, and the second method (section 3.6) appears in subroutine POTS (section 5.16).

4.0 ILL-POSED NATURE OF DESIGN METHOD WHEN APPLIED TO DUCTS

The design method applied to ducts requires two major inputs: (1) the upstream boundary configuration and (2) the velocity distribution on the lateral boundary. The lengths Δs of all streamlines on the boundary are precisely fixed because along each streamline

$$\Delta s = \int_{\varphi_U}^{\varphi_D} \frac{d\varphi}{q} \qquad (4.0.1)$$

where q is a known function of φ from equation (3.0.1) or, alternatively, is specified directly as a function of φ. Thus, for various upstream boundary configurations, which for a uniform (constant) upstream velocity with parallel flow must be plane, it appears unlikely that the downstream potential surface can also be plane with parallel streamlines normal to the surface, as required by the design method. If this is the case, boundary conditions are overprescribed and the design problem is ill posed.

For every prescribed upstream boundary configuration that lies on a flat, potential surface as assumed by the design method (section 7.2), there is an infinity of <u>compatible</u> velocity distributions that could exist on the lateral boundary, because there is an infinity of lateral boundary configurations for any upstream boundary shape. However, this consideration does not rule out the possibility of an infinity of lateral velocity distributions that are <u>not</u> compatible with the prescribed upstream boundary configuration.

Now, for a given duct configuration (completely specified) with upstream and downstream regions extended so that the upstream and downstream boundaries are flat potential surfaces, as assumed by the design method, a specific velocity distribution exists throughout the flow field and in particular on the lateral boundary. Presumably, this velocity distribution is unique to this duct shape (e.g., pp. 14 to 41, ref. 2); it then follows

12

that for a given lateral velocity distribution there is a unique upstream boundary config-
uration. Thus, although for a given upstream boundary an infinity of lateral velocity
distributions exists, as discussed in the previous paragraph, for a given lateral velocity
distribution there is only one compatible upstream area configuration. It is concluded
that the general design method when applied to ducts is ill posed because the boundary
conditions are overprescribed. However, fortunately, there are "degrees of incompati-
bility," as considered in the next section.

4.1 Compatibility between prescribed upstream boundary configuration and lateral
velocity distribution. - For a given lateral velocity distribution, some upstream boundary
configurations are less compatible than others. For example, a stellated upstream con-
figuration such as
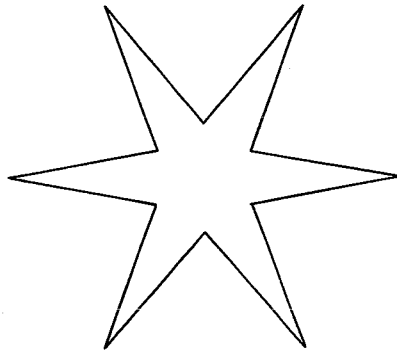
would be "highly incompatible" with a lateral velocity distribution corresponding to the
flow through an elbow of constant, circular cross section. An elliptical upstream con-
figuration with moderate aspect ratio should be "highly compatible" with such a lateral
velocity distribution.

Program DIN3D1 has been so constructed that stream-tube areas are adjusted to
local velocities (by means of the continuity parameters A and B; section 4.2 (con-
straint 6)), so that, unless the upstream boundary configuration is "highly incompatible,"
the continuity condition is essentially satisfied (the downstream-area error is
printed) for each of a relatively large number of major iterations (ITER; end of
section 3.3). The solution at first converges for each successive major iteration (as evi-
denced by decreasing maximum $\mathcal{R}$ in the flow field). Eventually, because boundary
conditions are overspecified, the solution must diverge and fail. For "highly incompatible"
upstream boundary configurations, divergence is rapid and occurs after only a few major
(ITER) iterations. For "highly compatible" cases, divergence is gradual and occurs only
after many iterations. Thus, excellent approximate solutions are obtained by stopping the
calculations before, or shortly after, divergence begins (section 4.4).

Finally, the program includes options (IVEL equals 2 or 3) for lateral velocity dis-
tributions that tend toward compatibility with the prescribed upstream boundary config-
uration. These "equilibrium" velocity distributions are based on the velocity distribution
in ducts of constant cross section and very large turning angle. Under these conditions,
near the middle of the turn, the velocity distribution on potential surfaces becomes a free
vortex (qr = constant) with r measured from the axis of the turn. A lateral velocity
distribution around the periphery of each potential surface, based on this free-vortex
distribution, and with r related to the upstream surface configuration, constitutes the
"equilibrium" velocity distribution on the lateral boundary (appendix A).

13

4.2 Constraints on calculation procedure. – Because of the ill-posed nature of the method when applied to ducts, it is beneficial to guide the calculations by imposing the following six constraints, all of which would be satisfied automatically in a well-posed case:

(1) The x,y,z coordinates of every internal grid point in the flow field are computed by two methods (sections 3.5 and 3.6), and the results are averaged according to the input value of CAVP, the decimal fraction of the first method that enters into the weighted average. Thus,

$$0.0 \leq CAVP \leq 1.0 \tag{4.2.1}$$

Although the optimum value of CAVP probably varies with the complexity of the upstream boundary configuration and with the lateral velocity distribution, a value of 0.5 is generally satisfactory (also see section 4.6).

(2) During the iterative calculations, values of the direction cosines computed from their gradients (eqs. (3.4.2), e.g.) can become greater than 1.0. If this occurs, the value is set equal to 1.0 by the program.

(3) Also, during the iterative calculations, the sum of the squares of the direction cosines may not equal 1.0, as required by equation (3.4.1). When this occurs, the program changes each cosine value by a factor k, where

$$k = \frac{1}{\left(\cos^2\alpha + \cos^2\beta + \cos^2\gamma\right)^{1/2}} \tag{4.2.2}$$

(4) At every interior grid point, the unit vector $\bar{e}_2$, which is tangent to the intersection of the η stream surface and the velocity potential surface φ, must be normal to the unit vector $\bar{e}_1$, which is in the direction of the velocity (fig. in section 3.1). Thus,

$$\bar{e}_1 \cdot \bar{e}_2 = 0 \tag{4.2.3}$$

or

$$\cos\alpha_1 \cos\alpha_2 + \cos\beta_1 \cos\beta_2 + \cos\gamma_1 \cos\gamma_2 = 0 \tag{4.2.4}$$

When this relation is not so, the direction cosines of $\bar{e}_2$ are changed by the program so that $\bar{e}_2$ becomes normal to $\bar{e}_1$ and the plane of $\bar{e}_1$ and $\bar{e}_2$ remains unchanged. This same "normality" condition is imposed on the direction cosines of the unit vector $\bar{e}_3$ in the same figure. (Also, see appendix B.)

(5) Also, from the figure in section 3.1,

$$\bar{e}_2 \cdot \bar{e}_3 = \cos\Theta \tag{4.2.5}$$

from which

$$\cos\Theta = \cos\alpha_2 \cos\alpha_3 + \cos\beta_2 \cos\beta_3 + \cos\gamma_2 \cos\gamma_3 \tag{4.2.6}$$

14

From the following figure, which shows a stream tube bounded by adjacent surfaces of
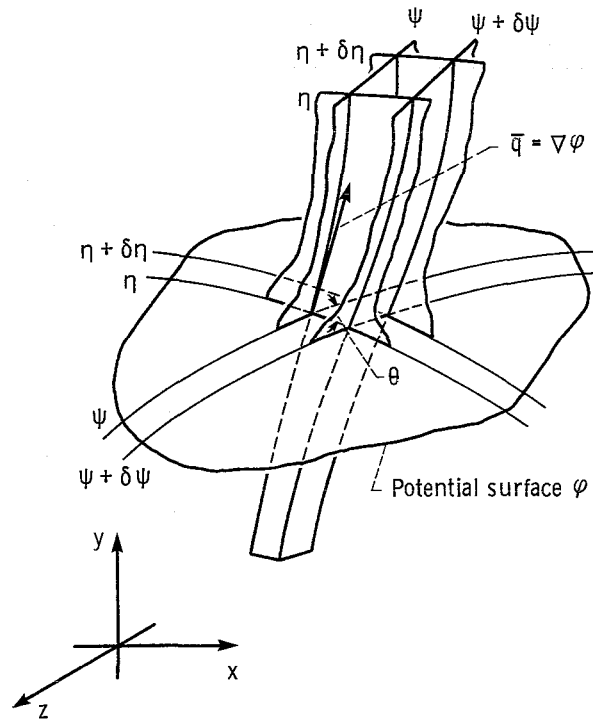
constant ψ and η, the value of Θ must be greater than $0.0°$ and less than $180.0°$; otherwise the stream-tube area becomes zero or negative. Thus, if from equation (4.2.6) the absolute value of $\cos \Theta$ is greater than 0.9962, the program sets $\cos \Theta$ equal to ± 0.9962 so that the "distortion" angle Θ lies in the range

$$5° \leq \Theta \leq 175° \qquad (4.2.7)$$

(6) Finally, the values of the continuity parameters A and B, as computed by equations (3.3.2) and (3.3.3), respectively, are changed by the same factor k so that the following continuity condition (eq. (10d), ref. 1) is satisfied:

$$AB = \frac{\rho \sin \Theta}{q} \qquad (4.2.8)$$

from which

$$k = \sqrt{\frac{\rho \sin \Theta}{qAB}} \qquad (4.2.9)$$

4.3 Mode of failure. - For those cases where total failure of the solution is approached after a sufficiently large number of major iterations (ITER), which number depends on the compatibility condition discussed in a previous section, 4.1, this failure usually occurs in the downstream region. Here the flow field in x,y,z space distorts as shown by the following examples.
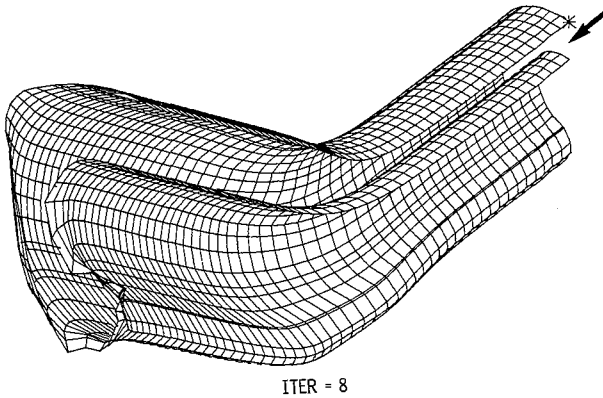
ITER = 8
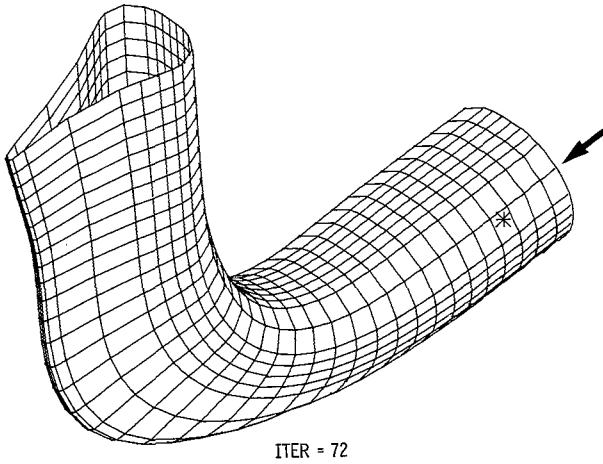
ITER = 72
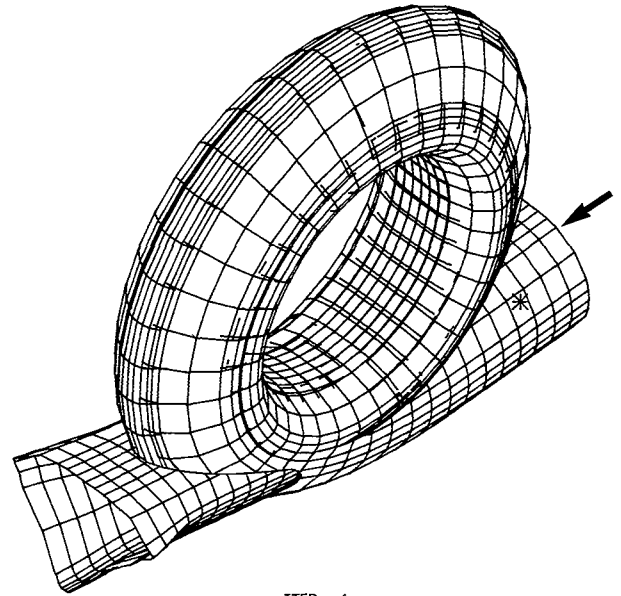
ITER = 6

The lateral surfaces diverge, and the "distortion" angle Θ (constraint (5), section 4.2) may vary rapidly and greatly from its initially undistorted value of 90° at the upstream boundary (fig. in section 3.5). All of these distortions result from an accumulation of unreal values of ln q near the downstream boundary. This accumulation appears to result from the relaxation procedure, which always starts at the upstream boundary and marches through to the exit, continually pushing the effects of the ill-posed problem toward the downstream boundary. The constraints discussed in section 4.2 maintain an apparently well-behaved flow field elsewhere. (In section 4.8 the distortion near the downstream boundary is found to be essentially independent of the extent of the downstream region, supporting the preceding reasoning.)

   4.4 Input option ISOLV. - As stated in section 4.1, excellent approximate solutions can be obtained for prescribed upstream boundary configurations and lateral velocity distributions that are moderately compatible. These solutions are achieved by stopping the calculations before or shortly after divergence begins. Input option ISOLV = 1 assumes that, because of the constraints discussed in section 4.2, an adequately converged solution is achieved after four or more major iterations (ITER), provided that the error in exit flow area, expressed as a decimal fraction, is less than 0.0033. Also, for ISOLV = 1, if these criteria are not met, the calculations are then stopped and the solution is printed out when the computed value of exit-area error changes sign - provided that the value of ITER is greater than 8. In this latter case, the solution may not be acceptable if the exit-area error (intermediate printout) is changing rapidly as the result of impending

failure. If none of the criteria are met, the solution continues until the number of major iterations equals the input value of ITERMX or until the solution fails entirely.

For an input value of ISOLV = 0, the solution continues until (1) the number of major iterations (ITER) equals the input value of ITERMX, (2) provided that ITER > 4, the maximum value of $\mathcal{R}$ (eq. (3.3.4)) in the entire flow field at the beginning of a major iteration is less than or equal to 0.0020, or (3) the solution fails.

4.5 Effect of ITER on solution. - Because of the ill-posed nature of the design method when applied to ducts, all examples must eventually fail (with rare exceptions in simple cases) as the number of major iterations (ITER) increases indefinitely. Thus, as shown, the solution changes with ITER. The changes are most pronounced in the

ITER = 4   ITER = 12   ITER = 24

ITER = 48   ITER = 72
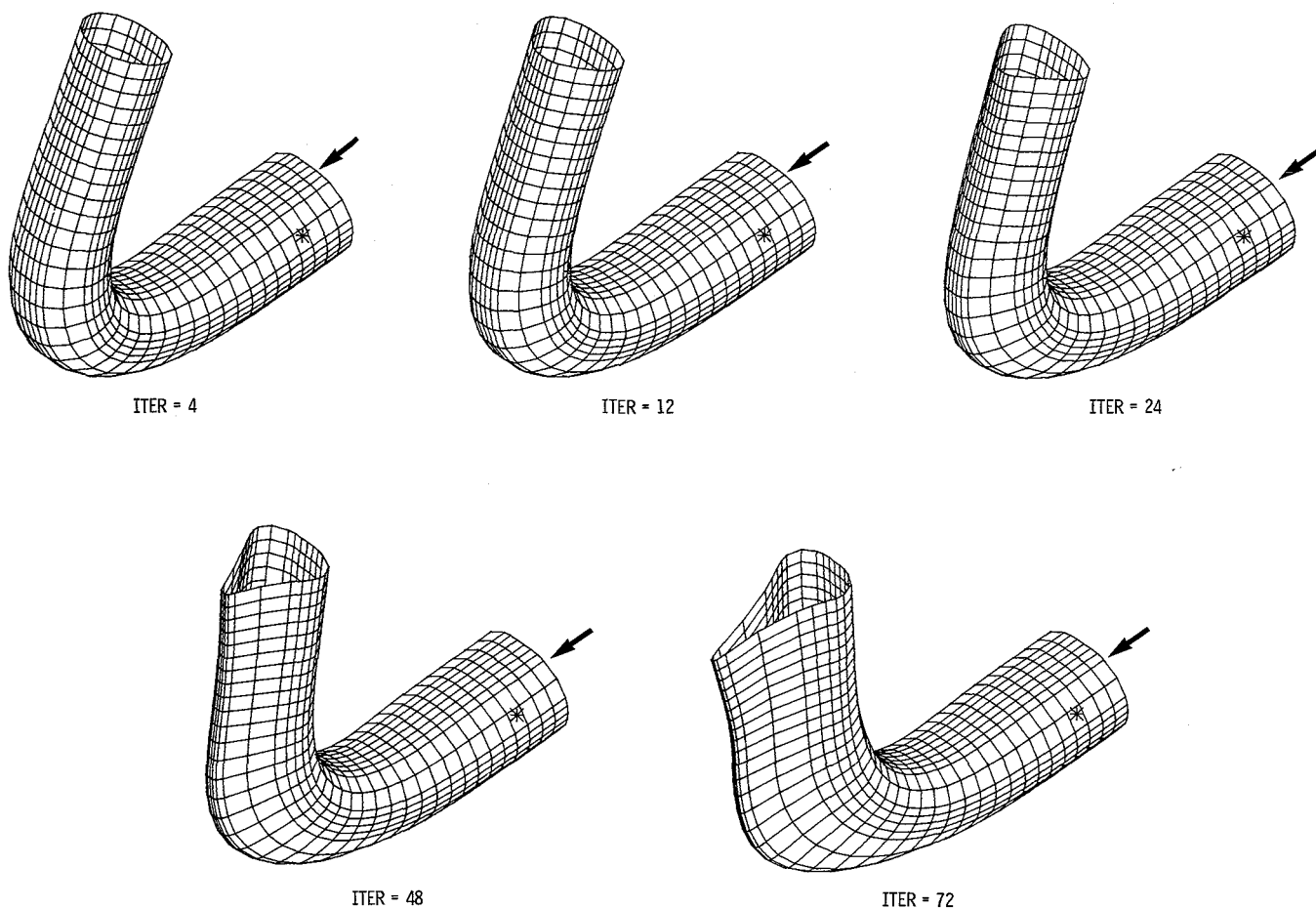
downstream-area configuration and to a lesser degree in the turning angle of the duct. It is suggested that, because the exit velocity is normal to the downstream boundary and therefore not influenced by its shape, large changes in the exit-area configuration can result from only minor changes in the lateral velocity distribution (appendix C). Likewise, for the same lateral velocity distribution during an approximate solution, small changes in the downstream boundary shape (but not in its area) can be expected from one major iteration (ITER) to the next. Because for the larger values of ITER the solution is approaching failure, the lower values of ITER are believed to give better approximate solutions. For ISOLV = 1, the solution is stopped at ITER = 4, provided certain criteria are met (section 4.4).

17

4.6 Effect of CAVP on solution. - In sections 3.5 and 3.6, two methods are discussed for computing the coordinates of the flow field in physical x,y,z space. The first method (section 3.5), which results in correct streamline lengths, determines x, y, and z by integrating along streamlines between adjacent potential surfaces. (For this method, the streamline lengths are correct, but the continuity condition may not be satisfied because of the ill-posed nature of the problem and its forced solution.) The second method (section 3.6), for which continuity is satisfied, starts from the "primary" streamline location (JX,KX; fig. in section 3.5) and determines the coordinates by integrating in the ψ and η directions on potential surfaces. (For this method, the continuity condition is satisfied by the essentially correct values of the continuity parameters A and B, but the streamline lengths may not be correct.) When moving from one potential surface to the next, these two sets of x,y,z coordinates are averaged by the input value of CAVP, which is the decimal fraction of the first set that enters into the weighted average of the two sets. As shown in the following figures, the effect of

CAVP = 0.0

CAVP = 0.2

CAVP = 0.4

CAVP = 0.6

CAVP = 0.8

CAVP = 1.0

18
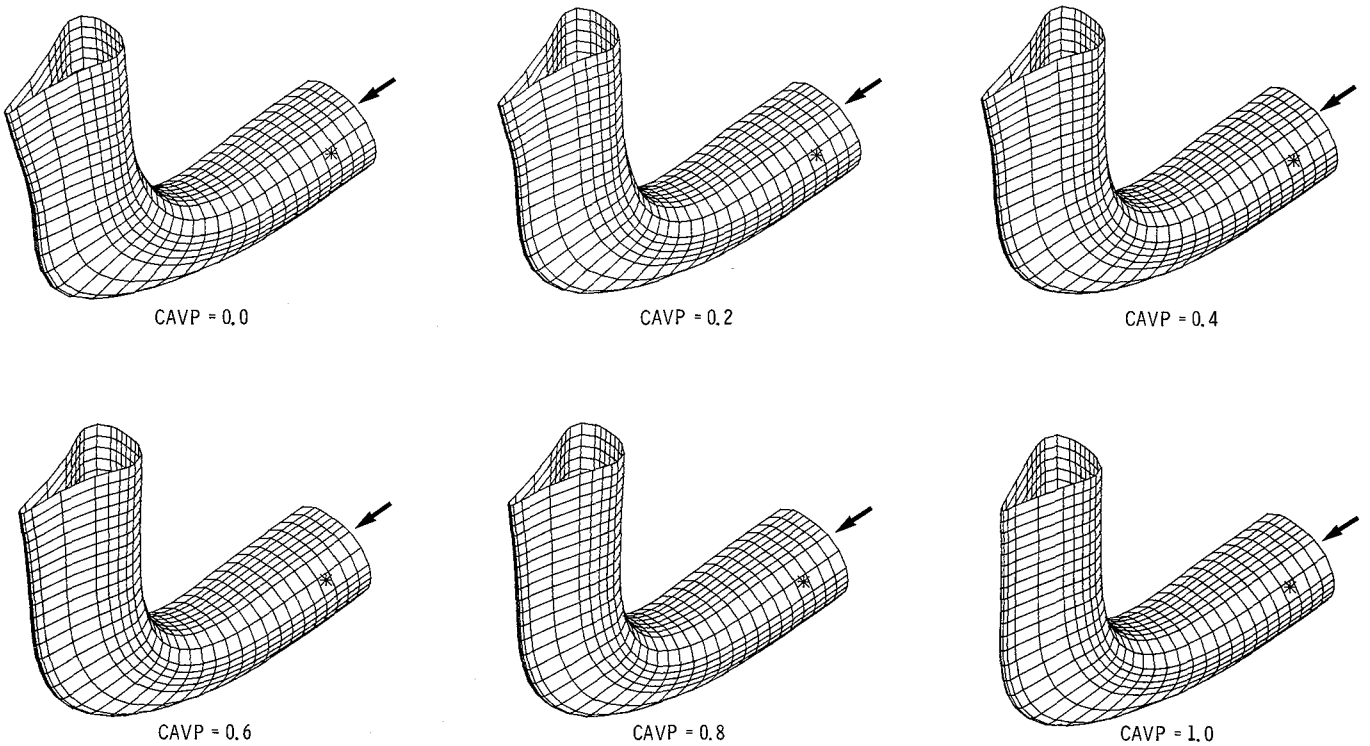
CAVP on the solution for ITER = 72 is to go from the case where streamlines are normal to the downstream potential surface but not parallel with each other (CAVP = 0.0) to the case where the streamlines are parallel but not normal to the potential surface (CAVP = 1.0). A clearer picture of the difference is given by two side views:

CAVP = 0.0

CAVP = 1.0
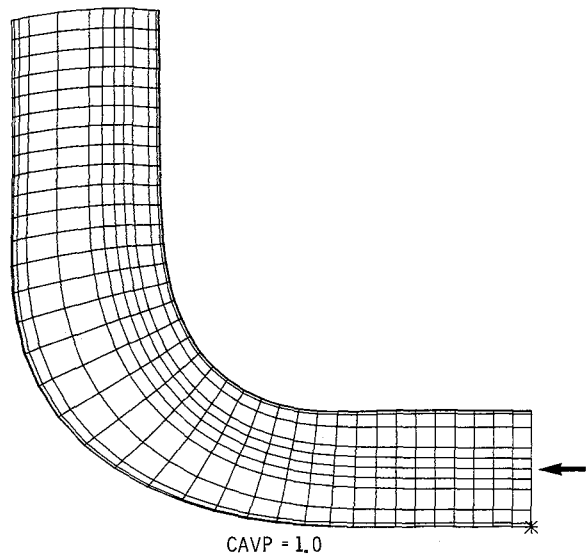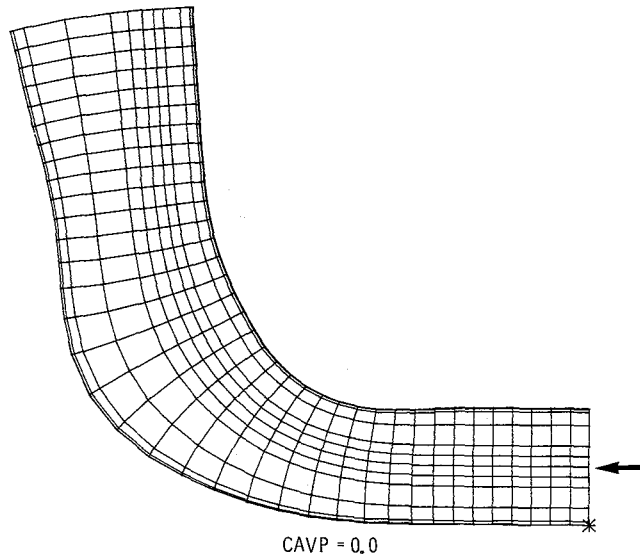
For less extreme examples (ITER << 72), the two methods of computing the x,y,z coordinates should give more nearly equal results, and a value of 0.5 for CAVP should usually be satisfactory. For more complex upstream boundary configurations and for problems involving less compatibility between the upstream boundary shape and the pre-

scribed lateral velocity distribution, where the solution starts to diverge at relatively low values of ITER, a better input value for CAVP might be as low as 0.2. However, in some cases, because of the numerical integration procedure used by the second method (section 3.6) on the potential surface, the duct wall may develop slightly rippled regions. The ripples can be reduced by increasing the input value of CAVP or eliminated by setting CAVP equal to 1.0.

4.7 Effect of duct turning angle on solution. - As might be expected, the greater the duct turning angle $\Delta\Theta$, the lower the value of ITER at which the solution begins to diverge. Or, as a corollary, for the same value of ITER, other things being equal, the greater $\Delta\Theta$, the greater the distortion (if any) near the downstream boundary, as shown by the following figures:

$\Delta\theta \approx 420^0$

$\Delta\theta \approx 720^0$

20
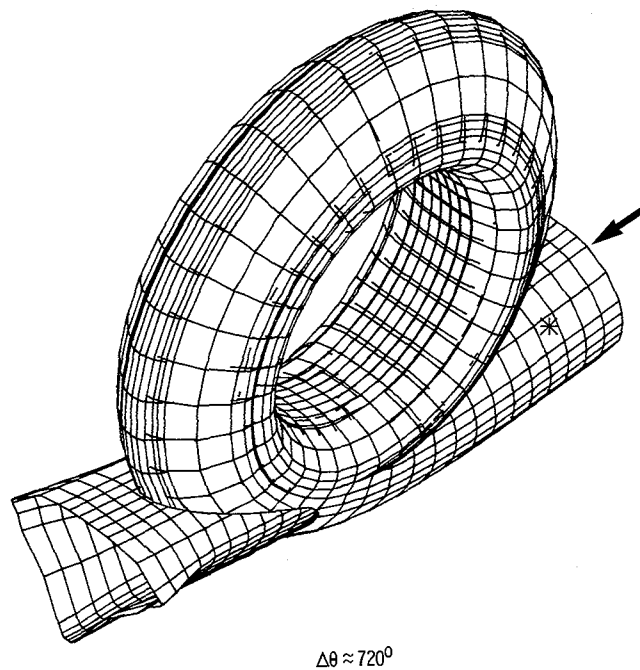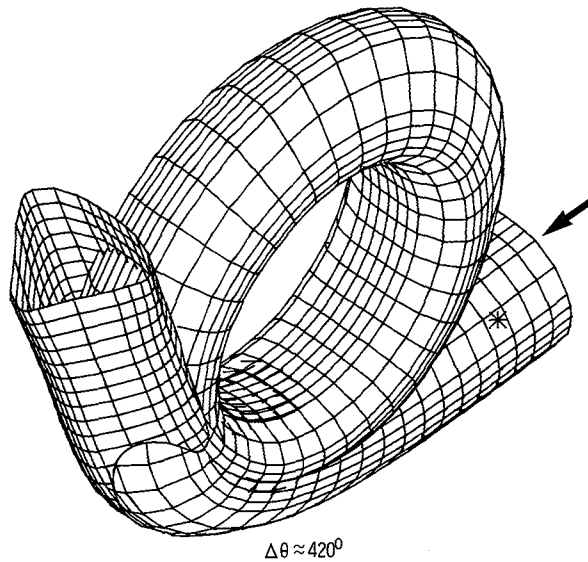
4.8 Effect of extent of downstream region on solution. - The downstream region is
that part of the duct near the downstream boundary where the lateral velocity is constant
and equal to its value at the downstream boundary. Because solutions apparently start to
diverge and distort near the downstream boundary, a question arises as to whether the
extent of the downstream region influences the magnitude and type of this distortion. As
the following figures indicate, the distortion is apparently not influenced appreciably by
the extent of the downstream region. This observation supports the discussion in
section 4.3 regarding the mode of failure, in program DIN3D1, for ill-posed problems.

Short exit   Extended exit
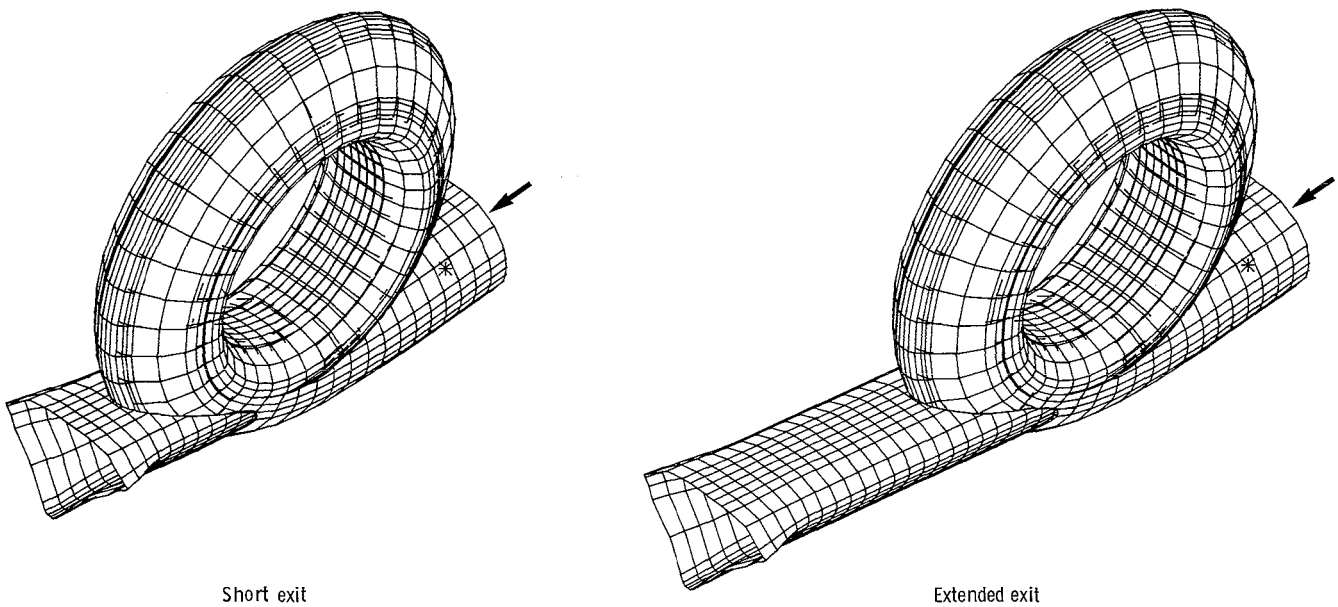
4.9 Effect of complexity of upstream boundary configuration on solution. - Exam-
ples of solutions with simple upstream boundary configurations and others with relatively
complex configurations are given by the figures on the next page. Solutions for complex
configurations require special care in prescribing lateral velocity distributions. Simple
upstream configurations involve no particular difficulty.

4.10 Remarks. - In concluding this major section on the ill-posed nature of the
general design method when applied to ducts, it is noted that the method is not ill posed
when applied to the external design problem (i.e., to the design of bodies with prescribed
velocities in infinite space). In this case, the velocity on the outer boundaries is every-
where constant, provided only that the upstream and downstream boundaries, which can
have any suitable shape (e.g., circular), are sufficiently large. This situation eliminates
the compatibility problem between prescribed boundary configuration and prescribed
velocity distribution, but other problems, such as body closure, remain.

Thus far, it has been implied that the general design method when applied to ducts
becomes well posed if the upstream boundary configuration is not specified. Under this
circumstance, it is not clear how, and may not even be possible, to carry out a practical
design procedure. Nor does it appear desirable, because the designer usually needs to
retain control over the upstream boundary configuration (which, by reversing the direction
of flow, becomes the downstream configuration, assuming that configuration needs to be
controlled).
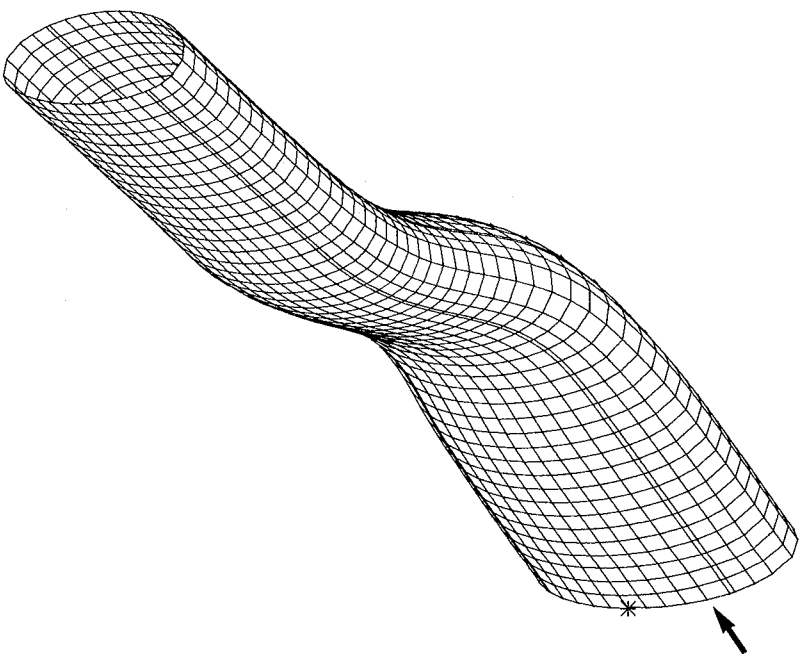
Simple (ellipse)
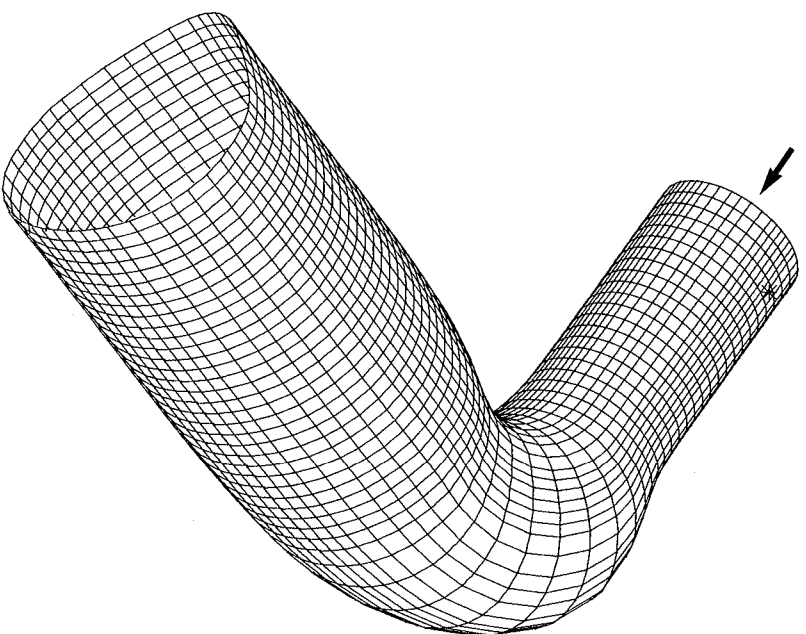
Simple (circle)
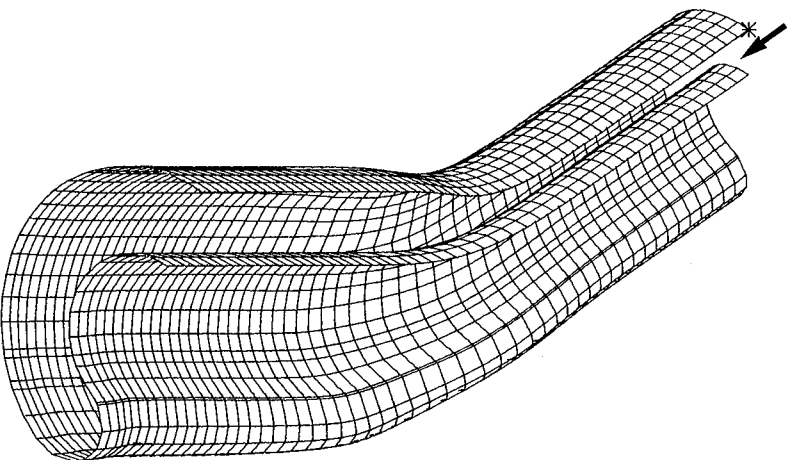
Complex (semiannulus)

Complex (general)

22
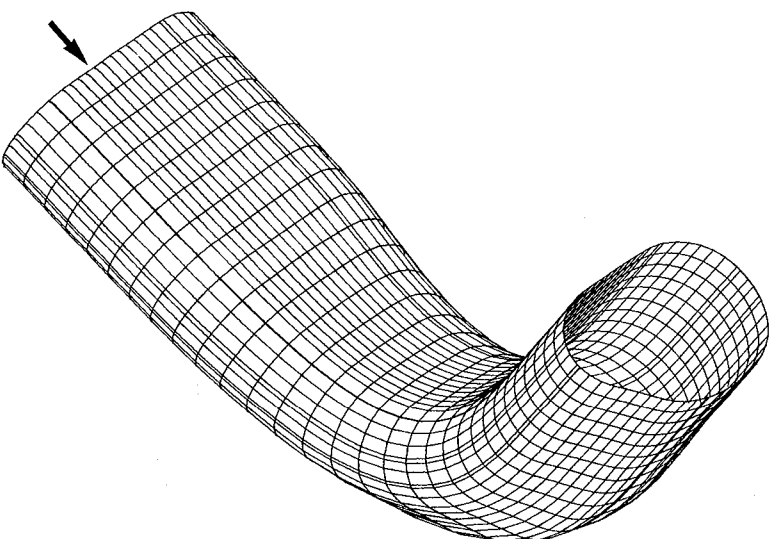
The difficulty of the three-dimensional duct design problem is further increased by the likelihood that, irrespective of the upstream boundary configuration, and unlike the two-dimensional case, proper solutions do not exist for every lateral velocity distribution. The situation is considered in more detail in appendix C.

5.0 BRIEF DESCRIPTION OF COMPUTER PROGRAM DIN3D1

Program DIN3D1 is written in standard Fortran IV. Double precision is required for computers with 32-bit words. In addition to the main program, there are 21 major sub-routines, 3 minor subroutines, and 8 external functions. The main program and the major subroutines are briefly described in this section.

5.1 Main program. - The main program governs the solution, as shown on the simplified flowchart. The integer I designates a potential surface, starting with 1 at the upstream boundary and ending with NI at the downstream boundary; the integer IT counts the number of passes through the entire flow field (I = 2 to I = NI - 1 = NI1), all with the same global set of coefficients in the finite-difference equation (3.3.4); and the integer ITER counts the number of major iterations, each with an improved set of coefficients determined from the previous major iteration.
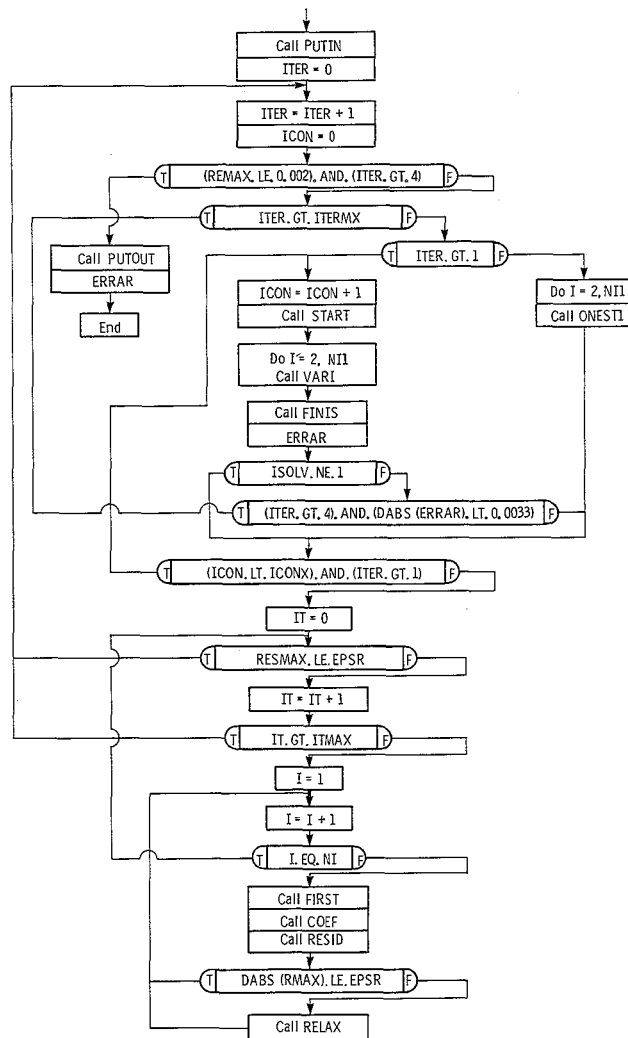
Simplified flowchart of main program

In general, the design procedure in program DIN3D1 is as outlined under Numerical Procedure on pages 56 and 57 in part I (ref. 1) of this report. The overall approach is to solve (in subroutine RELAX) the finite-difference form of the governing differential equation (3.3.4) everywhere on one potential surface at a time, starting at $I = 2$ (the first surface downstream from the upstream boundary) and marching through the entire flow field to $I = NI1$. This procedure is continued (counter IT), with the same global set of coefficients in the finite-difference equation (3.3.4), until the maximum residual error RESMAX (flowchart) encountered anywhere in the flow field is less than the input value of EPSR, or until IT equals the input value of ITMAX. At this point, a new set of coefficients is generated (in subroutine COEF, by using major parameters determined in subroutine VARI); the error (ERRAR) in the downstream boundary area (expressed as a decimal fraction of the correct value) is computed (flowchart); and the procedure is repeated. This process is continued (counter ITER) until the maximum residual error REMAX (flowchart) encountered anywhere in the flow field on the first pass with a new set of coefficients is less than 0.002 (provided ITER > 4), or until the value of ITER is equal to the input value of ITERMX (flowchart). This concludes the solution of the governing equation (3.3.4), which, as indicated on the flowchart, may also be concluded sooner if the input value of ISOLV is equal to 1 (section 4.4).

The flowchart for the main program involves 10 (of 21) major external subroutines. These are described shortly.

5.1.1 Input ICONX. - In the main program, to achieve better accuracy and to speed up the solution, the new global set of coefficients (for the governing equation) calculated after each major iteration (ITER) is iterated (counter ICON). This iteration is continued until ICON is equal to the input value of ICONX (flowchart). However, to further shorten the solution time, the value of ICONX is reduced by 1 after every seven major iterations (ITER) until a minimum value of 3 is attained, after which ICONX remains constant. (If the input value of ICONX is less than 3, it is changed to 3 in the main program and remains constant.)

5.2 Subroutine VARI. - Except for the main program, subroutine VARI is the most important routine in program DIN3D1. After each major iteration (ITER counter in main program), this subroutine determines, at every grid point in the flow field, the direction cosines of the unit vectors $\bar{e}_1$, $\bar{e}_2$, and $\bar{e}_3$ (section 3.4); the x, y, and z coordinates (section 3.5); and the parameters A, B, and Θ and the coefficient C_C (sections 3.3 and 4.2 (constraint 5)). The procedure is outlined in the simplified flowchart. In general, this procedure is as outlined in part I of this report (pp. 56 and 57, ref. 1). For a given potential surface I, the overall approach in subroutine VARI is to compute the direction cosines of the unit vectors $\bar{e}_1$, $\bar{e}_2$, and $\bar{e}_3$ on potential surface $I + 1$ from their known values on potential surface I and from their derivatives with respect to φ on both the I and $I + 1$ surfaces, as given by equation (3.4.2), for example. Because the derivatives of the direction cosines on surface $I + 1$ depend on the direction cosines themselves, the procedure is iterated three times (IT2.EQ.3, flowchart). Afterward (IT1.GT.1, flowchart) the direction cosines of the unit vector $\bar{e}_1$ are determined in subroutine ANGL (flowchart) by a new method based on their known values at the primary streamline location (specified by the input values of JX and KX; section 3.6 and fig. in section 3.5) on potential surface $I + 1$ and from their derivatives with respect to ψ and η.
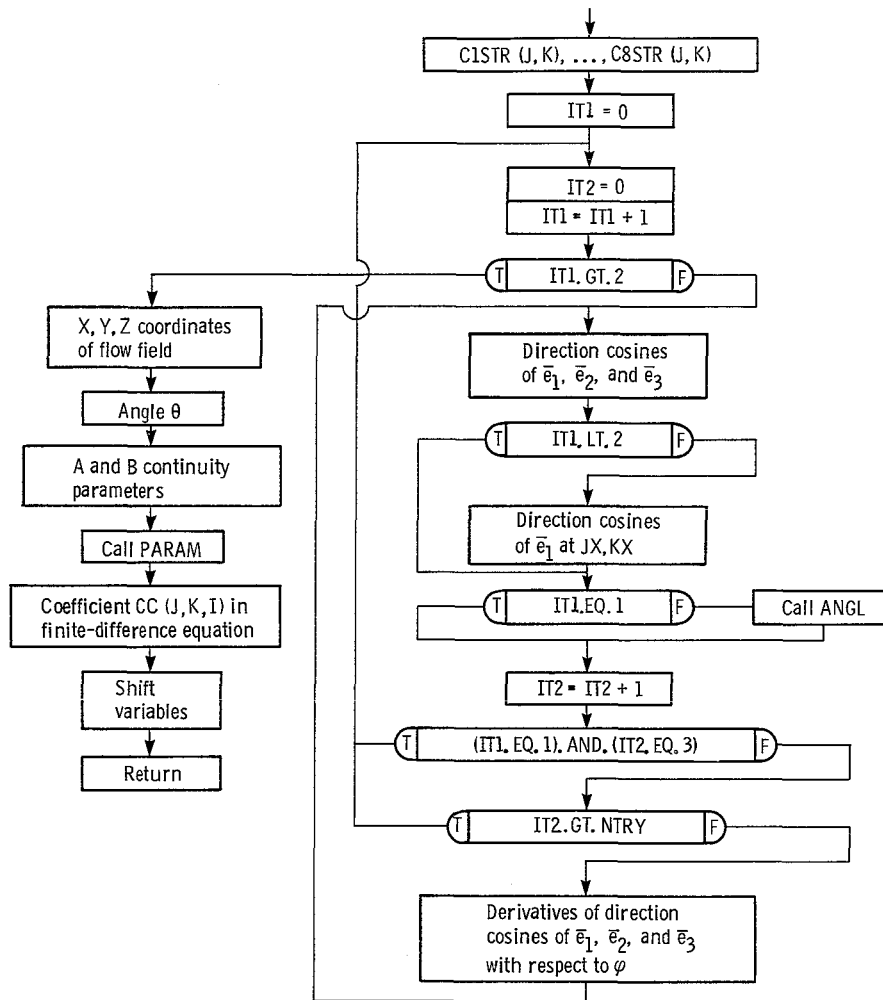
Simplified flowchart of subroutine VARI

These ψ and η derivatives of the three direction cosines of $\overline{e}_1$ are obtained by the following procedure. The derivatives with respect to ψ are obtained from the simultaneous solution of the following three equations: (1) the ψ derivative of the direction-cosine law (eq. (3.4.1)), (2) the continuity equation (16c) from reference 1, and (3) the equation (5.2.1). This equation is obtained by adding the irrotationality equations (14c) and (14d) from reference 1 to obtain $\partial \cos \Theta / \partial \varphi$, after which equations (13g), (16c), and (16d), also from reference 1, are introduced to give

$$\overline{e}_3 \cdot \frac{\partial \overline{e}_1}{\partial \psi} = \frac{1}{2B} \left[\frac{\partial \cos \Theta}{\partial \varphi} - \cos \Theta \left(2 \frac{\partial \ln q}{\partial \varphi} + \frac{\partial \ln A}{\partial \varphi} + \frac{\partial \ln B}{\partial \varphi} \right) \right] \qquad (5.2.1)$$

In a similar fashion, the derivatives with respect to η are obtained from (1) the direction-cosine law, (2) the continuity equation (16d), and (3) equation (5.2.1) combined with equation (13g) from reference 1 to give

$$\bar{e}_2 \cdot \frac{\partial \bar{e}_1}{\partial \eta} = \frac{1}{2A} \left[\frac{\partial \cos \Theta}{\partial \varphi} - \cos \Theta \left(2 \frac{\partial \ln q}{\partial \varphi} + \frac{\partial \ln A}{\partial \varphi} + \frac{\partial \ln B}{\partial \varphi} \right) \right] \qquad (5.2.2)$$

This new method for finding the direction cosines of $\bar{e}_1$ is needed to achieve truly parallel flow in the downstream boundary region. Using this method in subroutine ANGL, the procedure (in subroutine VARI) is to iterate NTRY additional times (where, if the input value of NTRY is less than 2, the program sets NTRY equal to 2).

Finally, as shown in the flowchart, subroutine VARI determines the x,y,z coordinates of the physical flow field (sections 3.5 and 3.6), the distortion angle Θ (section 4.2 (constraint 5)), the continuity parameters A and B (section 4.2 (constraint 6)), and the coefficient C_C, which is required by the finite-difference equation (3.3.4).

Subroutine VARI is called from the main program (section 5.1) and from subroutine PUTOUT (section 5.18).

5.2.1 ICX, ICY, and ITH counters. - If the three simultaneous equations (e.g., eq. (3.4.2)) for the derivatives of the three direction cosines of each of the unit vectors $\bar{e}_1$, $\bar{e}_2$, or $\bar{e}_3$ are not independent, their determinant D will become zero. Thus, in subroutine VARI, if $-0.00001 < D < 0.00001$, D is set equal to ± 0.00001, and the counter ICX is increased by 1. (This condition can occur when the solution is diverging, and failure usually occurs soon after.) If, for a given potential surface I, the value of ICX is greater than zero, a CAUTION note appears in the intermediate printout, or if the value is greater than 10, another note appears and the solution is stopped.

If the absolute value of any direction cosine, obtained in subroutine VARI from the derivatives of the three direction cosines, is greater than 1.0, that value is changed to ± 1.0, and the counter ICY is increased by 1. If, for a given potential surface I, the value of ICY is greater than zero, a CAUTION note appears in the intermediate printout. If the value is greater than 10, another note appears and the solution is stopped.

Also, in subroutine VARI, the "distortion" angle Θ is constrained to values between 5° and 175° (section 4.2 (constraint 5)). If Θ is less than 5° or greater than 175°, $\cos \Theta$ is set equal to 0.9962, and the counter ITH is increased by 1. If, for a given potential surface I, the value of ITH is greater than zero, a CAUTION note appears in the intermediate printout. If the value is greater than 10, another note appears and the solution is stopped.

5.2.2 Averaging coefficients CAVD, CAVN, CAVX, CAVY, and CAVZ. - In subroutine VARI, during the iterations involving direction cosines and their derivatives, the new values are averaged with the previous values by the input values of CAVX and CAVD, respectively, where CAVX and CAVD are the decimal fractions of the previous (old) values entering into the weighted average.

Likewise, the input values of CAVN, CAVY, and CAVZ are the decimal fractions of the previous values of the continuity parameters A and B, the coefficient C_C (eq. (3.3.4)), and the cosine of the "distortion" angle Θ, respectively, that enter into the weighted average with the respective new values.

For design problems involving lateral velocity distributions to achieve the desired shapes of the downstream boundary, the input value of CAVN can be as as low as 0.0, and certainly no higher than 0.1. In effect, the new values of A and B are not averaged with the previous values.

5.3 Subroutine AERIA. - Given the incremental lengths S1, ..., S6, shown in the figure, subroutine AERIA determines the incremental area DAREA of an incremental,
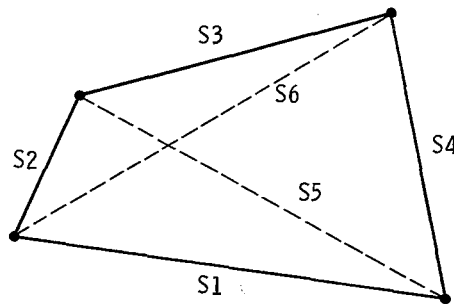
curved surface bounded by four, essentially straight, incremental lines. The area is divided into two sets of triangles by S5 and S6. For each of these four triangles

$$\Delta A = [s\,(s-a)(s-b)(s-c)]^{1/2} \tag{5.3.1}$$

where

$$s = \frac{a+b+c}{2} \tag{5.3.2}$$

Thus, s is the semiperimeter of the triangle, and a, b, and c are the lengths of its three sides. Subroutine AERIA is called from subroutine ERIA, where it is used to compute the area of potential surfaces. Starting with subroutine AERIA, the subroutines are discussed in alphabetical order.

5.4 Subroutine AKA. - Subroutine AKA assures that the sum of the direction cosines squared is equal to 1.0. (section 4.2 (constraint 3)). Subroutine AKA is called from subroutines ANGL, FINIS, and VARI.

5.5 Subroutine ANGL. - On potential surface I + 1, subroutine ANGL determines the distribution of the direction cosines of $\bar{e}_1$, starting from the location of the primary streamline (input values of JX and KX) and integrating along lines of constant ψ and η (eqs. (5.2.1) and (5.2.2)). Subroutine ANGL is called from subroutine VARI.

5.6 Subroutine BOUND. - The physical x,y,z coordinates of the flow field at all interior grid points are determined by subroutine VARI. Using these values on a given potential surface I, subroutine BOUND extrapolates to determine the coordinates XB, YB, and ZB (and the velocity QB) at every contour point along the boundary of the potential surface. Subroutine BOUND is called from subroutine PUTOUT.

5.7 Subroutine COEF. - On potential surface I, subroutine COEF determines the values of the coefficients C0, C1, C2, etc., in the finite-difference form of the governing differential equation (3.3.4). Subroutine COEF is called from the main program.

5.8 Subroutine ENGL. - On potential surface $I + 1$, subroutine ENGL determines the ψ and η derivatives of the direction cosines of $\bar{e}_1$. These derivatives are required to obtain the direction cosines of $\bar{e}_1$. Subroutine ENGL is called from subroutine ANGL.

5.9 Subroutine ERIA. - On potential surface I, subroutine ERIA computes the flow area (dimensional) of the potential surface. Subroutine ERIA is called from subroutine FINIS.

5.10 Subroutine FINIS. - Starting at potential surface $NI - 1$, subroutine FINIS determines the values of A, B, THET, and C_C, and of the x,y,z coordinates at every internal grid point on the downstream potential surface NI. This subroutine assumes that at the downstream boundary the φ derivatives of all direction cosines are zero. Subroutine FINIS obtains the downstream flow area at $NI - 1$ by calling subroutine ERIA. Subroutine FINIS is called from the main program and from subroutine PUTOUT.

5.11 Subroutine FIRST. - On potential surface I, subroutine FIRST establishes the values of the variables appearing in the coefficients (eqs. (3.3.5)) of the finite-difference form of the governing differential equation (3.3.5). Subroutine FIRST is called from the main program.

5.12 Subroutine FLAR. - Subroutine FLAR computes the sum (EXFLAR) of all incremental flow areas bounded by four internal grid points on potential surface I. Subroutine FLAR is called from subroutine ERIA, which adds to the value of EXFLAR all of the incremental areas adjacent to the potential surface contour.

5.13 Subroutine GRID. - Subroutine GRID determines the area of the upstream boundary surface and the distance P around its contour. This subroutine also determines the grid spacings a_2, a_3, a_5, and a_6 (second fig. in section 3.2) on the potential surfaces. Further details regarding the potential surface grid are given in section 7.1 of this report. Subroutine GRID is called from subroutine PUTIN.

5.14 Subroutine ONEST1. - On potential surface I, during the first major iteration (ITER = 1 only), subroutine ONEST1 determines the parameters A, B, C_C, and THET at every internal grid point. This subroutine assumes that the total curvatures K_η and K_ψ of the stream surfaces are zero, that cos Θ (i.e., THET) is also zero, that

$$A = \left(\frac{\rho}{q}\right)^{1/2} \tag{5.14.1}$$

and that

$$B = A \tag{5.14.2}$$

Subroutine ONEST1 is called from the main program.

5.15 Subroutine PARAM. - On potential surface I, subroutine PARAM determines the values of all variables required to compute the coefficient C_C in equation (3.3.4). Subroutine PARAM is called from subroutine VARI.

5.16 Subroutine POTS. - On potential surface $I + 1$, subroutine POTS determines the distribution of the x,y,z coordinates of the internal grid points, starting from the known values of x, y, and z for the primary streamline at JX,KX (fig. in section 3.5) and integrating in the ψ and η directions (section 3.6). Subroutine POTS is called from subroutine VARI.

28

5.17 Subroutine PUTIN. - Subroutine PUTIN reads and writes all input data required by program DIN3D1. Detailed descriptions of these data are given in section 7.3. Subroutine PUTIN is called from the main program.

5.18 Subroutine PUTOUT. - Subroutine PUTOUT prints those results of the solution that are requested by subroutine PUTIN. There are three output tables: (1) output table I (internal grid points), (2) output table II (coordinate points along contours of selected potential surfaces), and (3) output table III (coordinate points along selected streamlines). For details of the data reported in each of these tables, see section 8.0. Subroutine PUTOUT is called from the main program.

5.19 Subroutine RELAX. - At every interior grid point on potential surface I, subroutine RELAX reduces the residual error $\mathscr{R}$ (section 3.3) to an absolute value less than the current value of EPSX by varying the value of Q_0 in the finite-difference equation (3.3.4). (The initial value of EPSX, which is 400 times the input value of EPSR, decreases 12 times by a factor of 0.5, after which its final value is approximately 0.1 times the input value of EPSR.) This subroutine uses an overrelaxation coefficient, the input value of which is ORELAX. The relaxation process is continued until the maximum residual error everywhere on the potential surface is less than 0.1 times the input value of EPSR or until ITX is equal to the input value of ITXMAX, whichever occurs first.

During the relaxation process the program marches across the potential surface first from left to right (increasing ψ index J), then from top to bottom (decreasing η index K), next from right to left (decreasing J), and then from bottom to top (increasing K). Subroutine RELAX is called from the main program.

5.20 Subroutine RESID. - Subroutine RESID determines the residual error at every interior grid point on a given potential surface I. Subroutine RESID is called from the main program.

5.21 Subroutine START. - For ITER greater than 1, subroutine START establishes the values of certain variables ($\bar{e}_1$, $\bar{e}_2$, $\bar{e}_3$, x, y, z, Q, RHO, THET, A, and B) at potential surface I = 1. Subroutine START is called from the main program and from subroutine PUTOUT.

5.22 Subroutine VELD. - From various input data, subroutine VELD determines the input velocity distribution on the lateral boundary of the flow field. From this distribution, it estimates initial values of velocity at all interior grid points. For more detailed discussion of the input velocity distribution on the lateral boundary, see section 7.2. Subroutine VELD is called from subroutine PUTIN.

6.0 MISCELLANEOUS FEATURES OF PROGRAM

Various special features of the program, in addition to those already discussed, are described in this section. These features relate mainly to user options and to input parameters affecting the running time and accuracy of the calculations.

6.1 Option IFLUID. - The input option IFLUID relates to the type of fluid used in the duct design. At present, provision has been made for two types: incompressible fluids (IFLUID = 1), and perfect gases (IFLUID = 2). For incompressible fluids, no additional inputs are required (e.g., the fluid density is not required). For compressible fluids, two additional inputs are required: the upstream Mach number AMU, and the ratio of specific heats GAM.

The following three figures show that compressibility, as measured by AMU (all other factors, including the ratio 2.0 of downstream to upstream velocity, being equal),
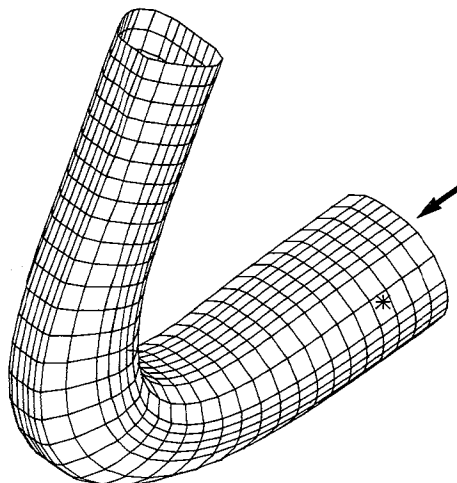
Incompressible; $\Delta\theta$ = 115.52°
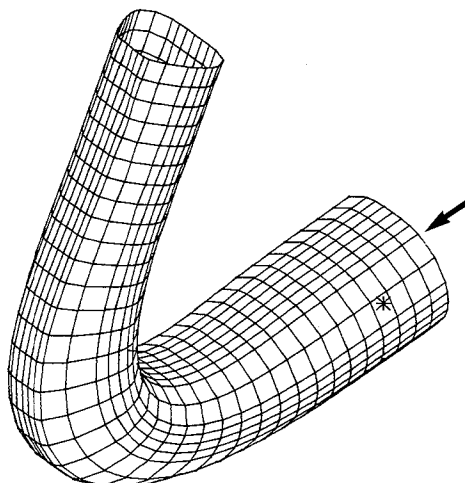
AMU = 0.01; $\Delta\theta$ = 115.52°
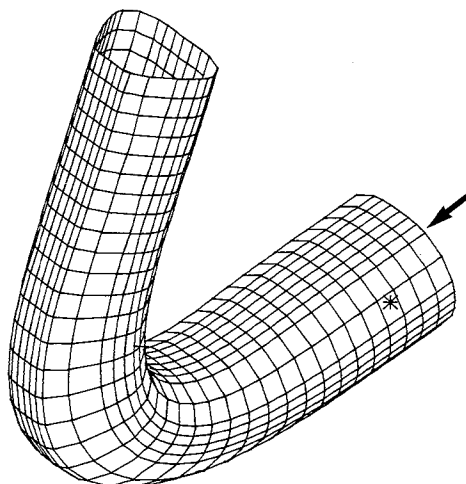
AMU = 0.40; $\Delta\theta$ = 110.96°

affects the turning angle, and of course, the magnitude of the downstream area. The incompressible solution and that for AMU = 0.01 are essentially equal.

If other types of fluid are required, additions can be made to the code in subroutine PUTIN. Of course, appropriate additions to the code must be made throughout the program, wherever the static density ratio ρ appears.

6.2 Option ISYM. - Many duct designs have planar symmetry; that is, the duct shape on one side of the plane is a mirror image of that on the other. If the prescribed lateral velocity distribution has planar symmetry, so also will the resulting design, provided that the prescribed upstream boundary configuration is also symmetrical about the plane. For cases involving planar symmetry, provision is made in the code for solving only one of the two flow fields on either side of the plane of symmetry. This provision cuts the running time roughly in half, or alternatively permits a finer grid with the existing 21-by-36 array size.

The input option ISYM relates to three types of symmetry: first (ISYM = 1), there is no symmetry, or if planar symmetry exists, it is not made use of; second (ISYM = 2), there is, as shown in the following figures,
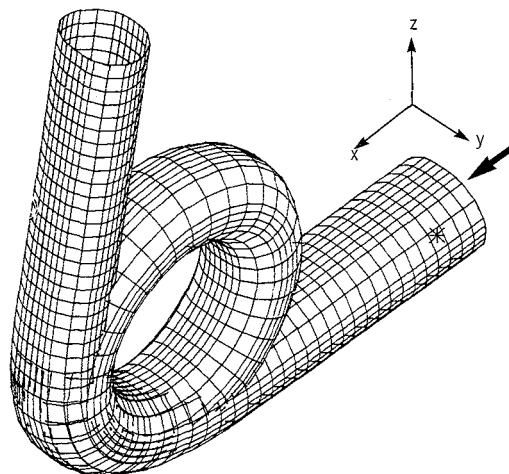
ISYM = 1
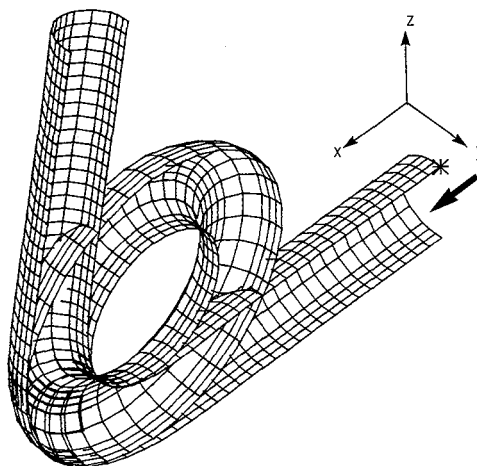
ISYM = 2

symmetry about a plane of constant y (i.e., a plane normal to the y axis of the upstream boundary (fig. in section 3.5)); and third (ISYM = 3), there is, as shown in the following figure, symmetry about a plane of constant z.

ISYM = 3
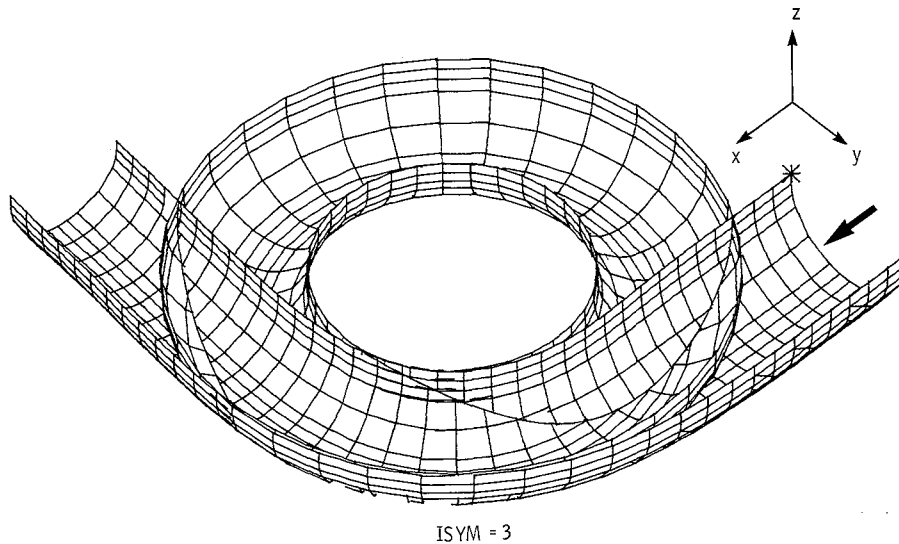
Both types of planar symmetry have been introduced because in program DIN3D1 the 21-by-36 arrays corresponding to the y and z directions, respectively, are not square.

6.3 Option IPLOT. - Because the output for three-dimensional solutions is usually very large, some sort of graphics display is almost a necessity. In program DIN3D1, the display data consist of the x,y,z coordinates of selected points along the contour of every selected potential surface IPS(200). These same points correspond to selected streamlines ISL(200) on the lateral boundary. The result is a three-dimensional plot of the lateral boundary of the flow field (i.e., the duct surface) consisting of a network of potential surface contours and streamlines as shown by figures in this report. (These same data are also printed in output table II (contour data, section 8.3) and output table III (streamline data, section 8.4).)

These display data are obtained by setting the input value of option IPLOT equal to 1. (For no graphics display data, the input value of IPLOT is zero.) These graphics data, which normally go to tape or disk, are provided for at the end of subroutine PUTOUT (section 5.18). It is assumed that a three-dimensional graphics program is available to the user, and only the following raw data, in the order presented, are supplied by program DIN3D1:

| NI | total number of potential surfaces from upstream boundary to downstream boundary. (NI is computed by the program from the input value of NP (number of potential surfaces for which data are specified) and NSD (number of equal subdivisions along the principal streamline between each of the NP potential surfaces); NI = (NP - 1) NSD + 1.) |
| NCP | total number of contour points around each potential surface. (Each contour point corresponds to a streamline on the lateral boundary, so there are NCP streamlines.) |

NPS	number of potential surfaces to be plotted and printed out in table II (maximum, 200)
NSL	number of streamlines to be plotted and printed out in table III (maximum, 200)
IPS(200)	index values IY of NPS potential surfaces to be plotted and printed (maximum, 200)
ISL(200)	index values IX of NSL streamlines to be plotted and printed (maximum, 200)
XB(ISL(IX),IPS(IY)) YB(ISL(IX),IPS(IY)) ZB(ISL(IX),IPS(IY))	x,y,z coordinates of contour points around potential surfaces and corresponding points along streamlines on lateral boundary

6.4 Overrelaxation factor (ORELAX). - At any point in the φ,ψ,η flow field, the residual error $\mathscr{R}$ in the governing equation (3.3.4) can be eliminated by an incremental change ΔQ_0 in the local value of Q_0. From equation (3.3.4), this value for ΔQ_0 is given by

$$\Delta Q_0 = \frac{\mathscr{R}}{C_0} \tag{6.4.1}$$

To speed up the iterative process involved in the global solution of equation (3.3.4), the local incremental changes given by equation (6.4.1) are multiplied by the input value of the overrelaxation factor ORELAX. Thus,

$$\Delta Q_0 = \left(\frac{\mathscr{R}}{C_0}\right)(ORELAX) \tag{6.4.2}$$

where

$$1.0 \le ORELAX < 2.0 \tag{6.4.3}$$

The optimum value of ORELAX for the shortest running time probably varies somewhat with the boundary conditions of the problem. A preliminary investigation indicated an approximate value of 1.35; however, the user is encouraged to try other input values.

6.5 Accuracy (EPS and EPSR). - The input values of EPS and EPSR determine the accuracy of various iterative processes in the program. The input value of EPSR relates to the solution of the governing equation (3.3.4) by finite-difference methods. It is the maximum allowable value of the residual error $\mathscr{R}$ at any point in the flow field after the iterative solution has been completed globally for a given (fixed) set of the coefficients $C_C, C_0,..., C_6$. The input value of EPS relates to other iterative processes.

The program uses double precision. The input values of EPS and EPSR used for the examples in this report were both 0.000005 and occasionally an order of magnitude less. Because of the dimensionless form under which the solutions are obtained, the magnitudes of EPS and EPSR are independent of the size of the flow field. However, for comparable accuracy in solving the governing equation (3.3.4), the greater the number of grid points on a potential surface, the smaller the input value of EPSR, because the smaller will be the dimensionless grid spacings $a_1,...,a_6$ in the coefficients of equation (3.3.4).

7.0 INPUT TO PROGRAM

The two major inputs to the program are the shape of the upstream boundary with its associated grid and the velocity distribution on the lateral boundary of the duct. These inputs are discussed in detail in the next two sections, after which a formatted, line-by-line description of the complete input is given. This latter section constitutes a users guide for preparation of the input.

7.1 Upstream boundary shape and associated grid. - The shape of the upstream boundary is specified by the coordinate points of its contour on the y,z plane for x = 0. These coordinate points are located at every intersection of the contour with a specified (input) grid of YG(J) and ZG(K) lines in the Y,Z plane. Thus,
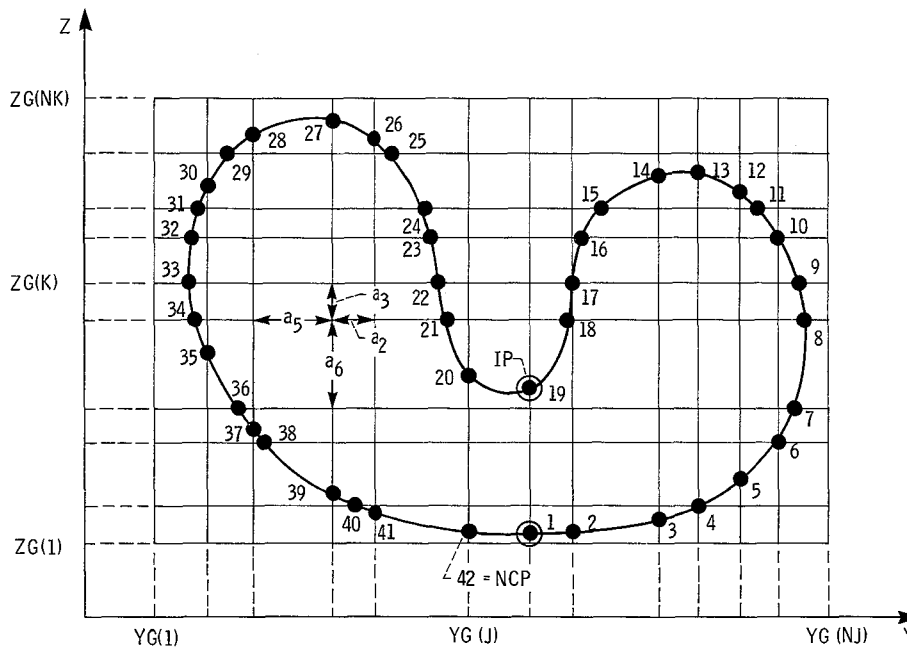
The coordinate points [YC(1), ZC(1)],..., (YC(NCP), ZC(NCP)] are numbered counter-clockwise and consecutively from 1 to NCP, where the maximum allowable value of NCP is 200. The starting point is arbitrary, except for cases using planar symmetry (ISYM equal to 2 or 3), which are discussed later. The YG(J) and ZG(K) grid lines, at which the contour coordinate points occur, are numbered 1 to NJ and 1 to NK, respectively, where the maximum allowable values of NJ and NK are 21 and 36, respectively.

The spacing (a_2, a_3, a_5, and a_6) of the grid lines is arbitrary, except that at least three internal grid points (i.e., intersections of grid lines) must lie along every internal grid line segment bounded by the contour and at least two external grid points must lie along every external grid line segment bounded by the contour. It is also prudent to keep the grid spacings as nearly constant as the contour shape and other considerations permit and not too different from the a_1 and a_4 spacing in the φ direction (second fig. in section 3.2). Of course, grid size affects running time. Doubling the grid spacing on potential surfaces, but leaving the spacing between potential surfaces unchanged, decreased CPU time by more than 75 percent in the following examples.

34
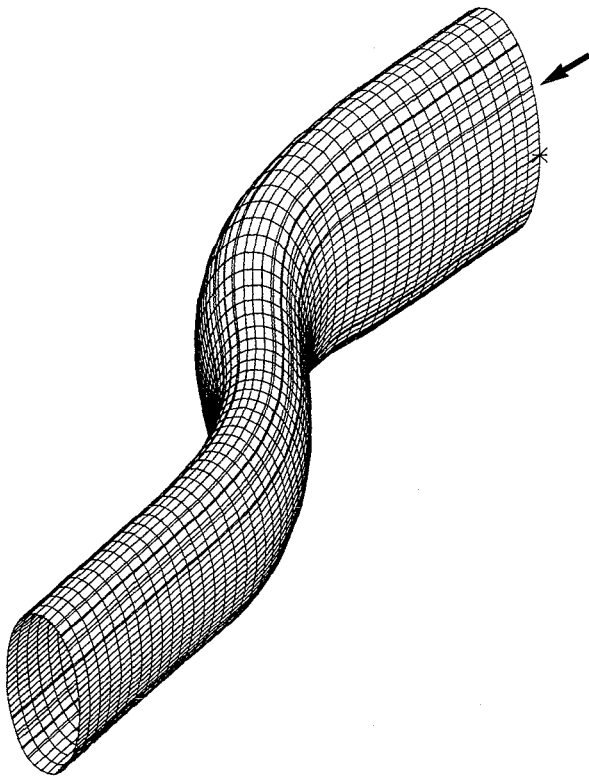
Fine grid; ITER = 10; 370/3033 CPU time, 132.01 min   Coarse grid (spacing doubled); ITER = 10; 370/3033 CPU time, 29.64 min
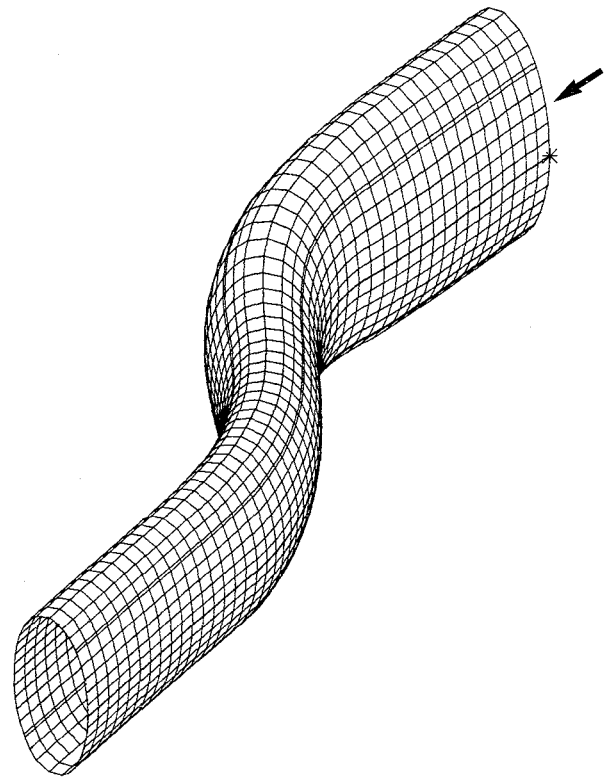
The shape of the contour is completely arbitrary (but see section 4.1) except that (see following figure) (1) every contour point must be the end point of at least one internal grid line, (2) any interior straight line drawn between two contour points that are not adjacent must cut at least one grid line, and (3) unless a contour point lies on a grid point, it must be at least 10 times the input value of EPS away from any interior grid point.

35
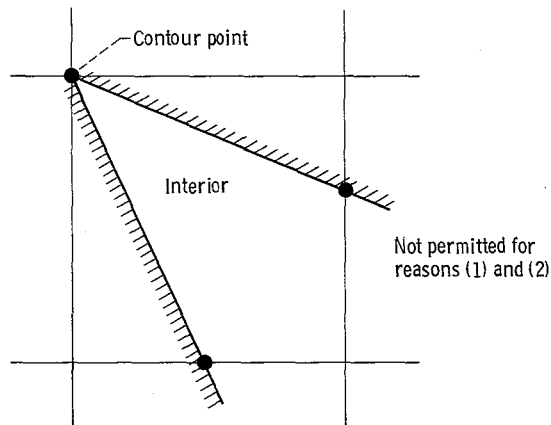
Because of the approximate nature of the solutions (section 4.0), a "kink" may develop in the duct boundary if an <u>external</u> grid point is too close to two adjacent contour points along the boundary, particularly if the upstream boundary configuration is too complex or convoluted. This "kink" occurs because the x,y,z coordinates at boundary
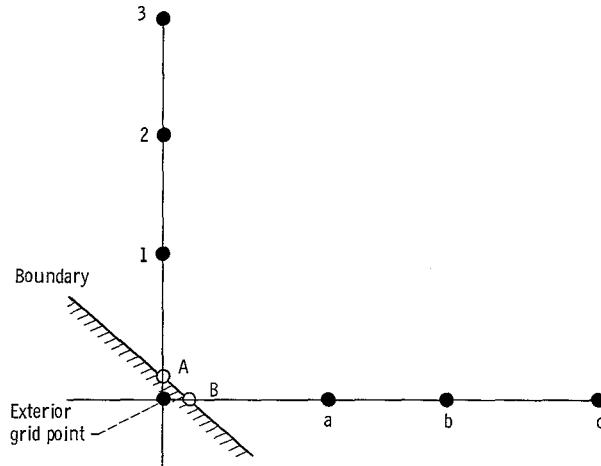
point A are obtained by extrapolating from the corresponding values at the interior points 1, 2, and 3, whereas the coordinates at boundary point B are obtained by extrapolating from the interior points a, b, and c. The "kink" is most easily eliminated by shifting one of the two grid lines so that the points A and B come together as shown in the following figure.
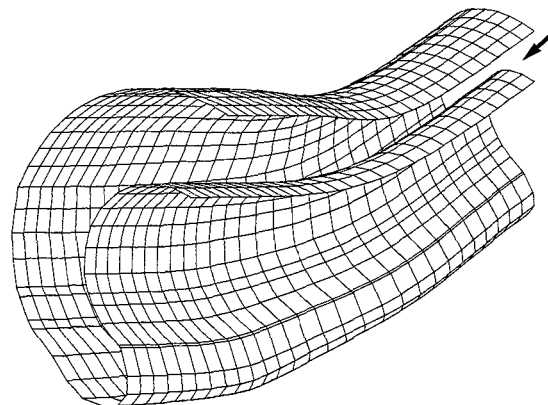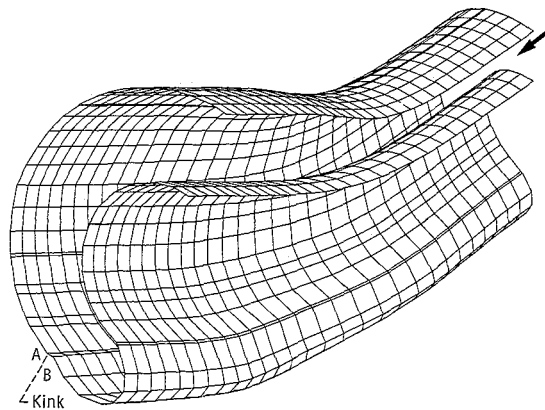
For planar symmetry solutions (section 6.2), only one of the two symmetrical halves of the upstream boundary configuration is used. If the plane of symmetry is normal to the Y axis (ISYM = 2) as shown, the left half must be used, and the contour points are numbered in the counterclockwise direction from 1 to NCP, starting at the plane of symmetry.
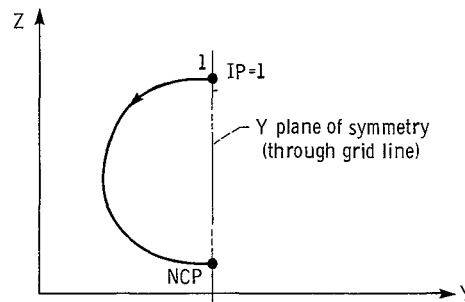
If the plane of symmetry is normal to the Z axis (ISYM = 3), the lower half must be used, and the contour points are numbered in the counterclockwise direction from 1 to NCP starting at the plane of symmetry as shown. Note that for ISYM equal to both 2
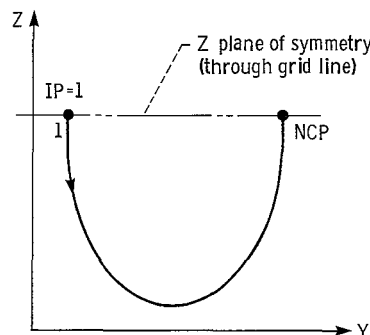
and 3, the input location (JX,KX) of the primary streamline must be on the plane of symmetry.

These various upstream boundary contours in physical X,Y,Z space are also the shapes of all potential surfaces in transformed φ,ψ,η space, because paired values of Y (equals ψ) and Z (equals η) are constant along streamlines (section 3.2).

7.2 Prescribed velocity distribution on surface of duct. - The velocity distribution on the lateral boundary of the duct could be specified in a perfectly general, continuous way (but see section 4.1) at each of the NCP coordinate points along the boundary contour (section 7.1) for each of the NI potential surfaces from the upstream boundary (I = 1) to the downstream boundary (I = NI), where the maximum allowable value for both NCP and NI is 200. Because this is a large amount of input data (200 x 200), for convenience, in program DIN3D1, the velocity distribution on the lateral surface is specified by two components. First, the distribution of velocity QP(I) is specified as a function of distance SP(I) along the principal streamline (input value of IP; figs. in section 7.1). Thus,
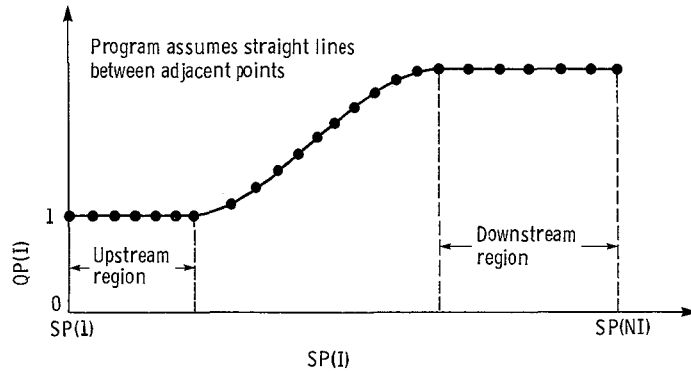
where QP(I) is expressed as a ratio of the upstream velocity, and the dimensional unit for SP(I) is the same as for YG(J) and ZG(K) (section 7.1). The velocity QP(I) is constant in the upstream and downstream regions, which regions should normally be at least two hydraulic diameters of their respective flow areas in extent. These regions of constant velocity on the lateral boundary are required to justify the assumption of constant velocity over the upstream and downstream flow areas.

Second, but only if the input value of option IVEL is 1, the velocity variation DQ around the contour of each potential surface, which contour in φ,ψ,η space is the same as the upstream contour (section 7.1), is specified by
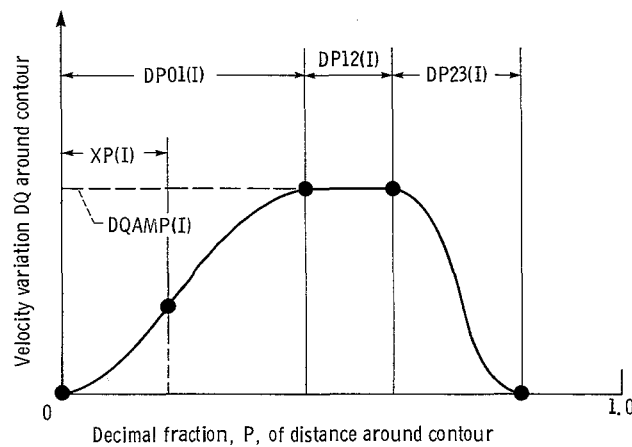
In this figure, DQAMP(I) is the amplitude (plus or minus) of the velocity variation DQ and P is the decimal fraction of the distance around the contour. The XP(I) value of P locates the principal streamline IP relative to the velocity variation with P. The variation in velocity with P is, therefore, specified for all potential surfaces by DP01(I), DP12(I), DP23(I), DQAMP(I), and XP(I) as functions of SP(I) from I = 1,...,NI. As for the distribution of QP(I) in the previous paragraph, the distributions of these parameters should also be constant in the upstream and downstream regions, and the values of DQAMP(I) must be zero.

In the regions of P defined by DP01(I) and DP23(I) in the figure, the velocity variation DQ is given by the cubic equation

$$DQ = a + bP + cP^2 + dP^3 \qquad (7.2.1)$$

38

where the four coefficients a, b, c, and d are fixed by the four conditions

$$\frac{d(DQ)}{dP} = 0 \qquad \text{at the two end points}$$

$$DQ = 0 \qquad \text{at one end point}$$

$$DQ = DQAMP(I) \qquad \text{at the other end point}$$

To simplify the input further, values of these parameters, as well as of QP(I), need not be specified at all values of I, but only at NP values, where

$$NI = (NP - 1) NSD + 1 \qquad (7.2.2)$$

in which NSD is the specified (input) number of equal subdivisions between adjacent, specified NP values of the parameters. The program assumes linear variations in the parameters between the specified values.

For the "equilibrium" velocity distributions described in appendix A (input values of option IVEL equal to 2 or 3), in addition to the prescribed velocity QP(I) as a function of distance SP(I) along the primary streamline, only the amplitude DQAMP(I) of the velocity variation DQ (see previous fig.) is specified. The parameters DP01(I), DP12(I), DP23(I), and XP(I) must be omitted. Also, if the input value of ISYM is 2, the input value of IVEL must not be 3; and if the input value of ISYM is 3, the input value of IVEL must not be 2.

Option IVEL = 4 can be used only with option ISYM equal to 2 or 3 (planar symmetry cases). Here, only the parameters DP23(I) and XP(I) must be omitted, it being understood that for planar symmetry

$$DP23(I) = DP01(I) \qquad (7.2.3)$$

and

$$XP(I) = 0.5 + DP01(I) + 0.5 \times DP12(I) \qquad (7.2.4)$$

As for optional input IFLUID (section 6.1), provision is also made in subroutine PUTIN for adding new types of option IVEL by additions to the code, and of course, appropriate additions to the code must also be made in subroutine VELD.

7.3 Line-by-line input for program DIN3D1. - This section should be used when preparing the formatted, line-by-line input for program DIN3D1. It is also recommended that sections 7.1 and 7.2 be reviewed before starting.

Line 1 - FORMAT(20A4)
    TITLE   title (center on field of 80 characters)

Line 2 - FORMAT(20A4)
    SUBT1   first subtitle (center on field of 80 characters)

Line 3 - FORMAT(20A4)
    SUBT2   second subtitle (center on field of 80 characters)

Line 4 -   FORMAT(7I10)

IFLUID   option equals 1 for incompressible flow, 2 for perfect gas (section 6.1)

ISYM   option equals 1 for complete flow field, 2 for half flow field with planar
                symmetry about y plane, and 3 for half flow field with planar symmetry
                about z plane (sections 6.2 and 7.1)

IGRID   option equals 1 for Cartesian YG(J),ZG(K) grid at upstream boundary
                (only option) (section 7.1)

IVEL   option equals 1 for standard, two-component, parametric method of
                specifying velocity distribution on lateral boundary of duct (section 7.2),
                2 for "equilibrium" velocity distribution with turn in y plane (sections
                4.1 and 7.2 and appendix A), 3 for "equilibrium" velocity distribution with
                turn in z plane (sections 4.1 and 7.2 and appendix A), and 4 for cases
                with ISYM values of 2 or 3 only (section 7.2)

IPLOT   option equals zero for no graphics output, 1 for three-dimensional
                graphics output (section 6.3)

ISOLV   option equals zero if built-in criteria for successful solution are not
                used, 1 if criteria are used (section 4.4)

ISPACE   option equals zero if grid spacings (second fig. in section 3.2) for all
                internal grid points are not printed in output (space-saving option), 1 if
                spacings are printed

Line 5 -   FORMAT(5I10)

ITERMX   maximum number of major iterations (ITER) allowed; value depends on
                circumstances of case involved (sections 3.3, 4.4, 4.5, and 5.1)

ITMAX   maximum number of IT iterations allowed (each iteration involves
                entire flow field; values of coefficients C_C, C_0, C_1,...,C_6 in equation
                (3.3.4) are unchanged for all IT iterations; recommended value is 250)
                (sections 3.3 and 5.1)

ITXMAX   maximum number of passes allowed for iterative, finite-difference
                solution of governing differential equation (3.3.4) on a given potential
                surface φ; recommended value is 100 (section 5.19)

ICONX   maximum number of ICON iterations, in main program, on coefficients
                of governing equation (3.3.4); recommended value is 4 and cannot be less
                than 3 (section 5.1.1)

NTRY   number of iterations, in subroutine VARI, on values of direction cosines;
                recommended value is 3 and cannot be less than 2

Line 6 -   FORMAT(6F10.3)

CAVD   coefficient for averaging new values of derivatives of direction cosines
                with previous values; recommended value is 0.5 (section 5.2.2)

40

CAVN   coefficient for averaging new values of continuity parameters A and B
            with previous values; recommended value is 0.5 or less (section 5.2.2 and
            appendix C)

CAVP   coefficient for averaging values (obtained by two methods) of x,y,z
            coordinates at each internal grid point; recommended value is 0.5 or less
            (sections 3.6, 4.2(constraint 1), and 4.6)

CAVX   coefficient for averaging new values of direction cosines with previous
            values; recommended value is 0.2 (section 5.2.2)

CAVY   coefficient for averaging new values of coefficient C_C, in the governing
            equation (3.3.4), with previous values; recommended value is 0.5 or less
            (section 5.2.2)

CAVZ   coefficient for averaging new values of THET (cosine of "distortion"
            angle Θ) with previous values; recommended value is 0.5 or less (section
            5.2.2)

[If IFLUID = 1, incompressible flow, go to line 8.]

Line 7 -   FORMAT(2F10.4)

AMU   upstream Mach number (section 6.1)

GAM   ratio of specific heats (section 6.1)

Line 8 -   FORMAT(2I10)

JX   value of J for primary streamline (fig. in section 3.5; sections 3.6, 5.2,
            and 7.1)

KX   value of K for primary streamline (fig. in section 3.5; sections 3.6, 5.2,
            and 7.1) (For input values of ISYM equal to 2 and 3, the primary
            streamline (JX,KX) must lie on the plane of symmetry.)

Line 9 -   FORMAT(3I10)

NJ   number of YG(J) grid lines; maximum value is 21 (section 7.1)

NK   number of ZG(K) grid lines; maximum value is 36 (section 7.1)

NCP   number of contour coordinate points around upstream potential surface;
            maximum value is 200 (sections 6.3 and 7.1)

Line 10 -   FORMAT(8F10.6)

YG(J)   NJ values of Y grid lines; same dimensional unit of length used for SP
            on line 15; 6-decimal accuracy recommended (sections 3.2, 3.5, and 7.1)

Line 11 -   FORMAT(8F10.6)

ZG(K)   NK values of Z grid lines; same dimensional unit of length used for SP
            on line 15; 6-decimal accuracy recommended (sections 3.2, 3.5, and 7.1)

41

YC(IX)   NCP values of Y for coordinate points along boundary contour starting
                at contour point 1 (which has arbitrary location for ISYM = 1 but must
                lie on the plane of symmetry for ISYM equal to 2 or 3); contour points
                must be read sequentially in counterclockwise direction; same
                dimensional unit of length used for SP on <u>line 15</u>; 6-decimal accuracy
                recommended (sections 3.2, 3.5, and 7.1)

Line 13 -   FORMAT(8F10.6)

ZC(IX)   NCP values of Z for coordinate points along boundary contour starting
                at contour point 1; see YC(IX), above, for further comments

Line 14 -   FORMAT(3I10)

IP   contour coordinate point corresponding to <u>principal</u> streamline; for
                ISYM equal to 2 or 3, IP must equal 1; for "equilibrium" velocity
                distributions (IVEL equal to 2 or 3), see appendix A (first and last figs. in
                section 7.1)

NP   number of stations (velocity potential surfaces) at which parameters are
                specified for velocity distribution on lateral surface; quantity
                (NP - 1)NSD + 1 must not exceed 200 (section 7.2)

NSD   number of subdivisions between each of the above NP stations
                (section 7.2)

Line 15 -   (NP lines, one for each station), FORMAT(6F10.5, F10.6)

QP(I)   velocity (ratio) distribution along <u>principal</u> streamline (IP), expressed as
                ratio of upstream velocity; 5-decimal accuracy recommended
                (section 7.2)

SP(I)   distance along <u>principal</u> streamline; any unit of length permitted, and
                value of SP(I) at upstream boundary need not be 0.0 (section 7.2)

DP01(I)   percent of contour length (second fig. in section 7.2); omit if IVEL
                equals 2 or 3 (section 7.2)

DP12(I)   percent of contour length (second fig. in section 7.2); omit if IVEL
                equals 2 or 3 (section 7.2)

DP23(I)   percent of contour length (second fig. in section 7.2); omit if IVEL
                equals 2, 3, or 4 (section 7.2)

DQAMP(I)   amplitude (second fig. in section 7.2) of velocity variation DQ around
                contour of potential surface; velocity expressed as ratio of upstream
                velocity; DQAMP(I) may be positive or negative; DQAMP(I) must be 0.0

in upstream and downstream regions of duct (first fig. in section 7.2; section 7.2)

XP(I)	location (percent of contour length) of <u>principal</u> streamline relative to velocity variation around contour of potential surface (second fig. in section 7.2); omit if IVEL equals 2, 3, or 4 (section 7.2)

Line 16 - <u>FORMAT(4I10)</u>

IA	I value of initial potential surface for which output data are printed in table I
IZ	I value of final potential surface for which output data are printed in table I; IZ $\leq$ NI (total number of potential surfaces; section 6.3); if IZ < IA, table I is omitted in printout
NPS	number of potential surfaces for which output data at boundary contour points are printed in table II (and saved for three-dimensional graphics if input value of IPLOT is 1); NPS $\leq$ 200; if NPS = 0, table II is omitted and input <u>line 17</u> is skipped (section 6.3)
NSL	number of boundary-surface streamlines for which output data are printed in table III (and saved for three-dimensional graphics if IPLOT is 1); NSL $\leq$ 200; if NSL = 0, table III is omitted and input <u>line 18</u> is skipped (section 6.3)

Line 17 - <u>FORMAT(8I10)</u>

IPS(I)	NPS values of the I values of potential surfaces for which output data are printed in table II; numbered sequentially, starting from lowest value, but numbers can be skipped (section 6.3)

Line 18 - <u>FORMAT(8I10)</u>

ISL(I)	NSL values of the I values of boundary contour points for which streamline data are printed in table III; numbered sequentially, starting from lowest value, but numbers can be skipped (section 6.3)

Line 19 - <u>FORMAT(2F10.7,F10.4)</u>

EPS	standard maximum allowable error in various iterative procedures; recommended value is 0.000005 (section 6.5)
EPSR	maximum allowable value of residual error $\mathscr{R}$ in finite-difference solutions of equation (3.3.4); recommended value is 0.000005 (sections 3.3, 5.19, and 6.5)
ORELAX	overrelaxation factor (sections 5.19 and 6.4)

43

7.4 Sample printout of input data. – Program DIN3D1 prints out the input data in the same order in which they are read in. A sample printout of the input data follows.

PROGRAM DIN3D1

DESIGN OF THREE-DIMENSIONAL INTERNAL FLOW FIELDS

FOR ARBITRARY PRESCRIBED VELOCITY DISTRIBUTIONS

ON LATERAL BOUNDARY SURFACE

CASE NO. V

ELBOW C2

QD/QU = 2.0   M-UP = 0.4

INPUT DATA

OPTIONS

IFLUID	ISYM	IGRID	IVEL	IPLOT	ISOLV	ISPACE
2	1	1	2	1	1	1

INPUT DATA FOR LIMITS ON VARIOUS ITERATION CYCLES

MAX ITER ITERATIONS	MAX IT ITERATIONS	MAX ITX ITERATIONS	ICONX ITERATIONS	NTRY ITERATIONS
12	250	100	4	3

INPUT DATA FOR VARIOUS DAMPING COEFFICIENTS

CAVD	CAVN	CAVP	CAVX	CAVY	CAVZ
0.500	0.500	0.200	0.200	0.500	0.500

INPUT DATA FOR PERFECT GAS (IFLUID = 2)

UPSTREAM MACH NO.	RATIO OF SPEC HTS
0.4000	1.4000

INPUT DATA FOR PRIMARY STREAMLINE

J-VALUE (JX)	K-VALUE (KX)
7	6

44

INPUT DATA FOR GRID SYSTEM ON UPSTREAM BOUNDARY SURFACE (IGRID = 1)

NO. OF Y GRID LINES	NO. OF Z GRID LINES	NO. OF POINTS ON BOUNDARY
13	11	28

INPUT DATA FOR UPSTREAM GRID (CONTINUED)

J	Y-VALUE OF GRID
1	1.000000
2	1.290635
3	2.318019
4	3.909010
5	4.704505
6	5.500000
7	6.295495
8	7.090990
9	7.886485
10	8.681980
11	10.272971
12	11.300355
13	11.590990

INPUT DATA FOR UPSTREAM GRID (CONTINUED)

K	Z-VALUE OF GRID
1	1.000000
2	1.290635
3	2.318019
4	3.909010
5	4.704505
6	5.500000
7	6.295495
8	7.090990
9	8.681981
10	9.709365
11	10.000000

INPUT DATA FOR UPSTREAM GRID (CONTINUED)

I	Y-VALUE OF CONTOUR	Z-VALUE OF CONTOUR
1	5.500000	1.000000
2	6.295495	1.000000
3	7.090990	1.000000
4	7.886485	1.070871
5	8.681980	1.290635
6	10.272971	2.318019
7	11.300355	3.909010
8	11.520119	4.704505
9	11.590990	5.500000
10	11.520119	6.295495
11	11.300355	7.090990
12	10.272971	8.681981
13	8.681980	9.709365
14	7.886485	9.929129
15	7.090990	10.000000
16	6.295495	10.000000
17	5.500000	10.000000
18	4.704505	9.929129
19	3.909010	9.709365

```
20      2.318019        8.681981
21      1.290635        7.090990
22      1.070871        6.295495
23      1.000000        5.500000
24      1.070871        4.704505
25      1.290635        3.909010
26      2.318019        2.318019
27      3.909010        1.290635
28      4.704505        1.070871
```

INPUT DATA FOR VELOCITY DISTRIBUTION ON LATERAL BOUNDARY SURFACE (IVEL = 1)

PRINCIPAL STREAMLINE	NO. OF SPEC. STATIONS	NO. OF SUBDIVISIONS
16	29	1

I	VEL. ON PRINCIPAL STREAMLINE	DISTANCE ALONG STREAMLINE	DEL-Q AMPLITUDE
1	1.000000	0.000000	0.000000
2	1.000000	1.500000	0.000000
3	1.000000	3.000000	0.000000
4	1.000000	4.500000	0.000000
5	1.000000	6.000000	0.000000
6	1.000000	7.500000	0.000000
7	1.000000	9.000000	0.000000
8	1.019700	10.500000	-0.019700
9	1.074100	12.000000	-0.074100
10	1.156300	13.500000	-0.156300
11	1.259300	15.000000	-0.259300
12	1.376200	16.500000	-0.356500
13	1.500000	18.000000	-0.425900
14	1.623800	19.500000	-0.467500
15	1.740700	21.000000	-0.481400
16	1.843800	22.500000	-0.467600
17	1.925900	24.000000	-0.425900
18	1.980300	25.500000	-0.356500
19	2.000000	27.000000	-0.259300
20	2.000000	28.500000	-0.156200
21	2.000000	30.000000	-0.074100
22	2.000000	31.500000	-0.019700
23	2.000000	33.000000	0.000000
24	2.000000	34.500000	0.000000
25	2.000000	36.000000	0.000000
26	2.000000	37.500000	0.000000
27	2.000000	39.000000	0.000000
28	2.000000	40.500000	0.000000
29	2.000000	42.000000	0.000000

INPUT DATA FOR PRINT FORMAT

MIN I-VALUE OF POT SURF (TABLE I)	MAX I-VALUE OF POT SURF (TABLE I)	NO OF POT SURFACES (TABLE II)	NO OF STREAMLINES (TABLE III)
1	29	29	28

46

INPUT DATA FOR POTENTIAL SURFACES (TABLE II)

    NUMBER (NPS) OF POTENTIAL SURFACES = 29

    I-VALUES OF POTENTIAL SURFACES:

1	2	3	4	5	6	7	8	9	10
11	12	13	14	15	16	17	18	19	20
21	22	23	24	25	26	27	28	29	

INPUT DATA FOR STREAMLINES (TABLE III)

    NUMBER (NSL) OF STREAMLINES = 28

    I-VALUES OF CONTOUR POINTS THROUGH WHICH STREAMLINES PASS:

1	2	3	4	5	6	7	8	9	10
11	12	13	14	15	16	17	18	19	20
21	22	23	24	25	26	27	28		

INPUT DATA RELATED TO ACCURACY OF CALCULATIONS

EPS	EPS-R	O-RELAX
0.0000005	0.0000005	1.3500

8.0 OUTPUT FROM PROGRAM

The five major outputs from the program are (1) an intermediate printout generated as the solution progresses; (2) output table I, with data at the internal grid points for the selected range (IA to IZ) of potential surfaces in x,y,z space; (3) output table II, with data around the contours of selected potential surfaces in x,y,z space; (4) output table III, with data along selected streamlines over the full range of potential surfaces (I equals 1 to NI); and (5) output data to tape or disk for three-dimensional graphics, provided that the input value of IPLOT is 1. Before printing these five outputs, the program prints out (1) the maximum Mach number along the principal streamline and (2) provided that the input value of ISPACE is 1, the values of the six grid spacings $a_1,...,a_6$ (second fig. in section 3.2) for all of the internal grid points.

8.1 Intermediate printout. – For each pass IT through the entire flow field for every major iteration ITER (with unchanged values of the coefficients C_C, C_0, $C_1,...,C_6$ in the governing equation (3.3.4)), the intermediate printout gives the magnitude and location (I-MAX, J-MAX, and K-MAX) of the absolute value of the maximum residual error $\mathscr{R}$ encountered during the pass. For a given value of ITER, after convergence ($\mathscr{R}$ < EPSR) or after IT becomes greater than the input value of ITMAX, the program prints the exit flow area EXFLAR (section 5.12) and its error ERRAR (section 5.1), expressed as a decimal fraction, for each of the ICON iterations (section 5.1.1). Also, any intermediate messages regarding, for example, the counters ICX, ICY, and ITH (section 5.2.1) are printed. A sample page of intermediate printout follows.

INTERMEDIATE PRINTOUT

ITERATION ITER	ITERATION IT	MAX RES IN IT	I-MAX	J-MAX	K-MAX	ITERATION ICON	EXIT FLOW AREA (DIM)	CORRECT FLOW AREA (DIM)	ERROR
1	1	0.8707286	8	7	10	...	...	...	...
1	2	0.3962490	8	7	8	...	...	...	...
1	3	U.2352487	7	7	7	...	...	...	...
1	4	0.1334014	7	7	7	...	...	...	...
1	5	0.0794694	6	7	7	...	...	...	...
1	6	0.0498247	6	7	6	...	...	...	...
1	7	0.0313226	6	7	6	...	...	...	...
1	8	0.0192473	6	7	6	...	...	...	...
1	9	0.0120385	5	7	6	...	...	...	...
1	10	0.0073951	5	7	6	...	...	...	...
1	11	0.0044359	5	7	6	...	...	...	...
1	12	0.0027005	4	7	6	...	...	...	...
1	13	0.0016138	4	7	6	...	...	...	...
1	14	0.0009475	4	7	6	...	...	...	...
1	15	0.0005484	4	7	6	...	...	...	...
1	16	0.0003137	4	7	6	...	...	...	...
1	17	0.0001780	4	7	6	...	...	...	...
1	18	0.0001002	4	7	6	...	...	...	...
1	19	0.0000562	4	7	6	...	...	...	...
1	20	0.0000315	4	7	6	...	...	...	...
1	21	0.0000176	4	7	6	...	...	...	...
1	22	0.0000098	4	7	6	...	...	...	...
1	23	0.0000055	4	7	6	...	...	...	...
1	24	0.0000031	4	7	6	...	...	...	...
1	25	0.0000017	3	7	6	...	...	...	...
1	26	0.0000010	4	7	6	...	...	...	...
1	27	0.0000005	7	7	6	...	...	...	...
1	27	...	...	...	...	1	49.3908	49.3932	-0.0000
1	27	...	...	...	...	2	49.3927	49.3932	-0.0000
1	27	...	...	...	...	3	49.3935	49.3932	0.0000
1	27	...	...	...	...	4	49.3939	49.3932	0.0000
2	1	0.0682211	12	7	2	...	...	...	...
2	2	0.0395768	12	7	6	...	...	...	...
2	3	0.0248684	12	7	6	...	...	...	...
2	4	0.0154618	11	7	6	...	...	...	...
2	5	0.0096363	10	7	6	...	...	...	...
2	6	0.0060232	10	7	6	...	...	...	...
2	7	0.0039346	9	7	6	...	...	...	...
2	8	0.0024947	8	7	6	...	...	...	...
2	9	0.0016270	8	7	6	...	...	...	...

8.2 Output table I. - Output table I gives the values of variables at all internal grid points for potential surfaces in the (input) range from IA to IZ. The headings in output table I are as follows:

I,J,K   grid-point indices in directions of increasing velocity potential PHI, stream function PSI, and stream function ETA, respectively

PHI, PSI,   at grid point (I,J,K), values of velocity potential and two stream
ETA   functions, respectively (sections 3.0 to 3.2)

X(DIM),Y(DIM),   at grid point (I,J,K), values of X,Y,Z coordinates, expressed in same
Z(DIM)   dimensional unit as input values of SP(I) (sections 3.5 and 3.6)

Q/Q-UP   at grid point (I,J,K), value of local velocity divided by upstream velocity (section 3.3)

MACH NO.   at grid point (I,J,K), value of local Mach number

RO/RO-UP   at grid point (I,J,K), value of local static density divided by upstream static density (section 3.3)

P/P-UP   at grid point (I,J,K), value of local static pressure divided by upstream static pressure. For incompressible flow (IFLUID = 1), P/P-UP is defined as local difference between total and static pressure divided by the same difference at upstream boundary (which definition is equivalent to square of Q/Q-UP) (section 3.3))

SIN(THET)   sine of "distortion" angle Θ (sections 3.1, 3.3, and 4.2 (constraint 5))

COS(AL1),...,   at grid point (I,J,K), values of direction cosines of three unit vectors
COS(GM3) $\bar{e}_1, \bar{e}_2,$ and $\bar{e}_3$ (sections 3.1, 3.4, and 4.2)

A,B   at grid point (I,J,K), values of continuity parameters (eqs. (3.3.2) and (3.3.3) and sections 3.4 and 5.2)

A sample page of output table I resulting from the sample input in section 7.4 follows.

OUTPUT TABLE NO. I (INTERNAL GRID POINTS)

I	J	K	PHI / COS(AL1)	PSI / COS(BT1)	ETA / COS(GM1)	X(DIM) / COS(AL2)	Y(DIM) / COS(BT2)	Z(DIM) / COS(GM2)	Q/Q-UP / COS(AL3)	MACH NO / COS(BT3)	RO/RO-UP / COS(GM3)	P/P-UP / A	SIN(THET) / B
14	10	9	2.51638	0.87683	0.87683	19.7331	7.4296	8.1175	1.5330	0.6269	0.8687	0.8212	1.0000
			0.9757	-0.0309	0.2171	0.0316	0.9995	0.0004	-0.2170	0.0065	0.9762	0.3018	0.7285
14	5	10	2.51638	0.42284	0.99409	19.5401	3.8690	8.9232	1.6026	0.6578	0.8509	0.7977	1.0000
			0.9783	0.0205	0.2060	-0.0209	0.9998	-0.0003	-0.2059	-0.0045	0.9786	0.7891	0.6952
14	6	10	2.51638	0.51363	0.99409	19.5290	4.5824	8.9232	1.6026	0.6577	0.8510	0.7978	1.0000
			0.9785	0.0103	0.2060	-0.0105	0.9999	-0.0001	-0.2060	-0.0023	0.9786	0.7890	0.6954
14	7	10	2.51638	0.60443	0.99409	19.5252	5.2955	8.9233	1.6026	0.6577	0.8510	0.7978	1.0000
			0.9786	0.0000	0.2060	-0.0000	1.0000	-0.0000	-0.2060	-0.0000	0.9786	0.7889	0.6955
14	8	10	2.51638	0.69523	0.99409	19.5290	6.0086	8.9232	1.6026	0.6577	0.8510	0.7978	1.0000
			0.9785	-0.0103	0.2060	0.0105	0.9999	0.0001	-0.2060	0.0023	0.9786	0.7890	0.6954
14	9	10	2.51638	0.78603	0.99409	19.5401	6.7220	8.9232	1.6026	0.6578	0.8509	0.7977	1.0000
			0.9783	-0.0205	0.2060	0.0209	0.9998	0.0003	-0.2059	0.0045	0.9786	0.7891	0.6952
15	5	2	2.80440	0.42284	0.03317	23.4195	3.9438	2.3670	1.2708	0.5134	0.9277	0.9003	1.0000
			0.9258	0.0180	0.3775	-0.0196	0.9998	0.0003	-0.3775	-0.0063	0.9260	0.3083	0.9264
15	6	2	2.80440	0.51363	0.03317	23.4093	4.6195	2.3671	1.2709	0.5134	0.9277	0.9003	1.0000
			0.9259	0.0090	0.3776	-0.0097	1.0000	-0.0000	-0.3776	-0.0032	0.9260	0.3083	0.9263
15	7	2	2.80440	0.60443	0.03317	23.4060	5.2955	2.3672	1.2709	0.5134	0.9277	0.9003	1.0000
			0.9260	0.0000	0.3776	-0.0000	1.0000	-0.0000	-0.3776	-0.0000	0.9260	0.3083	0.9262
15	8	2	2.80440	0.69523	0.03317	23.4093	5.9714	2.3671	1.2709	0.5134	0.9277	0.9003	1.0000
			0.9259	-0.0090	0.3776	0.0097	1.0000	0.0000	-0.3776	0.0032	0.9260	0.3083	0.9263
15	9	2	2.80440	0.78603	0.03317	23.4195	6.6472	2.3670	1.2708	0.5134	0.9277	0.9003	1.0000
			0.9258	-0.0180	0.3775	0.0196	0.9998	-0.0003	-0.3775	0.0063	0.9260	0.3083	0.9264
15	4	3	2.80440	0.33204	0.15044	23.0727	3.2591	3.2840	1.3129	0.5313	0.9190	0.8885	1.0000
			0.9318	0.0275	0.3620	-0.0297	0.9996	0.0006	-0.3619	-0.0088	0.9322	0.3046	0.8928
15	5	3	2.80440	0.42284	0.15044	23.0555	3.9377	3.2842	1.3130	0.5314	0.9192	0.8887	1.0000
			0.9319	0.0182	0.3621	-0.0197	0.9998	0.0004	-0.3621	-0.0059	0.9321	0.3043	0.8930
15	6	3	2.80440	0.51363	0.15044	23.0453	4.6164	3.2843	1.3131	0.5314	0.9192	0.8888	1.0000
			0.9321	0.0091	0.3622	-0.0098	1.0000	0.0001	-0.3622	-0.0030	0.9321	0.3044	0.8929
15	7	3	2.80440	0.60443	0.15044	23.0419	5.2955	3.2843	1.3131	0.5314	0.9192	0.8888	1.0000
			0.9321	0.0000	0.3622	-0.0000	1.0000	-0.0000	-0.3622	-0.0000	0.9321	0.3044	0.8928
15	8	3	2.80440	0.69523	0.15044	23.0453	5.9745	3.2843	1.3131	0.5314	0.9192	0.8888	1.0000
			0.9321	-0.0091	0.3622	0.0098	1.0000	-0.0001	-0.3622	0.0030	0.9321	0.3044	0.8929
15	9	3	2.80440	0.78603	0.15044	23.0555	6.6533	3.2842	1.3130	0.5314	0.9192	0.8887	1.0000
			0.9319	-0.0182	0.3621	0.0197	0.9998	-0.0004	-0.3621	0.0059	0.9321	0.3043	0.8930
15	10	3	2.80440	0.87683	0.15044	23.0727	7.3319	3.2840	1.3129	0.5313	0.9190	0.8885	1.0000
			0.9318	-0.0275	0.3620	0.0297	0.9996	-0.0006	-0.3619	0.0088	0.9322	0.3046	0.8928
15	3	4	2.80440	0.15044	0.33204	22.6111	1.8814	4.6653	1.3828	0.5614	0.9037	0.8678	1.0000
			0.9389	0.0473	0.3408	-0.0505	0.9937	0.0004	-0.3405	-0.0143	0.9401	0.7969	0.8427
15	4	4	2.80440	0.33204	0.33204	22.5550	3.2461	4.6653	1.3828	0.5614	0.9042	0.8685	1.0000
			0.9396	0.0279	0.3410	-0.0298	0.9996	0.0003	-0.3409	-0.0085	0.9401	0.7971	0.8425
15	5	4	2.80440	0.42284	0.33204	22.5376	3.9290	4.6653	1.3828	0.5614	0.9044	0.8687	1.0000
			0.9399	0.0185	0.3410	-0.0197	0.9998	0.0002	-0.3410	-0.0056	0.9400	0.7972	0.8424
15	6	4	2.80440	0.51363	0.33204	22.5273	4.6122	4.6654	1.3829	0.5614	0.9044	0.8688	1.0000
			0.9400	0.0092	0.3411	-0.0098	1.0000	0.0001	-0.3411	-0.0028	0.9400	0.7973	0.8423

8.3 Output table II. - Output table II gives the values of variables along the boundary contour of potential surfaces selected by the input. The headings in output table II are as follows:

I	index number for potential surface (constant PHI)
ICP	index number for contour point along boundary of potential surface I
X-CP(DIM), Y-CP(DIM), Z-CP(DIM)	at contour point ICP of potential surface I, values of X,Y,Z coordinates, expressed in same dimensional units as input values of SP(I) (sections 5.6 and 6.3)

Remaining headings for table II are defined under output table I (section 8.2). A sample page of output table II resulting from the sample input in section 7.4 follows.

OUTPUT TABLE NO. II (COORDINATE POINTS ALONG CONTOURS OF SELECTED POTENTIAL SURFACES)

I	ICP	X-CP(DIM)	Y-CP(DIM)	Z-CP(DIM)	Q/Q-UP	MACH NO	RO/RO-UP	P/P-UP
17	16	23.7339	5.2955	10.6006	1.9259	0.8061	0.7972	0.7281
17	17	23.7365	4.6218	10.6002	1.9259	0.8061	0.7972	0.7281
17	18	23.7679	3.9486	10.5500	1.9216	0.8041	0.7983	0.7295
17	19	23.8549	3.2775	10.3952	1.9084	0.7978	0.8019	0.7341
17	20	24.2432	1.9506	9.6664	1.8490	0.7700	0.8176	0.7543
17	21	24.8302	1.1218	8.5152	1.7640	0.7307	0.8395	0.7828
17	22	25.1230	0.9565	7.9289	1.7244	0.7126	0.8495	0.7959
17	23	25.4175	0.9150	7.3359	1.6865	0.6954	0.8589	0.8082
17	24	25.7139	0.9903	6.7365	1.6502	0.6791	0.8678	0.8199
17	25	26.0126	1.1871	6.1306	1.6155	0.6635	0.8762	0.8310
17	26	26.6218	2.0544	4.9016	1.5502	0.6345	0.8915	0.8515
17	27	27.0248	3.3597	4.1001	1.5108	0.6171	0.9005	0.8636
17	28	27.1104	4.0064	3.9286	1.5026	0.6135	0.9024	0.8661
18	1	28.7558	4.6607	4.8332	1.6238	0.6672	0.8742	0.8284
18	2	28.7537	5.2955	4.8339	1.6238	0.6672	0.8742	0.8284
18	3	28.7558	5.9303	4.8332	1.6238	0.6672	0.8742	0.8284
18	4	28.7292	6.5655	4.8844	1.6261	0.6683	0.8736	0.8276
18	5	28.6372	7.2027	5.0450	1.6333	0.6715	0.8719	0.8254
18	6	28.2048	8.4895	5.7998	1.6678	0.6870	0.8635	0.8143
17	7	27.5470	9.3456	6.9658	1.7241	0.7125	0.8496	0.7960
18	8	27.2229	9.5406	7.5442	1.7538	0.7260	0.8421	0.7862
18	9	26.9008	9.6161	8.1186	1.7844	0.7401	0.8343	0.7760
18	10	26.5803	9.5763	8.6890	1.8162	0.7548	0.8261	0.7654
18	11	26.2611	9.4142	9.2552	1.8491	0.7700	0.8176	0.7543
18	12	25.6212	8.5980	10.3732	1.9186	0.8026	0.7991	0.7306
18	13	25.1999	7.2887	11.0851	1.9664	0.8253	0.7862	0.7141
18	14	25.1064	6.6260	11.2367	1.9769	0.8303	0.7833	0.7104
18	15	25.0736	5.9610	11.2864	1.9803	0.8320	0.7824	0.7093
18	16	25.0714	5.2955	11.2870	1.9803	0.8320	0.7824	0.7093
18	17	25.0736	4.6300	11.2864	1.9803	0.8320	0.7824	0.7093
18	18	25.1064	3.9650	11.2367	1.9769	0.8303	0.7833	0.7104
18	19	25.1999	3.3023	11.0851	1.9664	0.8253	0.7862	0.7141
18	20	25.6212	1.9930	10.3732	1.9186	0.8026	0.7991	0.7306
18	21	26.2611	1.1768	9.2552	1.8491	0.7700	0.8176	0.7543
18	22	26.5803	1.0147	8.6890	1.8162	0.7548	0.8261	0.7654
18	23	26.9008	0.9749	8.1186	1.7844	0.7401	0.8343	0.7760
18	24	27.2229	1.0504	7.5442	1.7538	0.7260	0.8421	0.7862
18	25	27.5470	1.2453	6.9658	1.7241	0.7125	0.8496	0.7960
18	26	28.2048	2.1015	5.7998	1.6678	0.6870	0.8635	0.8143
18	27	28.6372	3.3883	5.0450	1.6333	0.6715	0.8719	0.8254
18	28	28.7292	4.0255	4.8844	1.6261	0.6683	0.8736	0.8276
19	1	30.2546	4.6668	5.7945	1.7407	0.7201	0.8454	0.7905
19	2	30.2529	5.2955	5.7954	1.7407	0.7201	0.8454	0.7905
19	3	30.2546	5.9242	5.7945	1.7407	0.7201	0.8454	0.7905
19	4	30.2261	6.5533	5.8428	1.7425	0.7209	0.8450	0.7899
19	5	30.1303	7.1844	5.9950	1.7480	0.7234	0.8436	0.7881

8.4 Output table III. - Output table III gives the values of various variables along streamlines (constant ICP) selected by the input. X-SL(DIM), Y-SL(DIM), and Z-SL(DIM) are values of the X,Y,Z coordinates, respectively, along the streamline. The next four headings are the same as defined for output table II (section 8.3). The last two headings are the lengths (same dimension as SP(I)) of the streamline ICP computed in two ways as follows:

$$S\text{-}I(DIM) = \sum_{I=2}^{I=I} \left[(\Delta X)^2 + (\Delta Y)^2 + (\Delta Z)^2\right]^{1/2} \tag{8.4.1}$$

where $\Delta X = X(I) - X(I - 1)$, etc.

and

$$S\text{-}II(DIM) = \int_0^\varphi \frac{d\varphi}{q} \tag{8.4.2}$$

A sample page of output table III resulting from the sample input in section 7.4 follows:

OUTPUT TABLE NO. III (COORDINATE POINTS ALONG SELECTED STREAMLINES)

ICP	I	X-SL(DIM)	Y-SL(DIM)	Z-SL(DIM)	Q/Q-UP	MACH NO	RO/RO-UP	P/P-UP	S-I(DIM)	S-II(DIM)
10	18	26.5803	9.5763	8.6890	1.8162	0.7548	0.8261	0.7654	27.1785	27.2304
10	19	27.9671	9.5391	9.4967	1.8845	0.7866	0.8082	0.7422	28.7838	28.8444
10	20	29.2937	9.5172	10.3293	1.9326	0.8093	0.7954	0.7257	30.3502	30.4165
10	21	30.5765	9.5046	11.1714	1.9688	0.8265	0.7855	0.7132	31.8848	31.9545
10	22	31.8326	9.4984	12.0154	1.9918	0.8375	0.7792	0.7052	33.3981	33.4695
10	23	33.0760	9.4972	12.8591	2.0000	0.8414	0.7770	0.7024	34.9008	34.9725
10	24	34.3162	9.4984	13.7032	2.0000	0.8414	0.7770	0.7024	36.4009	36.4725
10	25	35.5565	9.4995	14.5477	2.0000	0.8414	0.7770	0.7024	37.9015	37.9725
10	26	36.7971	9.5000	15.3922	2.0000	0.8414	0.7770	0.7024	39.4022	39.4725
10	27	38.0374	9.5000	16.2365	2.0000	0.8414	0.7770	0.7024	40.9025	40.9725
10	28	39.2769	9.5001	17.0808	2.0000	0.8414	0.7770	0.7024	42.4023	42.4725
10	29	40.5163	9.5003	17.9258	2.0000	0.8414	0.7770	0.7024	43.9023	43.9725
11	1	0.0000	10.3004	6.0910	1.0000	0.4000	1.0000	1.0000	0.0000	0.0000
11	2	1.5000	10.3002	6.0909	1.0000	0.4000	1.0000	1.0000	1.5000	1.5000
11	3	3.0010	10.2995	6.0906	1.0000	0.4000	1.0000	1.0000	3.0010	3.0000
11	4	4.5015	10.2985	6.0902	1.0000	0.4000	1.0000	1.0000	4.5015	4.5000
11	5	6.0020	10.2964	6.0894	1.0000	0.4000	1.0000	1.0000	6.0020	6.0000
11	6	7.5024	10.2921	6.0878	1.0000	0.4000	1.0000	1.0000	7.5024	7.5000
11	7	9.0025	10.2823	6.0851	1.0000	0.4000	1.0000	1.0000	9.0026	9.0000
11	8	10.5069	10.2566	6.0810	1.0132	0.4055	0.9979	0.9970	10.5072	10.5049
11	9	12.0288	10.2086	6.0801	1.0490	0.4203	0.9920	0.9888	12.0298	12.0283
11	10	13.5837	10.1430	6.0961	1.1007	0.4418	0.9832	0.9765	13.5862	13.5855
11	11	15.1835	10.0662	6.1518	1.1619	0.4674	0.9722	0.9613	15.1888	15.1881
11	12	16.8276	9.9757	6.2757	1.2365	0.4988	0.9582	0.9420	16.8401	16.8380
11	13	18.4936	9.8688	6.4955	1.3296	0.5385	0.9397	0.9166	18.5239	18.5215
11	14	20.1495	9.7535	6.8298	1.4361	0.5845	0.9172	0.8860	20.2171	20.2182
11	15	21.7684	9.6423	7.2840	1.5493	0.6341	0.8917	0.8518	21.9022	21.9112
11	16	23.3319	9.5457	7.8511	1.6613	0.6841	0.8651	0.8164	23.5681	23.5879
11	17	24.8302	9.4692	8.5152	1.7640	0.7307	0.8395	0.7828	25.2088	25.2402
11	18	26.2611	9.4142	9.2552	1.8491	0.7700	0.8176	0.7543	26.8207	26.8627
11	19	27.6287	9.3790	10.0476	1.9081	0.7977	0.8019	0.7342	28.4017	28.4522
11	20	28.9431	9.3581	10.8699	1.9467	0.8159	0.7915	0.7209	29.9523	30.0088
11	21	30.2195	9.3459	11.7059	1.9754	0.8296	0.7837	0.7109	31.4781	31.5387
11	22	31.4729	9.3399	12.5468	1.9936	0.8383	0.7788	0.7046	32.9875	33.0504
11	23	32.7158	9.3386	13.3892	2.0000	0.8414	0.7770	0.7024	34.4889	34.5529
11	24	33.9559	9.3397	14.2327	2.0000	0.8414	0.7770	0.7024	35.9887	36.0529
11	25	35.1962	9.3408	15.0770	2.0000	0.8414	0.7770	0.7024	37.4891	37.5529
11	26	36.4367	9.3412	15.9216	2.0000	0.8414	0.7770	0.7024	38.9898	39.0529
11	27	37.6768	9.3412	16.7659	2.0000	0.8414	0.7770	0.7024	40.4901	40.5529
11	28	38.9162	9.3412	17.6102	2.0000	0.8414	0.7770	0.7024	41.9898	42.0529
11	29	40.1557	9.3414	18.4550	2.0000	0.8414	0.7770	0.7024	43.4898	43.5529
12	1	0.0000	9.2730	7.6820	1.0000	0.4000	1.0000	1.0000	0.0000	0.0000
12	2	1.5000	9.2727	7.6818	1.0000	0.4000	1.0000	1.0000	1.5000	1.5000
12	3	3.0009	9.2720	7.6814	1.0000	0.4000	1.0000	1.0000	3.0000	3.0000
12	4	4.5014	9.2707	7.6808	1.0000	0.4000	1.0000	1.0000	4.5014	4.5000
12	5	6.0019	9.2682	7.6793	1.0000	0.4000	1.0000	1.0000	6.0019	6.0000

8.5 Output to tape or disk for three-dimensional graphics. - Output to tape or disk for three-dimensional graphics occurs at the end of subroutine PUTOUT and is described in section 6.3. A three-dimensional plot resulting from the sample input in section 7.4 follows. Running time on an IBM 370/3033 was 6.50 min.
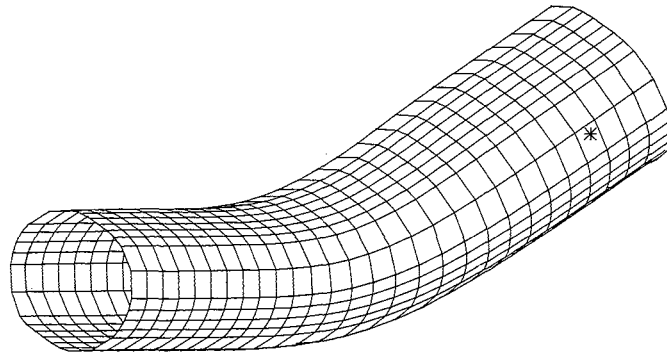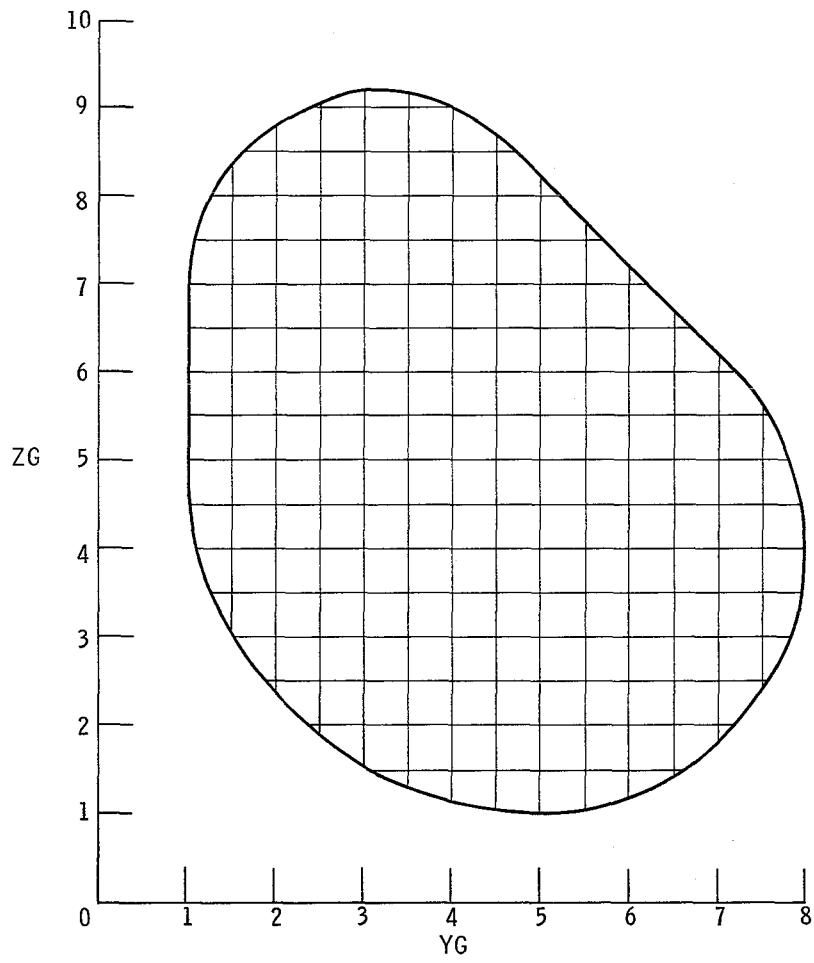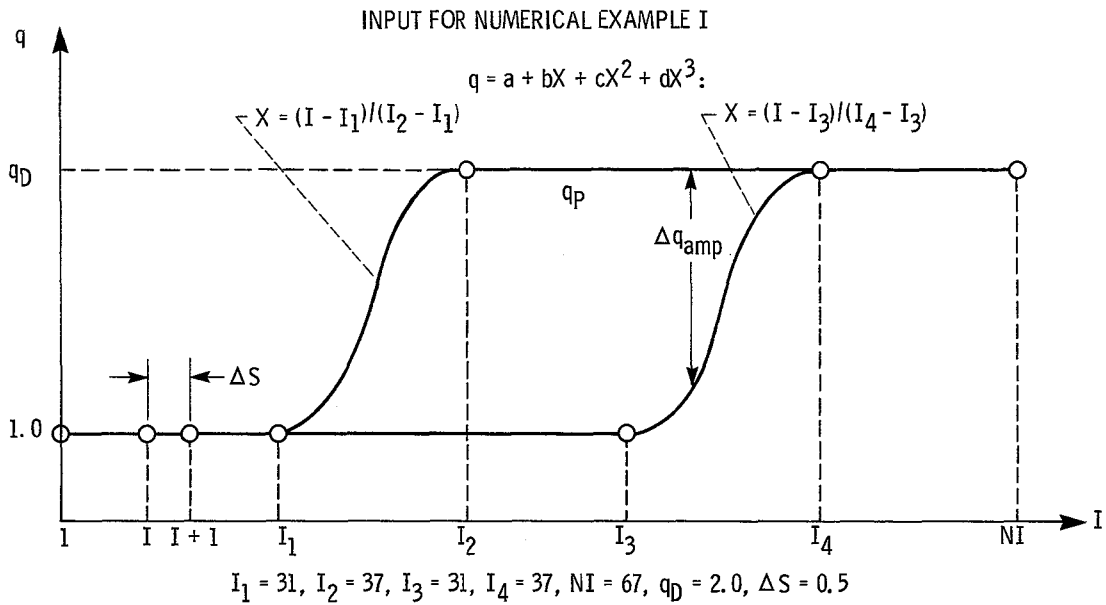
9.0 NUMERICAL EXAMPLES

Five numerical examples of ducts are presented. For each example, the upstream boundary configuration and associated grid are given together with the prescribed velocity distribution on the lateral surface and a number of key input parameters. The results are presented by three-dimensional graphs. The first example is a completely general three-dimensional nozzle with a nonsymmetrical upstream boundary configuration and rapid acceleration of the flow with no deceleration along the surface streamlines. The second example is an accelerating elbow with the same upstream boundary configuration and again no deceleration along the surface streamlines. The third example is an accelerating S-duct with an elliptical upstream boundary configuration. The fourth example is a rapidly decelerating elbow with a circular upstream boundary and an unusually sharp turning angle. This solution, like the others, can be reversed to give, in this case, a rapidly accelerating elbow with no deceleration along the surface streamlines. Of special interest in this example is the pronounced initial turning of the inner wall in a direction opposite to that of the elbow itself. This phenomenon has also been observed (ref. 3) in designs of two-dimensional ducts. The last example is a preliminary design of a side-inlet duct such as might be used with various types of turbomachinery. The solution has planar symmetry (with a small amount of overlap in one region), and for the reverse flow case, is an accelerating flow into a circular annulus with no deceleration anywhere along the duct walls.

9.1 <u>Numerical example I</u>. - Straight, three-dimensional nozzle with rapid acceleration (no deceleration along streamlines)
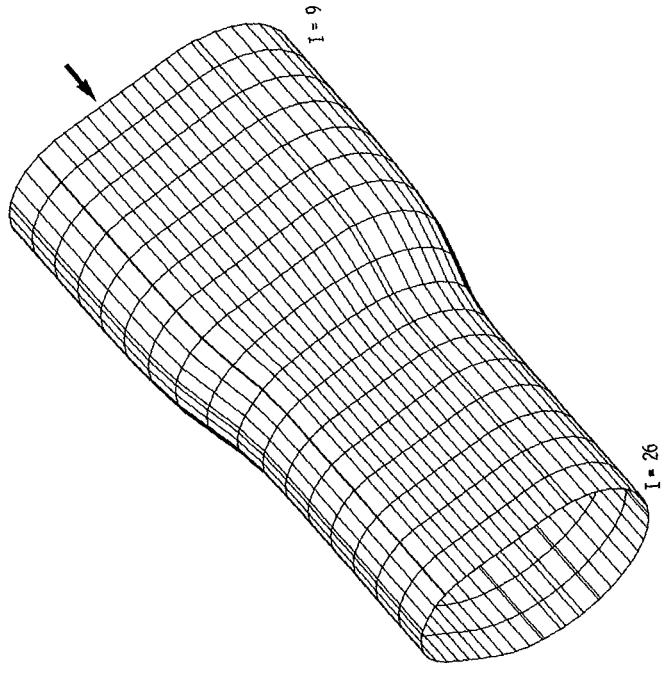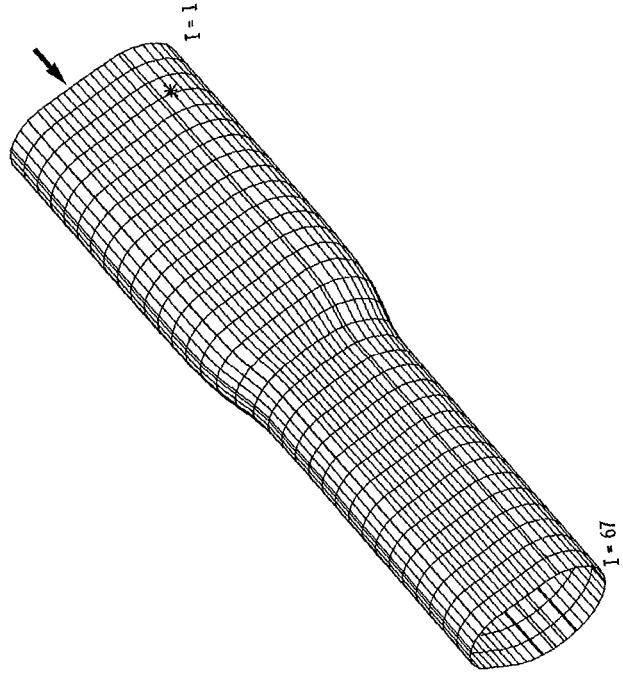
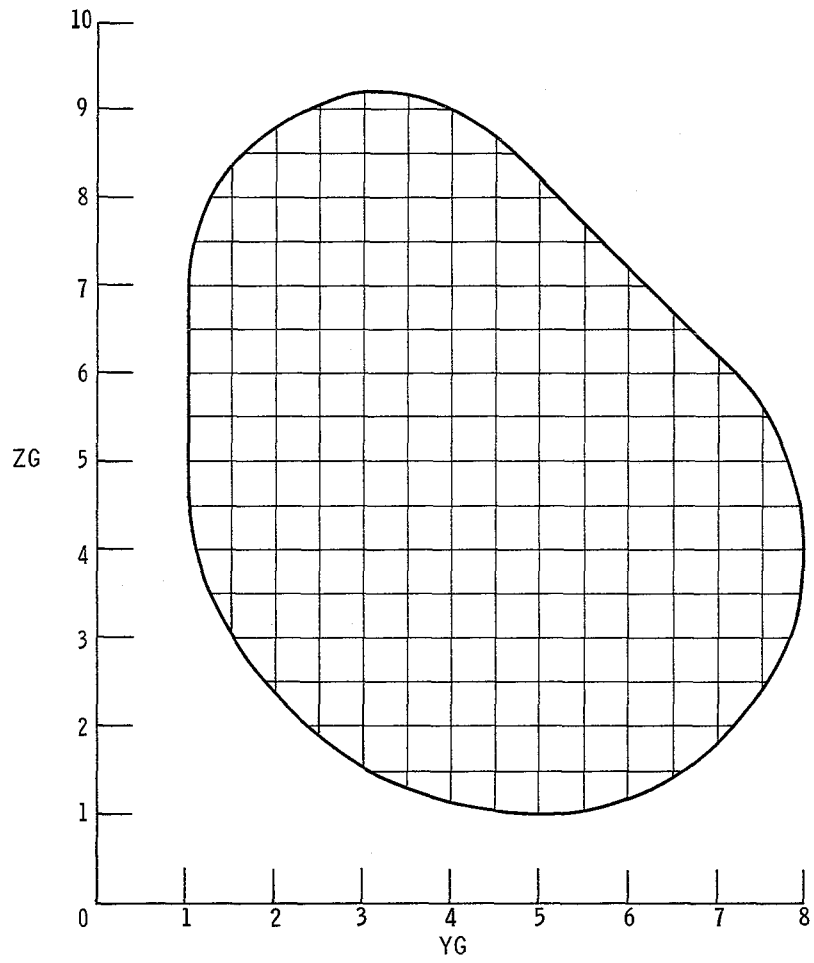NUMERICAL EXAMPLE I – UPSTREAM BOUNDARY AND ASSOCIATED GRID

INPUT FOR NUMERICAL EXAMPLE I

$$q = a + bX + cX^2 + dX^3:$$

$X = (I - I_1)/(I_2 - I_1)$

$X = (I - I_3)/(I_4 - I_3)$

q_D

q_P

Δq_{amp}

ΔS

1.0

$I_1 = 31,\ I_2 = 37,\ I_3 = 31,\ I_4 = 37,\ NI = 67,\ q_D = 2.0,\ \Delta S = 0.5$

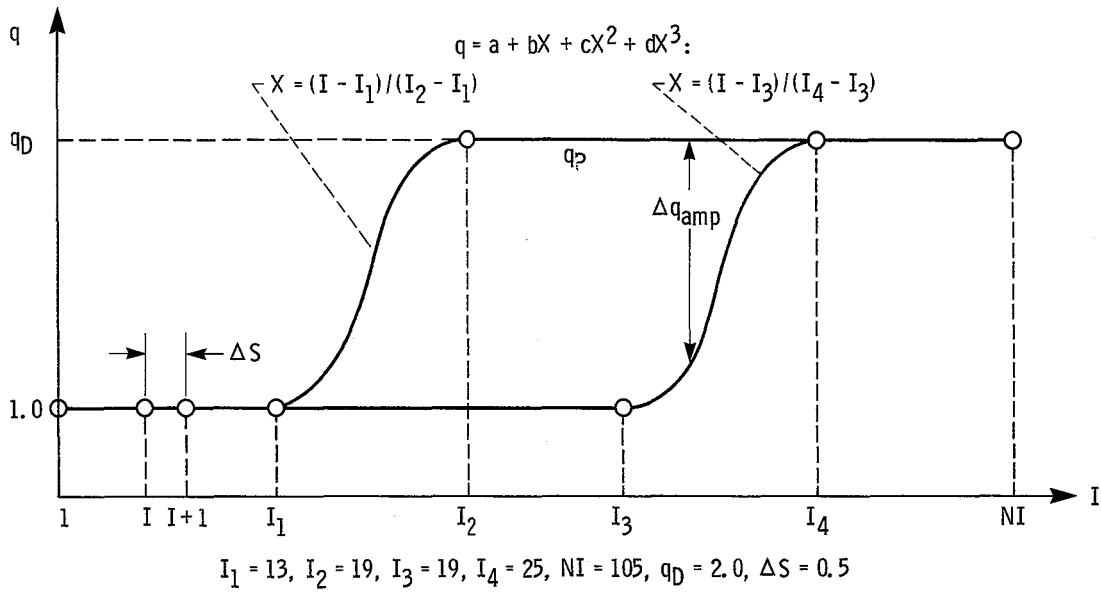|			
Option ISYM	= 1	Accuracy of finite-difference solution (EPSR)	= 0.000005
Option IVEL	= 1	Overrelaxation factor (ORELAX)	= 1.35
Major iterations (ITER)	= 4	Exit-area error (ERRAR)	= 0.0005
Coefficient to average x, y, z (CAVP)	= 0.5	Running time (370/3033), min	= 55.69
Upstream Mach number (AMU)	= 0.4	DEL-P-01	= 0.3
Ratio of specific heats (GAM)	= 1.4	DEL-P-12	= 0.2
J location of primary streamline (JX)	= 9	DEL-P-23	= 0.3
K location of primary streamline (KX)	= 12	Location of principal streamline (XP)	= 0.9
Number of subdivisions between adjacent input values of I (NSD)	= 1		

NUMERICAL EXAMPLE I

I = 1

I = 67

I = 9

I = 26

9.2 Numerical example II. – General case of three-dimensional accelerating elbow (no deceleration along streamlines)

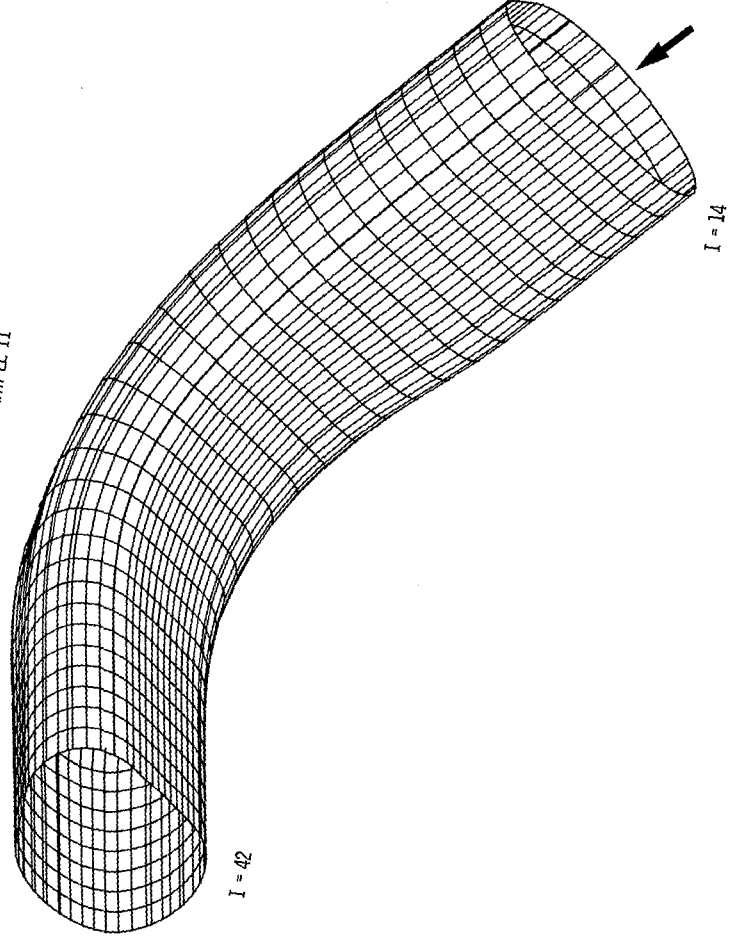NUMERICAL EXAMPLE II - UPSTREAM BOUNDARY AND ASSOCIATED GRID
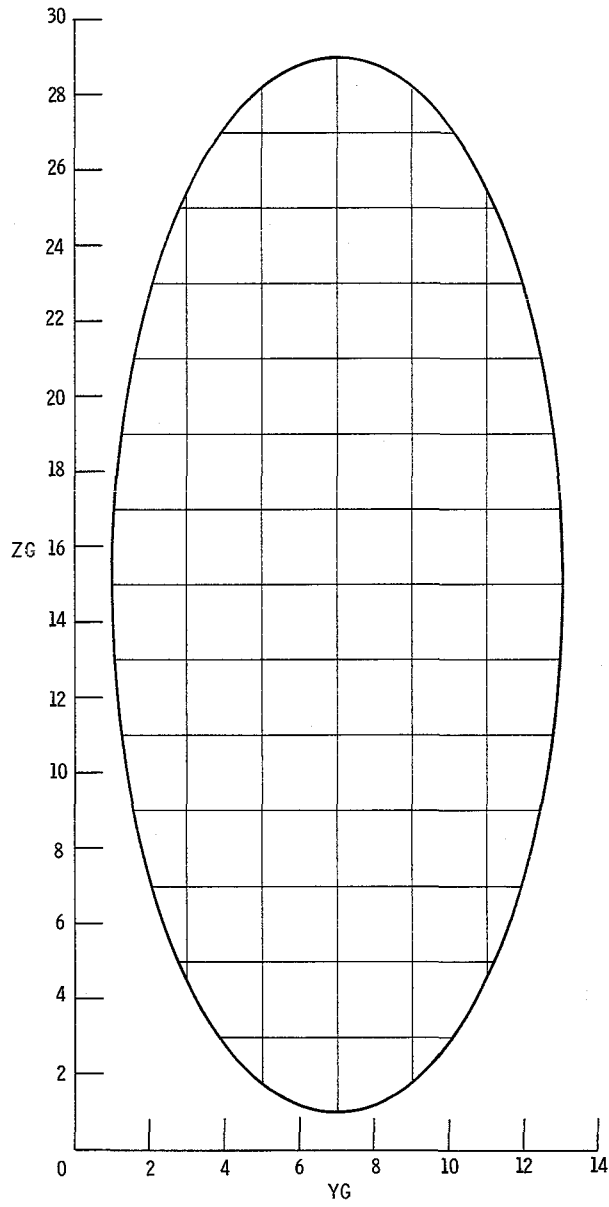
INPUT FOR NUMERICAL EXAMPLE II

$$q = a + bX + cX^2 + dX^3:$$

$$X = (I - I_1)/(I_2 - I_1)$$

$$X = (I - I_3)/(I_4 - I_3)$$

q

q_D

q_p

Δq_{amp}

ΔS

1.0

1   I I+1 I_1 I_2 I_3 I_4 NI   I

$$I_1 = 13, \ I_2 = 19, \ I_3 = 19, \ I_4 = 25, \ NI = 105, \ q_D = 2.0, \ \Delta S = 0.5$$

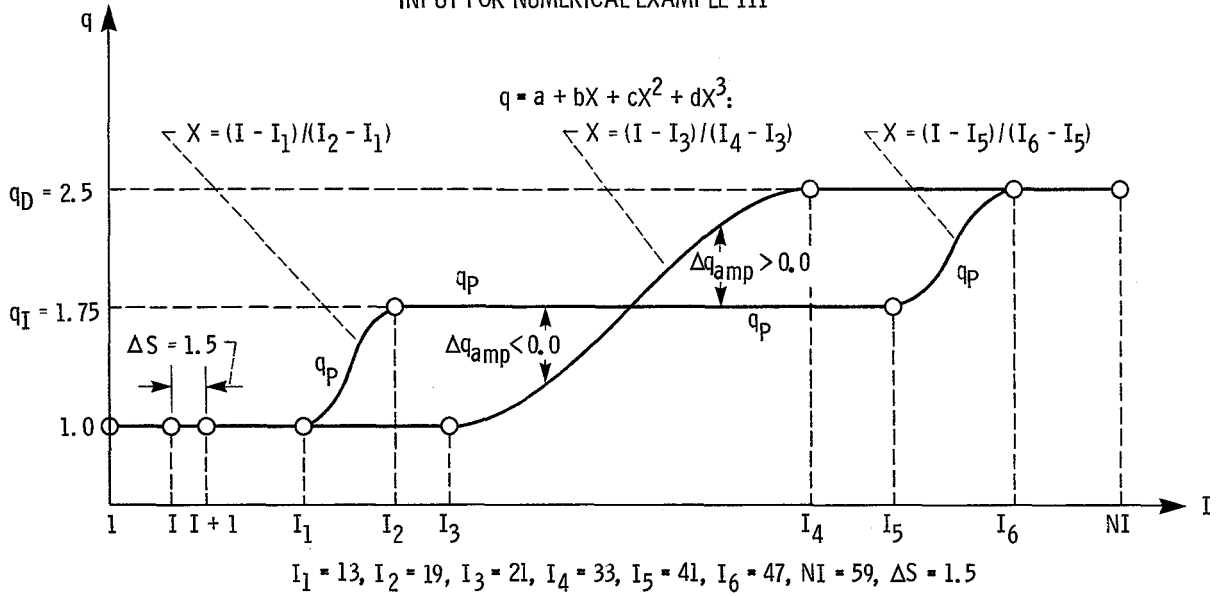|				
Option ISYM	= 1	Accuracy of finite-difference solution (EPSR)	=	0.000005
Option IVEL	= 1	Overrelaxation factor (ORELAX)	=	1.30
Major iterations (ITER)	= 4	Exit-area error (ERRAR)	=	-0.0019
Coefficient to average x, y, z (CAVP)	= 0.2	Running time (370/3033), min	=	103.14
Upstream Mach number (AMU)	= 0.4	DEL-P-01	=	0.3
Ratio of specific heats (GAM)	= 1.4	DEL-P-12	=	0.2
J location of primary streamline (JX)	= 9	DEL-P-23	=	0.3
K location of primary streamline (KX)	= 12	Location of principal streamline (XP)	=	0.9
Number of subdivisions between adjacent input values of I (NSD)	= 3			

NUMERICAL EXAMPLE II

I = 42

I = 14

9.3 Numerical example III. – Accelerating S-duct with elliptical upstream boundary (no deceleration along streamlines)

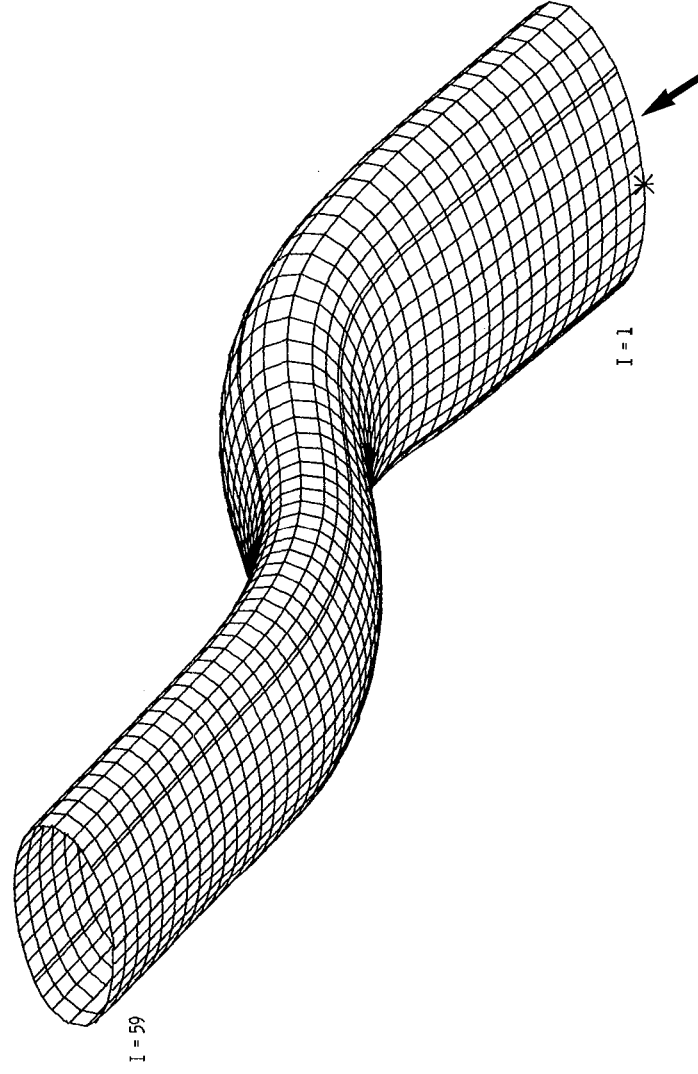NUMERICAL EXAMPLE III - UPSTREAM BOUNDARY
AND ASSOCIATED GRID

INPUT FOR NUMERICAL EXAMPLE III

$q = a + bX + cX^2 + dX^3$:

$X = (I - I_1)/(I_2 - I_1)$ $X = (I - I_3)/(I_4 - I_3)$ $X = (I - I_5)/(I_6 - I_5)$

$q_D = 2.5$

$q_I = 1.75$

$\Delta q_{amp} > 0.0$

q_P

q_P

q_P

$\Delta S = 1.5$

q_P

$\Delta q_{amp} < 0.0$

q_P

1.0

$1 \quad I \ I+1 \quad I_1 \quad I_2 \ I_3 \qquad\qquad I_4 \ I_5 \qquad I_6 \qquad NI$

I

$I_1 = 13, \ I_2 = 19, \ I_3 = 21, \ I_4 = 33, \ I_5 = 41, \ I_6 = 47, \ NI = 59, \ \Delta S = 1.5$

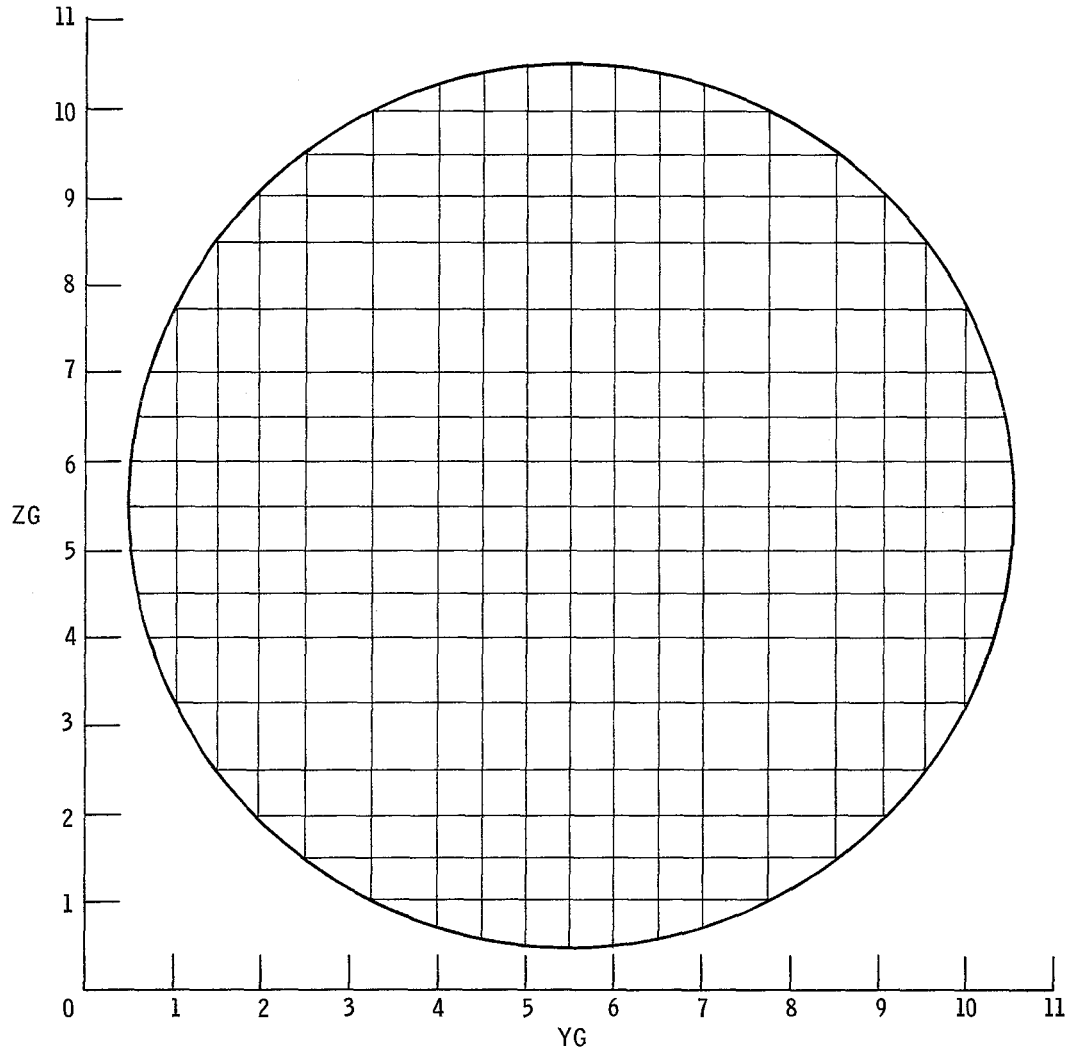|			
Option ISYM	= 1 ;	Accuracy of finite-difference solution (EPSR)	= 0.000005
Option IVEL	= 3 ;	Overrelaxation factor (ORELAX)	= 1.30
Major iterations (ITER)	= 10 ;	Exit-area error (ERRAR)	= 0.0005
Coefficient to average x, y, z (CAVP)	= 0.2 ;	Running time (370/3033), min	= 29.64
Upstream Mach number (AMU)	= 0.3 ;	DEL-P-01	= *
Ratio of specific heats (GAM)	= 1.4 ;	DEL-P-12	= *
J location of primary streamline (JX)	= 4 ;	DEL-P-23	= *
K location of primary streamline (KX)	= 8 ;	Location of principal streamline (XP)	= *
Number of subdivisions between adjacent input values of I (NSD)	= 1 ;		

*Not applicable.

64

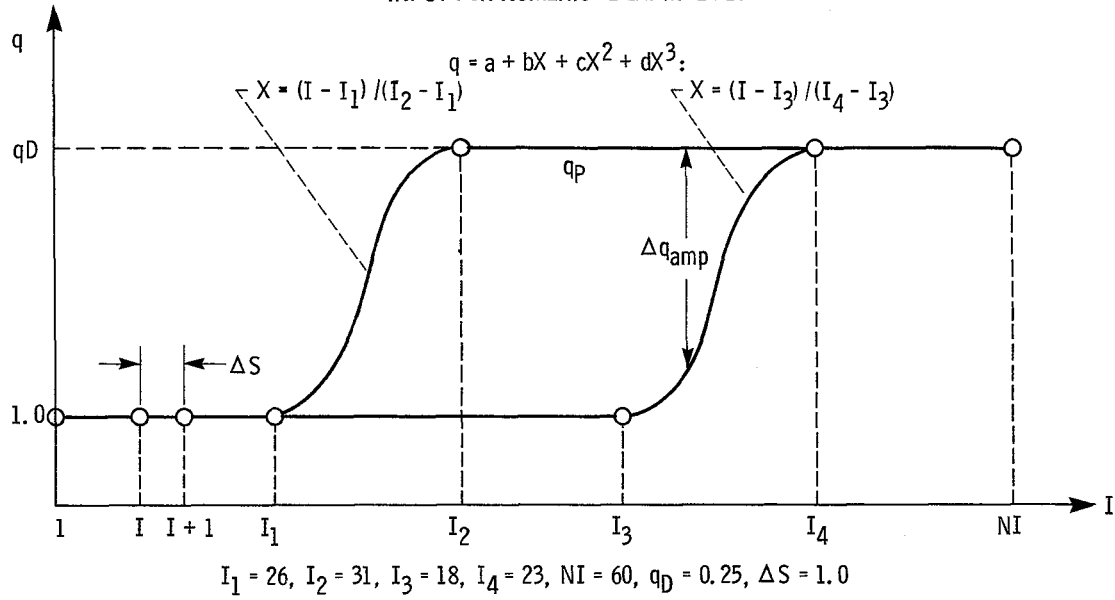NUMERICAL EXAMPLE III

I = 59

I = 1

9.4 <u>Numerical example IV</u>. – Decelerating elbow with sharp turn and circular upstream boundary (no deceleration for reversed flow)

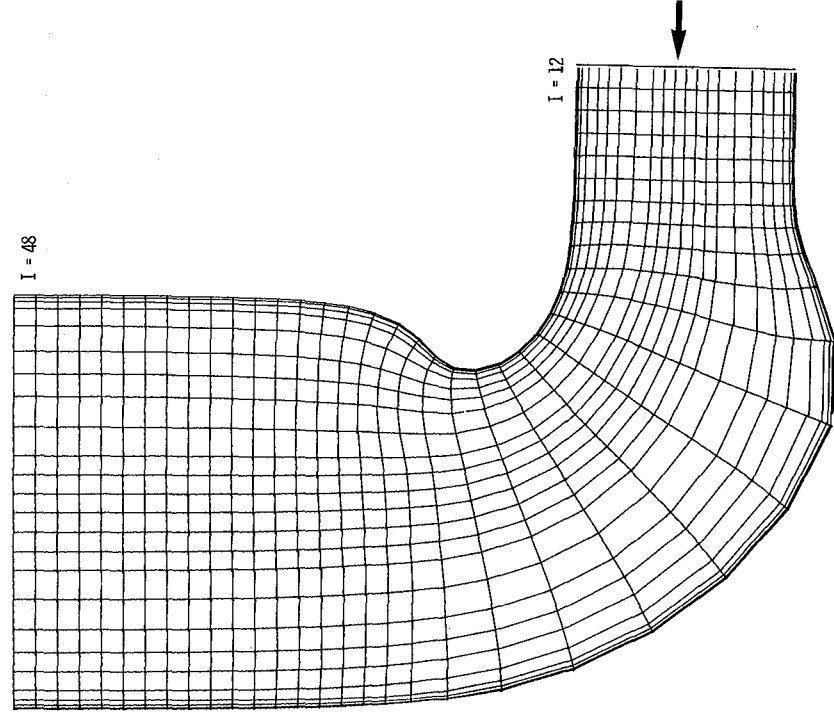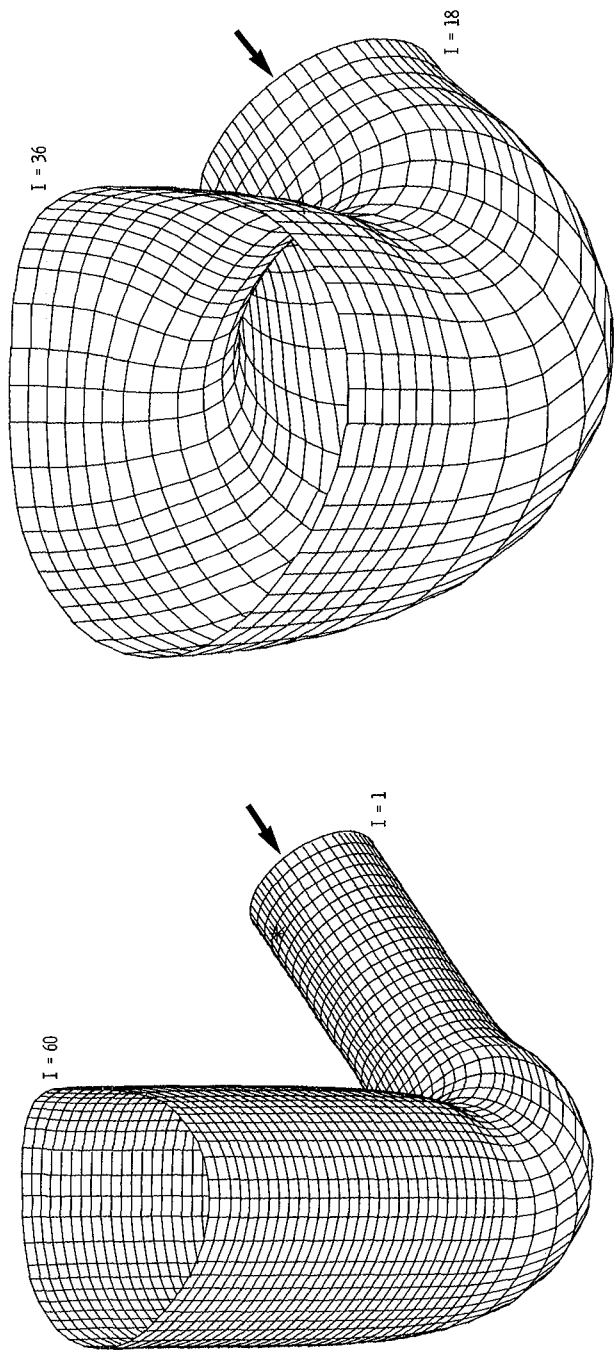NUMERICAL EXAMPLE IV - UPSTREAM BOUNDARY AND ASSOCIATED GRID

INPUT FOR NUMERICAL EXAMPLE IV

$q = a + bX + cX^2 + dX^3$:

$X = (I - I_1)/(I_2 - I_1)$

$X = (I - I_3)/(I_4 - I_3)$

$I_1 = 26, I_2 = 31, I_3 = 18, I_4 = 23, NI = 60, q_D = 0.25, \Delta S = 1.0$

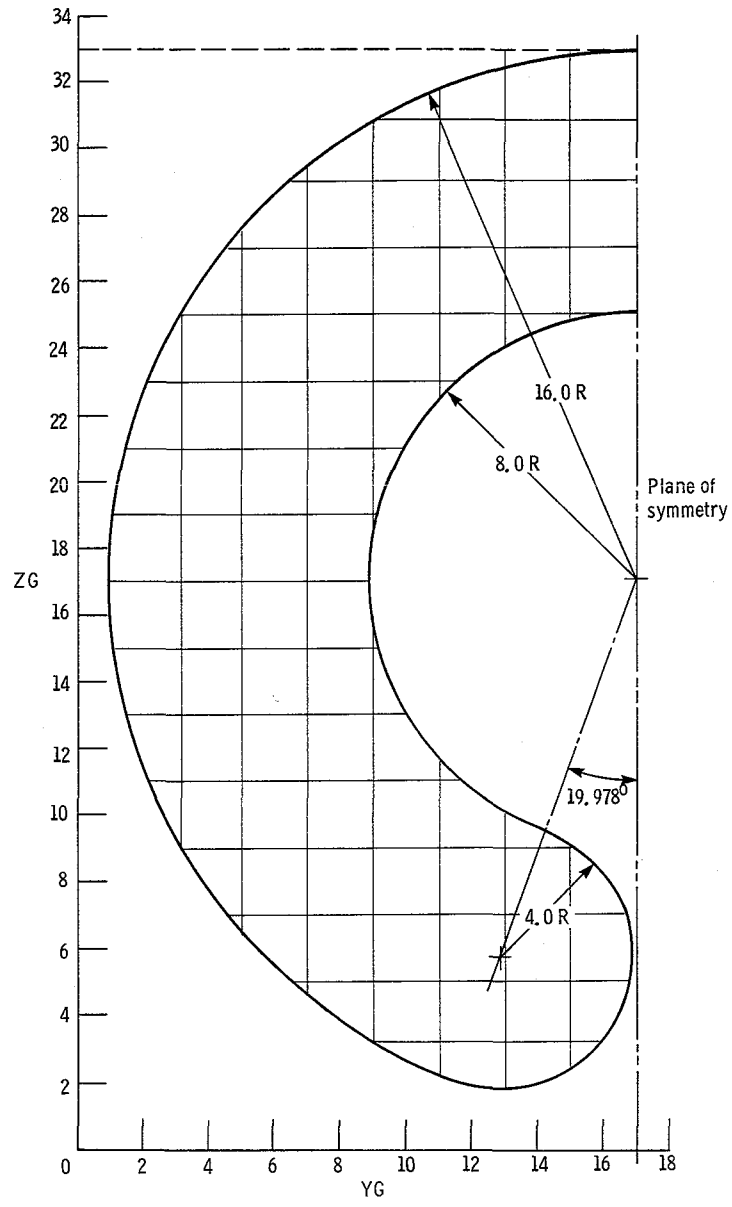|				
Option ISYM	= 1	Accuracy of finite-difference solution (EPSR)	=	0.000005
Option IVEL	= 2	Overrelaxation factor (ORELAX)	=	1.30
Major iterations (ITER)	= 4	Exit-area error (ERRAR)	=	0.0024
Coefficient to average x, y, z (CAVP)	= 0.0	Running time (370/3033), min	=	121.88
Upstream Mach number (AMU)	= 0.6	DEL-P-01	=	*
Ratio of specific heats (GAM)	= 1.4	DEL-P-12	=	*
J location of primary streamline (JX)	= 10	DEL-P-23	=	*
K location of primary streamline (KX)	= 10	Location of principal streamline (XP)	=	*
Number of subdivisions between adjacent input values of I (NSD)	= 1			

* Not applicable.

68

NUMERICAL EXAMPLE IV
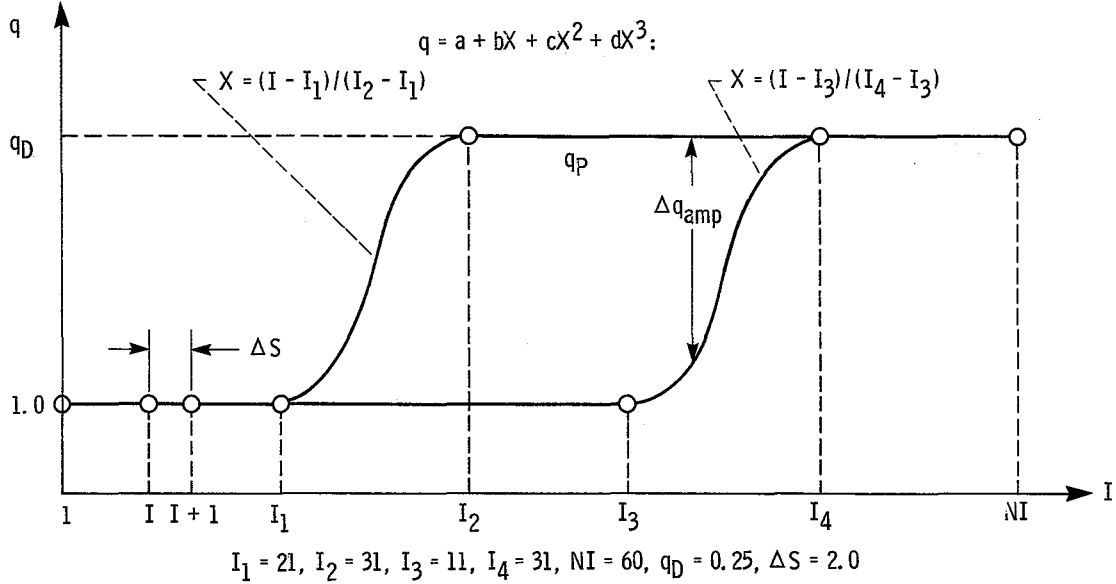
I = 36

I = 18

I = 1

I = 60

I = 48

I = 12

9.5 Numerical example V. - Planar symmetry solution for side inlet (in reversed-flow case; no deceleration for reversed-flow direction)

NUMERICAL EXAMPLE V – UPSTREAM BOUNDARY AND ASSOCIATED GRID

INPUT FOR NUMERICAL EXAMPLE V

$$q = a + bX + cX^2 + dX^3:$$

$X = (I - I_1)/(I_2 - I_1)$

$X = (I - I_3)/(I_4 - I_3)$

$I_1 = 21, \ I_2 = 31, \ I_3 = 11, \ I_4 = 31, \ NI = 60, \ q_D = 0.25, \ \Delta S = 2.0$

Option ISYM	= 2	Accuracy of finite-difference solution (EPSR)	= 0.000005
Option IVEL	= 2	Overrelaxation factor (ORELAX)	= 1.30
Major iterations (ITER)	= 6	Exit-area error (ERRAR)	= 0.0110
Coefficient to average x, y, z (CAVP)	= 0.0	Running time (370/3033), min	= 33.05
Upstream Mach number (AMU)	= 0.6	DEL-P-01	= *
Ratio of specific heats (GAM)	= 1.4	DEL-P-12	= *
J location of primary streamline (JX)	= 9	DEL-P-23	= *
K location of primary streamline (KX)	= 15	Location of principal streamline (XP)	= *
Number of subdivisions between adjacent input values of I (NSD)	= 1		

---

* Not applicable.

NUMERICAL EXAMPLE V

I = 60

I = 1

73
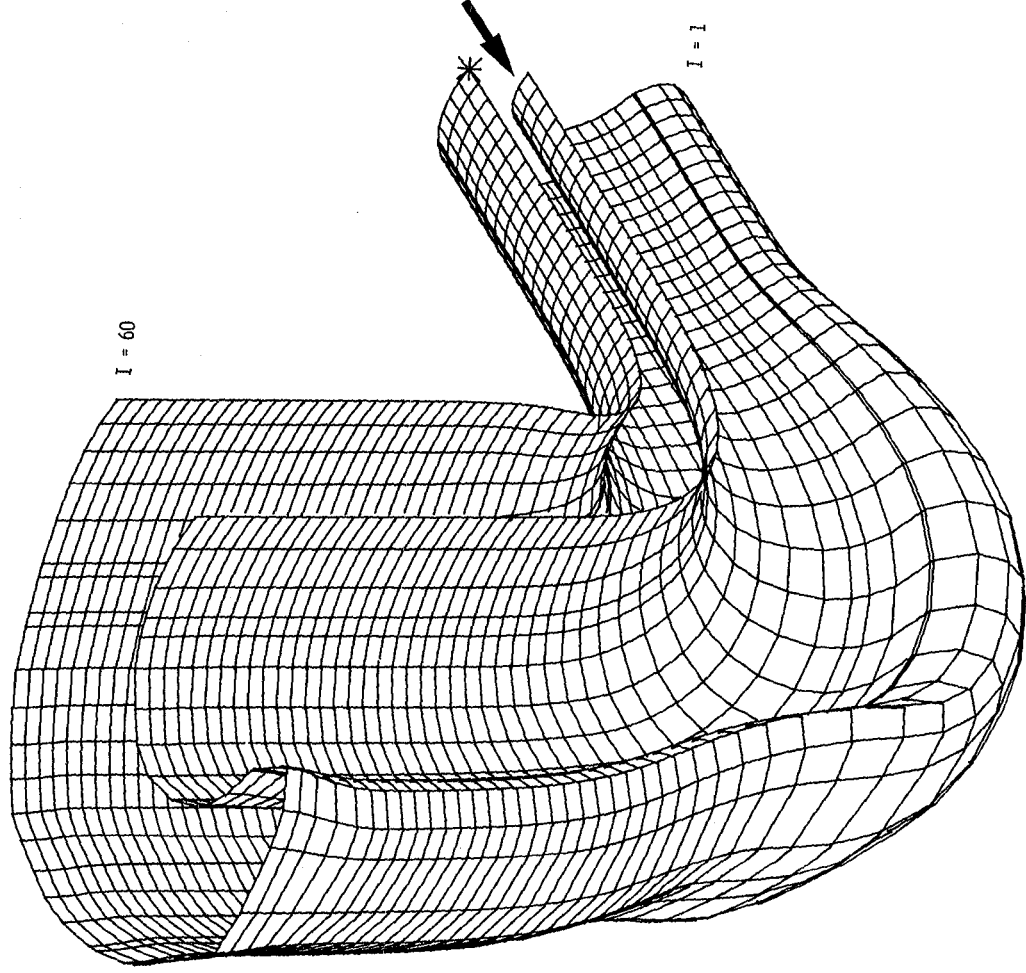
10.0 CONCLUDING REMARKS

The general design method for three-dimensional, potential flow developed in part I of this report (ref. 1) is herein applied to the design of simple, unbranched ducts. A computer program, DIN3D1, is developed and five numerical examples are presented, including a nozzle, two elbows, an S-duct, and the preliminary design of a side inlet for turbomachines. The two major inputs to the program are the upstream boundary configuration and the lateral velocity distribution on the duct wall. As a result of these inputs, boundary conditions of the problem are overprescribed and the problem is ill posed. However, it appears that there are degrees of "compatibility" between the two major inputs and that for reasonably compatible inputs satisfactory, reliable solutions can be obtained. By not prescribing the shape of the upstream boundary, the problem presumably becomes well posed, but it is not clear how to carry out a practical design method under this circumstance. Nor does it appear desirable, because the designer usually needs to retain control over the upstream (or downstream) boundary configuration.

The problem is further complicated by the fact that, unlike the two-dimensional case, and irrespective of the upstream boundary shape, some prescribed lateral velocity distributions do not have proper solutions (appendix C).

The input data for an example solution together with example output tables and a three-dimensional plot of the solution are given in sections 7.4 and 8.1 to 8.5, respectively.

APPENDIX A

"EQUILIBRIUM" VELOCITY DISTRIBUTIONS FOR
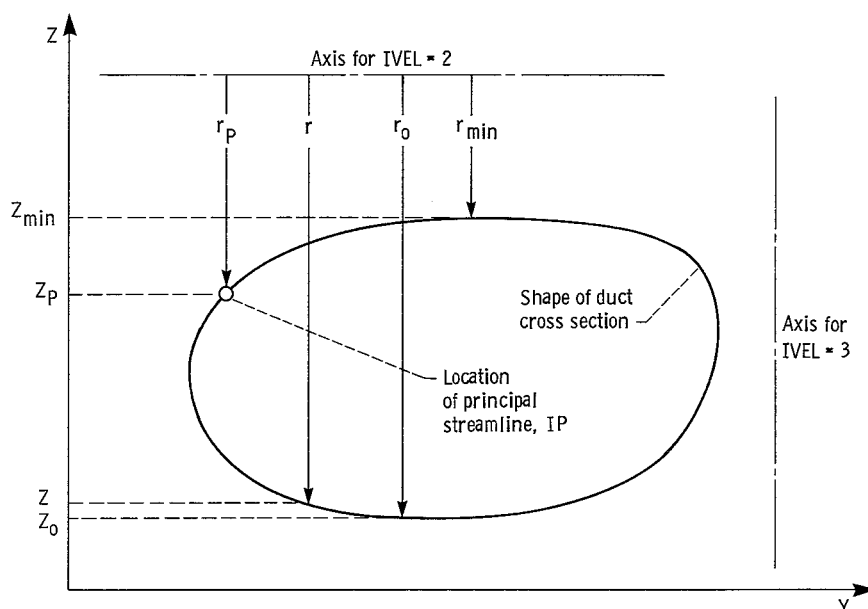
INPUT OPTION IVEL EQUAL TO 2 OR 3

The "equilibrium" velocity distributions for input option IVEL equal to 2 or 3 refer to the velocity distributions around the contours of the potential surfaces; the velocity distribution along the principal streamline (section 7.2) is not affected. Variation in the velocity distribution around the contour (e.g., DQ in second fig. of section 7.2) causes the duct to bend and may be looked upon as the duct "loading."

Consider potential flow in an infinitely long duct with constant loading. Such a duct will turn an infinite number of degrees, and the duct cross section will be constant. Under these circumstances, the potential surfaces are flat planes, and the "equilibrium" velocity distribution normal to the planes is a free vortex

$$qr = \text{constant} \tag{A1}$$

where the radius r is measured from the axis about which the duct bends.

Such an equilibrium duct shape halfway between $\pm\infty$ can be considered to lie on the Y,Z plane corresponding to the upstream boundary. Thus,

Z

Axis for IVEL = 2

r_p r r_0 r_{min}

Z_{min}

Z_p

Shape of duct
cross section

Axis for
IVEL = 3

Location
of principal
streamline, IP

Z
Z_0

Y

For IVEL = 2, the axis of the bend is a line of constant Z; and for IVEL = 3, the axis is a line of constant Y, as shown.

For IVEL equal to 2 or 3, the "equilibrium" shape is assumed to be the input shape of the upstream boundary and the lateral velocity distribution corresponds to the "equilibrium" velocity based on that shape. (Other shapes could be used, but these would entail additional input and probably would not achieve the same degree of compatibility (section 4.1) between the prescribed upstream boundary shape and the prescribed lateral velocity distribution.)

For IVEL = 2, equation (A1) gives

$$qr = q_P r_P = \left(q_P + \Delta q_{amp}\right) r_o \tag{A2}$$

where (preceding figure) the subscript P refers to the principal streamline (at which q_P is the input value of $QP(I)$) and subscript o refers to the maximum (outer) radius where q is equal to $q_P + \Delta q_{amp}$ and Δq_{amp} is the input value (negative) of $DQAMP(I)$ at potential surface I. (Note that $DQAMP(I)$ for IVEL options 2 and 3, as opposed to option 1, is the difference between the minimum velocity, which occurs at r_o in the figure, and the input velocity $QP(I)$ of the principal streamline.)

In the figure, the radius r is related to the Z coordinate by

$$r = r_P + \left(r_o - r_P\right)\left(\frac{Z_P - Z}{Z_P - Z_o}\right) \tag{A3}$$

and

$$r_o - r_P = Z_P - Z_o \tag{A4}$$

From equations (A2) and (A4),

$$q_P r_P = \left(q_P + \Delta q_{amp}\right)\left[r_P + \left(Z_P - Z_o\right)\right]$$

or

$$r_P = \frac{q_P + \Delta q_{amp}}{-\Delta q_{amp}}\left(Z_P - Z_o\right) \tag{A5}$$

and from equations (A2), (A3), and (A5),

76

$$q = \frac{q_p r_p}{r} = \frac{q_p}{1 - \dfrac{\Delta q_{amp}}{q_p + \Delta q_{amp}} \left(\dfrac{Z_p - Z}{Z_p - Z_o} \right)} \tag{A6}$$

Thus, at each potential surface I, for IVEL = 2, equation (A6) gives the lateral distribution of velocity q as a function of the coordinate Z around the upstream boundary contour.

As shown in the preceding figure, r_p (at which radius $q = q_p$) can be greater than r_{min} (at which radius $q = q_{max}$), but r_p must be reasonably greater than r_o (at which radius $q = q_{min}$). In subroutine VELD, for IVEL = 2, if

$$\frac{r_o - r_p}{r_o - r_{min}} = \frac{Z_p - Z_o}{Z_{min} - Z_o} < 0.5 \tag{A7}$$

the solution is stopped.

In a similar fashion, for IVEL = 3,

$$q = \frac{q_p r_p}{r} = \frac{q_p}{1 - \dfrac{\Delta q_{amp}}{q_p + \Delta q_{amp}} \left(\dfrac{Y_p - Y}{Y_p - Y_o} \right)} \tag{A8}$$
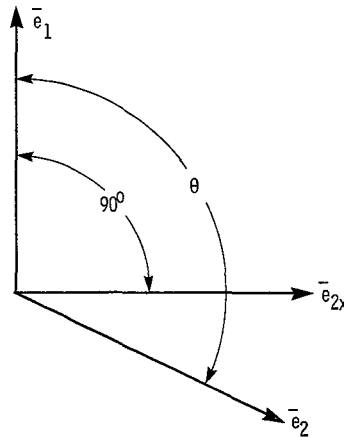
and the solution is stopped if

$$\frac{r_o - r_p}{r_o - r_{min}} = \frac{Y_p - Y_o}{Y_{min} - Y_o} < 0.5 \tag{A9}$$

APPENDIX B

CONDITION FOR NORMALITY OF UNIT VECTORS $\bar{e}_2$ and $\bar{e}_3$
WITH UNIT VECTOR $\bar{e}_1$

Consider the case in which the unit vectors $\bar{e}_1$ and $\bar{e}_2$ are not normal and find the direction cosines for a third unit vector $\bar{e}_{2x}$, which lies in the plane of $\bar{e}_1$ and $\bar{e}_2$ and is normal to $\bar{e}_1$. Thus,

Because the three vectors are coplanar, they are related by

$$\bar{e}_{2x} = k_1 \bar{e}_1 + k_2 \bar{e}_2 \tag{B1}$$

from which

$$
\left.
\begin{aligned}
\cos \alpha_{2x} &= k_1 \cos \alpha_1 + k_2 \cos \alpha_2 \\
\cos \beta_{2x} &= k_1 \cos \beta_1 + k_2 \cos \beta_2 \\
\cos \gamma_{2x} &= k_1 \cos \gamma_1 + k_2 \cos \gamma_2
\end{aligned}
\right\} \tag{B2}
$$

where $\cos \alpha_{2x}, ..., \cos \gamma_2$ are the direction cosines of $\bar{e}_{2x}, \bar{e}_1,$ and $\bar{e}_2$ and k_1 and k_2 are constants.

The constants k_1 and k_2 are determined from equation (B1) as follows:

$$\bar{e}_{2x} \cdot \bar{e}_1 = 0 = k_1 + k_2 \cos \Theta$$

and

$$\bar{e}_{2x} \cdot \bar{e}_2 = \cos (\Theta - 90°) = \sin \Theta = k_1 \cos \Theta + k_2$$

from which

$$k_1 = -\frac{1}{\tan \Theta} \tag{B3}$$

and

$$k_2 = \frac{1}{\sin \Theta} \tag{B4}$$

Thus, the direction cosines for $\bar{e}_{2x}$, which is $\bar{e}_2$ adjusted to satisfy the normality condition, are known from equations (B2) to (B4).

In a similar fashion, the adjusted direction cosines for $\bar{e}_3$ are given by

$$\left. \begin{array}{l} \cos \alpha_{3x} = k_1 \cos \alpha_1 + k_2 \cos \alpha_3 \\ \cos \beta_{3x} = k_1 \cos \beta_1 + k_2 \cos \beta_3 \\ \cos \gamma_{3x} = k_1 \cos \gamma_1 + k_2 \cos \gamma_3 \end{array} \right\} \tag{B5}$$

where k_1 and k_2 are given by equations (B3) and (B4), respectively.

APPENDIX C

PROBLEMS AND LIMITATIONS OF THE THREE-DIMENSIONAL DESIGN METHOD

The ill-posed nature of the three-dimensional duct design method when both the upstream boundary configuration and the lateral velocity distribution are prescribed is discussed in section 4.0. This ill-posed nature negates a proper solution. However, for relatively "compatible" upstream boundary configurations and lateral velocity distributions, reasonable solutions are forced by introduction of the six constraints in section 4.2 and by limiting the number of major iterations (ITER) to a range over which the solution is converging, as evidenced by decreasing maximum residuals $\mathscr{R}$. This appendix considers other problems and limitations of the design method, and for this purpose it is assumed that a method exists for assuring an absolutely compatible upstream boundary configuration (if such exists) for a given prescribed, lateral-velocity distribution. Also, without destroying the generality of the discussion, it is convenient to assume planar symmetry.

For the classical, two-dimensional, duct design problem (ref. 3) a solution exists for every prescribed, piecewise-continuous, velocity distribution along the duct walls. For the three-dimensional problem this universal existence does not appear to be the case. For example, consider a straight duct (which, if the velocity is not constant, implies two planes of symmetry at right angle, with the duct centerline along the intersection). Presumably, if the duct is straight, the upstream boundary configuration has biplanar symmetry, but is otherwise general. Thus,
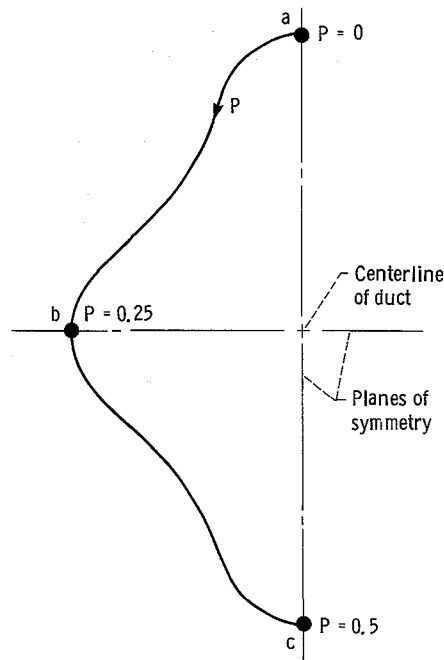
where P is the decimal fraction of distance around the contour. In the upstream and downstream regions (section 7.2), the lateral velocity q, expressed as a ratio of the upstream velocity, is 1.0 along every boundary streamline. Elsewhere, let the prescribed velocity be 1.0 along the streamlines through a and c (P = 0.0 and 0.5, respectively), and let the velocity decrease along the contour in an arbitrary fashion, but with biplanar symmetry, to a finite value approaching zero for the streamline through b (P = 0.25). If this distribution of velocity with P is maintained along the boundary streamlines over a large range of the velocity potential $\Delta\varphi$, then from equation (3.0.1)

$$\Delta\varphi = q_{a,c}(\Delta s)_{a,c} = q_b (\Delta s)_b \tag{C1}$$

so that over the range $\Delta\varphi$

$$(\Delta s)_b = \left(\frac{q_{a,c}}{q_b}\right)(\Delta s)_{a,c} \tag{C2}$$

from which the length $(\Delta s)_b$ of streamline b becomes many times larger than the streamline length $(\Delta s)_{a,c}$, and no solution (i.e., shape of flow field) appears likely. It might be argued that the large $(\Delta s)_b$ could be accommodated by a rapid outward fanning of streamline b, but the pressure gradients associated with the velocity distribution preclude this. (The rapid outward fanning of streamline b would approach a two-dimensional configuration in which streamlines a and c come together, lie on the duct centerline, and have a velocity distribution that adjusts to the prescribed velocity of boundary streamline b. In the three-dimensional case, however, the velocity distributions along streamlines a and c are prescribed and thus cannot adjust. This inability to adjust is probably the center of the problem.)

Finally, for the example just discussed the velocity q along the straight streamline on the centerline of the duct can be no higher than 1.0 (which is the highest velocity on the boundary streamlines in this example) and will be less than 1.0 where influenced by velocities less than 1.0 on the boundary. The lengths of the streamlines between the upstream and downstream potential surfaces are given by

$$\Delta s = \int_0^{\Delta\varphi} \frac{d\varphi}{q} \tag{C3}$$

Thus, Δs for the centerline streamline with velocities less than 1.0 is _longer_ than Δs for the boundary streamlines a and c, which have a constant prescribed velocity of 1.0. However, in contradiction, the centerline streamline must be _shorter_ than the boundary streamlines a and c, because it is straight and normal to the upstream and downstream potential surfaces, which are flat and parallel. It is concluded that for three-dimensional design problems not every prescribed velocity distribution has a proper solution.

For velocity distributions without proper solutions program DIN3D1, using the constraints in section 4.2 and limiting the number of major iterations (ITER), forces a "reasonable" solution. A measure of this reasonableness is the difference in streamline lengths S-I and S-II (output table III), which lengths should be equal.

Another problem area in the application of program DIN3D1 occurs when certain characteristics in the shape of the _downstream_ boundary configuration are desired. (There is, of course, no way to achieve a precise shape, because the downstream config-uration is dictated by the upstream configuration and the prescribed lateral velocity dis-tribution.) For example, consider a straight duct with a transition section in which the duct cross section changes from a circular upstream shape to an elliptical downstream shape of the same area. A normal design procedure, based on one-dimensional consider-ations, would keep the duct area constant and employ a linear variation in the fineness ratio of the elliptical cross section starting from 1.0 for the circle and ending with the desired value for the downstream shape. Here, to avoid large losses, the designer's objective is to keep the velocity on the duct wall constant (i.e., $q = 1.0$ along the boundary streamlines); and provided that the transition length is not too short, this objective should be nearly achieved. Thus for this type of three-dimensional design problem very _large_

81

changes in the duct cross section occur for very _small_ changes in the prescribed lateral velocity distribution. It is not easy to determine just how large and where these small changes in velocity should be. Furthermore because this type of problem is so sensitive to small changes in lateral velocity distribution, the downstream boundary shape is also sensitive to the necessarily approximate methods used in the forced, finite-difference solution of the governing differential equation (3.3.1). That is, the downstream shape varies appreciably with number of iterations (ITER), with upstream grid size and arrangement (section 7.1), with various damping coefficients (sections 4.6 and 5.2.2), and perhaps with such lesser iterations as ICONX (section 5.1.1) and NTRY (section 7.3).

In summary, it is not easy to control the _downstream_ boundary shape of the duct by the prescribed _lateral_ velocity distribution; although it is relatively easy to control the _streamwise_ shape of the duct by this means. However, substantial differences in the downstream shape need not imply significantly different lateral velocity distributions, provided that the downstream areas are equal in size. Finally, in those cases where the downstream shape is important, the solution becomes more sensitive to the lateral velocity distribution, if the damping coefficient CAVN is reduced to 0.0, or at most is not greater than 0.1.

82

REFERENCES

1. Stanitz, John D.: General Design Method for Three-Dimensional, Potential Flow Fields. I - Theory. NASA CR-3288, 1980.

2. Petrovsky, Ivan Georgievich (A. Shenitzer, transl.): Lectures on Partial Differential Equations. Interscience Publishers, New York, 1954.

3. Stanitz, John D.: Design of Two-Dimensional Channels with Prescribed Velocity Distributions Along the Channel Walls. NACA Rep. 1115, 1953.

1. Report No.	2. Government Accession No.	3. Recipient's Catalog No.
NASA CR-3926		

4. Title and Subtitle	5. Report Date
General Design Method for Three-Dimensional, Potential Flow Fields II - Computer Program DIN3D1 for Simple, Unbranched Ducts	September 1985
	6. Performing Organization Code

7. Author(s)	8. Performing Organization Report No.
John D. Stanitz	E-2388
	10. Work Unit No.

9. Performing Organization Name and Address	11. Contract or Grant No.
John D. Stanitz, Consulting Engineer 14475 East Carroll Boulevard University Heights, Ohio 44118	NAS3-21991
	13. Type of Report and Period Covered

12. Sponsoring Agency Name and Address	Contractor Report
National Aeronautics and Space Administration Washington, D.C. 20546	14. Sponsoring Agency Code

15. Supplementary Notes

Lewis Technical Monitor: Theodore Katsanis
Final Report

16. Abstract

The general design method for three-dimensional, potential, incompressible or subsonic-compressible flow developed in part I of this report is applied to the design of simple, unbranched ducts. A computer program, DIN3D1, is developed and five numerical examples are presented: a nozzle, two elbows, an S-duct, and the preliminary design of a side inlet for turbomachines. The two major inputs to the program are the upstream boundary shape and the lateral velocity distribution on the duct wall. As a result of these inputs, boundary conditions are overprescribed and the problem is ill posed. However, it appears that there are degrees of "compatibility" between these two major inputs and that, for reasonably compatible inputs, satisfactory solutions can be obtained. By not prescribing the shape of the upstream boundary, the problem presumably becomes well posed, but it is not clear how to formulate a practical design method under this circumstance. Nor does it appear desirable, because the designer usually needs to retain control over the upstream (or downstream) boundary shape. The problem is further complicated by the fact that, unlike the two-dimensional case, and irrespective of the upstream boundary shape, some prescribed lateral velocity distributions do not have proper solutions.

17. Key Words (Suggested by Author(s))	18. Distribution Statement
Design; Three dimensional; Internal fluid dynamics; Compressible; Incompressible S-ducts; Side inlets; Elbows	Unclassified - unlimited STAR Category 02

19. Security Classif. (of this report)	20. Security Classif. (of this page)	21. No. of pages	22. Price*
Unclassified	Unclassified	85	A05

End of Document